MASTER THESIS

# DESIGN OF A PROTOTYPE MACHINE FOR 3D PRINTING WITH CONTINUOUS FIBRE REINFORCEMENT


Menno-Jan Rietema

FACULTY OF MECHANICAL ENGINEERING

DESIGN, PRODUCTION AND MANAGEMENT


**EXAMINATION COMMITTEE**
Prof.dr.ir. F.J.A.M. van Houten
Dr.ir. T.H.J. Vaneker
Dr.ir. H.A. Visser


**DOCUMENT NUMBER**
OPM - 1285


UNIVERSITY OF TWENTE.

15-06-2015

## Summary

Continuous fibre deposition techniques are used in high tech industries to create very light and stiff structures like for example airplane hulls. Fused Deposition Modelling (FDM) is a 3D printing process that uses thermoplastics materials to create smaller but more complex shapes. In this study a machine and process are defined that combine the forming freedom of the FDM process with the strength to weight ratio of composite products. The study is a continuation of prior research at the University of Twente.

As a first step a pultrusion setup is designed and built. This process is used to create a filament based on a matrix of polypropylene with E-glass fibre reinforcement. This new feed material is used as basis for the printing process. Next an existing open source FDM printer has been adapted with a new printing head, optimized to handle the new feed material. Finally this new setup required a dedicated cutting mechanism, typically not found in standard FDM processes.

With this new feed material and machine setup samples were printed. Basic geometries were defined to test the ability to print small but complex structures. It was found that a minimal radius of 20mm could be printed and that a minimal fibre length of 6mm was possible.
Also mechanical test samples were printed. These samples were subjected to a microscopic study and three point bending tests to determine their quality. Results are evaluated to discover insights between machine design, process parameters and mechanical properties of the printed composites.

# Preface

I performed most of the research for this study at the WOT (Werkgroep OntwikkelingsTechnieken), which is one of the most beautiful places on the campus of the University of Twente. A place where the High Tech of the university meets the Human Touch of development work. I spent a large fraction of my study time as a member of this association, developing techniques to be used in developing countries. In the middle of these activities (somewhere between designing a wind generator for mobile phones and building a small scale bio digester ), I did my Masters research on a 3D printer to be used for high end composite materials. Since this has no direct link to the WOT activities, I would like to thank the people of the WOT for the work space and the use of the well equipped workshop. And not in the last place for their ability to withstand the smell of melted polypropylene.

During the design of the 3D printer, I enjoyed the multidisciplinary aspect of mechanics, electronics and software. The last fields of engineering were not competences that I learned directly during the courses of Mechanical Engineering. For that I want to thank Freddy Alferink, who helped me to pick up the basics years ago, and who always was an encyclopaedia to find answers on new questions.

Further I want to thank my supervisor Tom Vaneker for his support, especially during the last part of my research where I broke a lot of his deadlines.

# Table of contents

# 1 Introduction

Fibre reinforced products are gaining popularity in many areas. Not only in consumer products, but also in aerospace, sports and industrial applications such as pressure vessels and wind turbines. The main reason being their relative high strength/weight ratio. Still there is a lot of work to do, especially in the field of automating manufacturing [1]. Most of production methods for fibre reinforced products involve a large amount of manual labour and are therefore costly.

The market of the most used form of 3D printing, Fused Deposition Modelling, is also rapidly growing. Especially for the ability to manufacture complex shapes in low quantity products. Specifications of printers improve, and new materials are introduced to enhance the quality of manufactured products and the speed of production. Frequently used materials involve, but are not limited to ABS, PLA, PC and Nylon.

The combination of the FDM process and the mechanical properties of fibre reinforced materials could merge the freedom of creating complex shaped forms and the strength of composites. For this reason it has a huge potential to become an attractive production method. In the past few years a first step is made by some suppliers that offer FDM filaments that are reinforced with small chopped fibres [2]. These short fibres offer only a fraction of the mechanical properties that could be achieved with continuous fibres.

This potential was recognized by T.A. de Bruijn, who graduated with his research “DEVELOPING A PROCESS FOR CONTINUOUS FIBRES IN FUSED DEPOSITION MODELLING” at the University of Twente in 2013 [3]. This research gave a good insight in backgrounds of additive manufacturing and a proof of concept that combined FDM and fibre reinforced thermoplastics. This research is a follow up of the research in this report, and has a slight emphasis on the practical implementation of the process into an existing FDM printer. The goal is to design a working process to manufacture continuous fibre reinforced products with the same ease as regular FDM products.

To combine the continuous fibre reinforcement with the FDM process, the two fields of automated manufacturing are investigated in the first sub chapter. Then the previous work on this topic of T.A. de Bruijn is investigated, to determine the direction of the current research. The last sub chapter will describe the goal and the requirements for the current research.

## 1.1 State of technology

This sub chapter contains an overview of the two fields of automated manufacturing that are combined in this research into a new process. In the first sub chapter, the state of current technologies in the area of automated manufacturing methods with respect to fibre reinforced polymers is given. Then the state of technology regarding to the 3D printing process of FDM is described.

### 1.1.1 ATL and AFP

Automated Tape Layering machines use robotic heads to place thermosetting or thermoplastic fibre reinforced tape onto an existing (3 dimensional) surface. Tape width range from 1 to 12 inch, maximum linear speeds are up to 30.48 m/s with a mass deposition rate of 22.7 – 27.2 kg/h[4]. Consolidation forces are in the range of 445N (for 75mm thermoset tape) to 1000N (for 300mm thermoset tape), which corresponds with a consolidation pressure of approximately 0.1MPa [5]. For thermoplastic materials a much higher consolidation pressure is found, ranging from 1.4 MPa for APC-2 at 316 °C [5] to 3.6MPa [6]. Most of the systems have a minimum course length of around 100mm [5], which is the minimal length the machine put down. Start/stop accuracy is reported to be around 0.75 mm [4]. Cutting of the fibres is commonly done with ultrasonic knives.

Automated Fibre Placement (AFP) machines differ from ATL machines mainly in the width of tape that is applied. Typically it ranges between 3.2 to 12.7 mm, but several tapes can be placed in one movement[5]. Each tape speed can be individually controlled and consolidated, allowing for more complex shapes to be created. Production speeds and mass deposition is generally half the speed of ATL, since more complex parts are made. Tapes can be placed with slight curvatures with maximal radii in the range of 50.8 mm, compared to 610 mm for ATL setup with tape of 150mm. Minimal course lengths are usually around 50 mm [5].

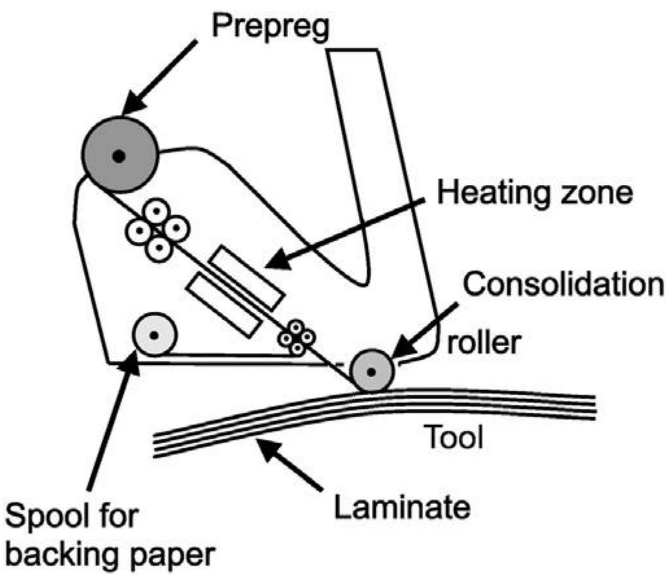


Figure 1: Schematic of an ATL lay up head [7]

### 1.1.2 FDM

Fused deposition modelling machines use a heated printing head to melt thermoplastic polymers.

These are then pressed through a small nozzle onto a print bed. Typical nozzle diameters range from 0.1 – 0.5 mm, and achieved speeds are reported up to 128mm/s (nozzle diameter 0.5mm, ABS), which leads to a deposition of 90 $cm^3$/h or 97gr/h [8]. Most of the machines use solid filament that are fed into the hot end with drive wheels. Typical diameters of filament are 1.75 and 3 mm.

Typical configurations use a gantry system or a delta robot to move the nozzle in 3 translational degrees. Controlling of 6 degrees of freedom is not seen very often, however researchers from different groups  are creating prototypes working with 6 DOF delta robots or robotic arms [9][10].

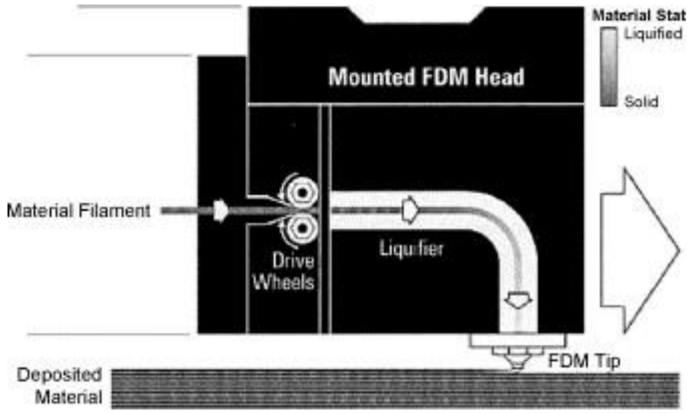


Figure 2: Fused deposition modelling process

## 1.2 Research Phase 1

The first phase of research at the University to the potential in the field between ATL and FDM is performed by T.A. de Bruijn. His work titled: “DEVELOPING A PROCESS FOR CONTINUOUS FIBRES IN FUSED DEPOSITION MODELLING” [3] is the start point for the current research.  In the first subchapter the main findings and achievements are noted. The research is reviewed in the next sub chapter. In the last sub chapter, a short summary of the review is given with a conclusion.

### 1.2.1 Achievements Phase 1

In this work several samples are created with continuous fibres of 30%v E-glass nested in a matrix of Polypropylene. The feed material exists of PP tape with dimensions of 5 x 0.5mm. The practical setup exists of an aluminium heater block with a channel to guide the tape while it is heated (see Figure 4). Heating is done with a 300W, 220AC resistor, controlled by a relay switch. This hot end is bolted to an existing Fab@Home 3D printer ([11]) as its printing head. In the research it is concluded that pressing of fibre reinforced tape through a heating channel is not possible in general, since buckling of the fibres occur easily and block the channel. This observation has led to the design where the fibre reinforced filament is pulled through the heater block without an active drive system.

Test are performed on printed specimen. Results of a three point bending test are reported to have a Young’s modulus of around 18 GPa, in comparison to a 2 GPa modulus of an FDM printed ABS part. Specimens of the same reinforced material but constructed in a heated press show a 20 to 30 percent higher Young’s modulus than the printed specimen.  Air pockets are seen between layers when insufficient force is applied to the printing head, resulting in a Young’s modulus of 4.3GPa. Specimen constructed with enough downward force on the printing head show no significant air pockets. Quantification of applied bonding forces or pressures is not given.

A maximum print speed with the used test setup is found to be around 25 mm/s. This corresponds with a deposition rate of 225 $cm^3/h$, or 390 gr/h.

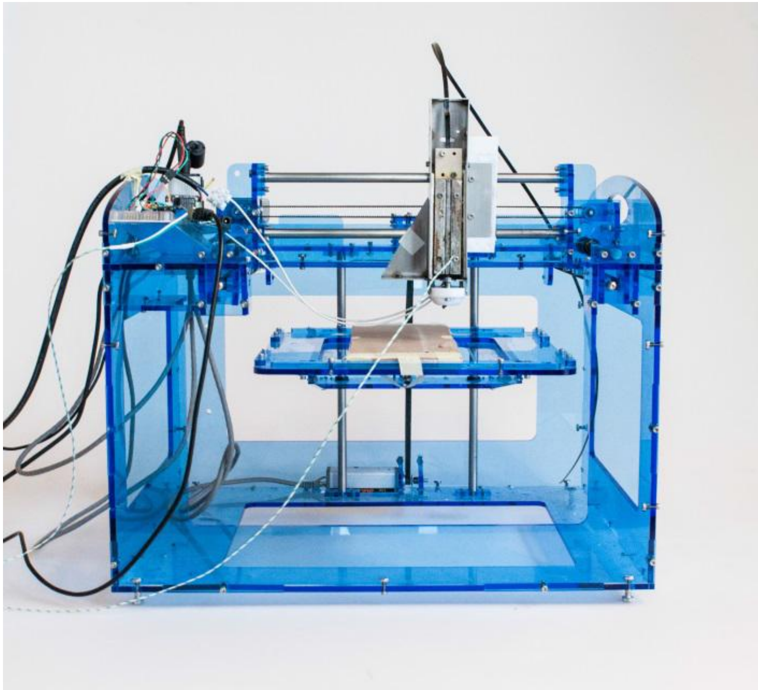

Figure 3: Fab@Home printer with developed printing head [3]

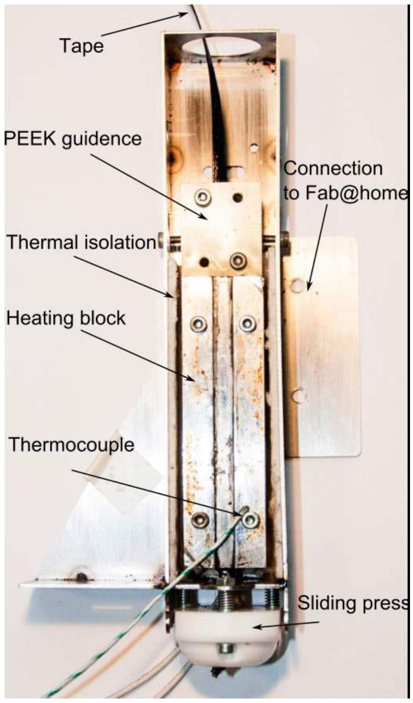


Figure 4: An overview of the CFFDM printing head prototype [3]

A schematic of the developed process is given in Figure 5.

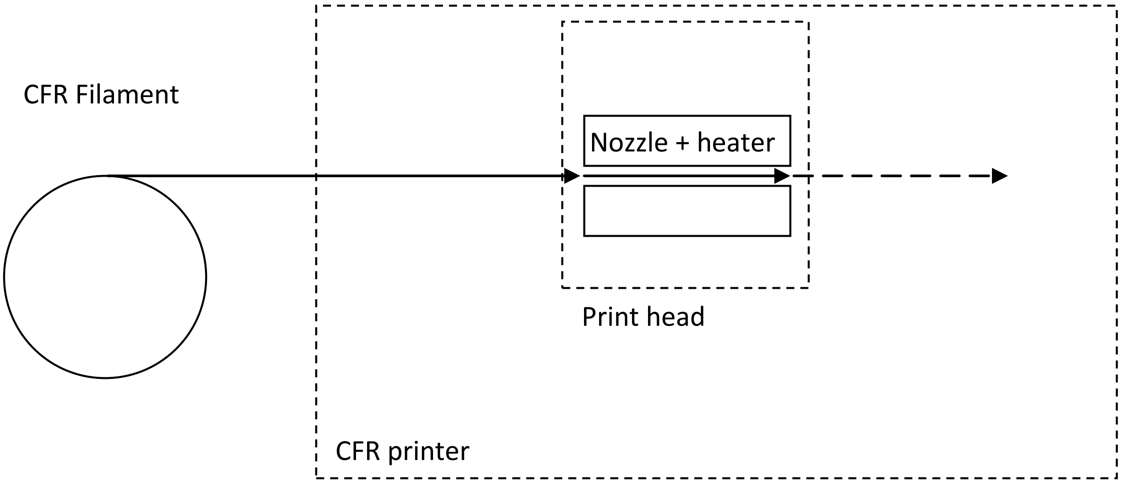


Figure 5: Process steps of Research phase 1

### 1.2.2 Evaluation of research Phase 1

In this sub chapter a review is given of the report "DEVELOPING A PROCESS FOR CONTINUOUS FIBRES IN FUSED DEPOSITION MODELLING" [3]. First the temperature control is discussed. In the second sub chapter the design of the heater block is evaluated. Then the selection of the feed material for the process is discussed, and the obtained results from the three point bending tests are analysed.

#### 1.2.2.1 Temperature control

The heat control in the heater block of the design is done with an Arduino, which drives a relay switch. Connections between sensor, relay and thermocouple amplifier shield is done with a breadboard. A picture of the system is given in Figure 6.

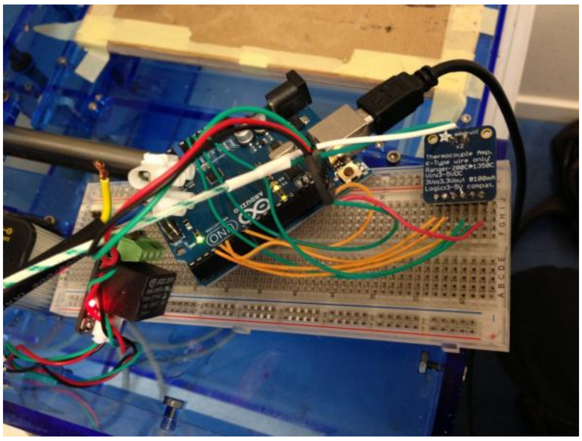

Figure 6: Temperature control system

The heater block is divided in two parts which are bolted together. The heating is done in one part, and the measurement is taken on the surface of the other element. During experiments, a small film of degraded PP has settled on the surfaces between the two parts. This decreases heat flow from the heated part to the monitored part. This causes a difference in measured temperature and actual temperature, where maximum measured values will be lower than maximum actual temperatures.

The temperature control is done with an on-off controller. It checks the temperature approximately once per 70ms, and when it drops under the configured setpoint, it powers the relay which switches net power to the resistor. With a relative long thermal distance from the sensor to the heating source and a significant thermal mass, this gives an overshoot that reaches >250°C with a setpoint of 230°C [[3] p.33]. A logged plot of the temperature over time is given in Figure 7 for various print speeds.

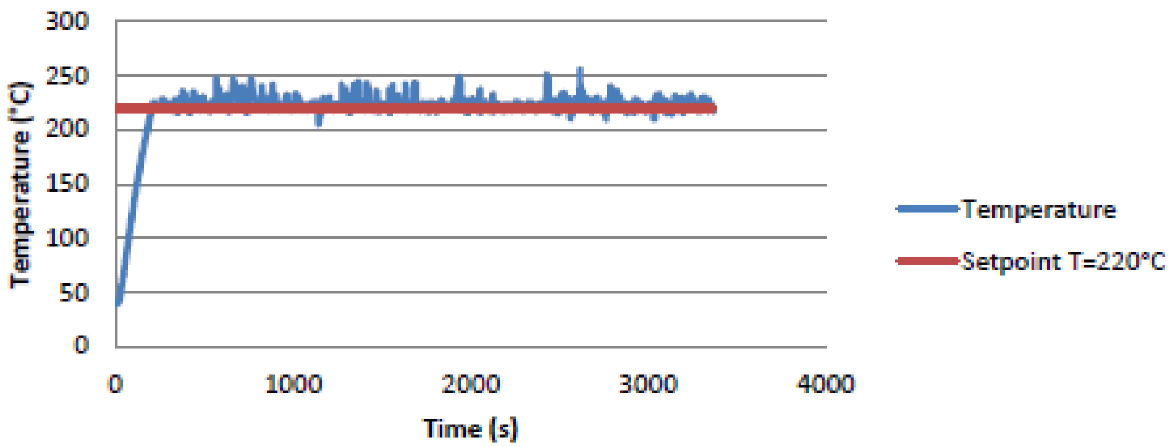


Figure 7: Measured temperature of the heater block, printing at various speeds. [1]

In the report is stated that a desirable temperature to process PP is between 220 and 230 degrees Celsius. This is very common for injection moulding of PP resins. Also for butt fusion welding of PP a temperature of 200-220 degrees C is advised [12]. The temperature at which certain filler materials in PP resin start to degrade at an undesirable rate is 232 $^{o}$C [13]. Fiber Glass Industries Inc advises a processing temperature of 180 – 230 degrees C[14]. Data of the used tape [15] is not sufficient to determine a maximum temperature for extrusion, but since the matrix material consists of PP, it will not deviate much from earlier mentioned values.

The above stated issues make it likely that the PP used in this study has degraded to a significant extend in the printing head since the actual temperature in the channel was significantly higher than the desired maximum processing temperature of 230°C. To obtain good bonding and healing between printed layers, this degradation is not desired.

In order to test a prototype printing head for continuous fibres, temperature control is advised to be improved to avoid over heating due to control issues. The thermal connection between heater and sensor needs to be improved in order to measure the actual temperature in the heating channel.

#### *1.2.2.2 Design of the heater block*

A picture of the heater block is given in Figure 8. The dimensions are 90 x 25 x 25 mm.

**Figure 8: Design of the heater block with PEEK guidance**

Nothing is mentioned in the report about the argumentations of the dimensions of the heater block. On page 28 of the report is stated that pushing the tape through a conductive heating channel is not possible in general, unless the matrix material is not heated totally (to remain stronger in buckling), or heating the tape is done without contact (so the friction force, which causes the buckling, is omitted). There is no evidence in the report to prove the statement for the *general* case. The conclusion of this pushing test is therefore only valid for the current design.

Below is demonstrated that the outcome of buckling fibres in the tape is the only possible outcome for the used design.

#### 1.2.2.2.1 Minimal length of the heater block.

For obvious reasons as friction, the length of the heating channel should be as small as possible, regardless of pulling or pushing the tape. When designing a test for pushing the tape through the heater block (see page 28 [3]), friction at the wall of the channel is the main force that causes buckling of the fibres.

#### 1.2.2.2.2 The dimensions of the heating channel

The dimensions of the tape cross section are 5 x 0.5 mm. To prevent buckling of the fibres, the cross sectional area of the tape should remain the same during the whole process. If this changes, the length of the tape changes because of conservation of volume. The dimensions of the channel in the heater block are measured to be approximately 6.2 x 1.5 mm. This is more than three times the cross section of the tape. Pushing melted tape in the heater will fill the channel, automatically shorten the original length more than three times. This obviously causes the fibres inside the channel to bend and buckle. A test with a channel dimension of exact the same as the nominal cross sectional area of the tape might give totally different results for this reason.

### *1.2.2.3 Applying of pressure*

The force which is exerted to bond a newly print layer onto an existing layer is very important to realize intermolecular fusion [p.19[3]].

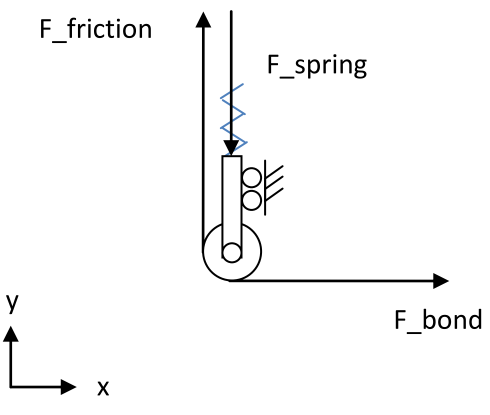


Figure 9: Simplified free body diagram of glider

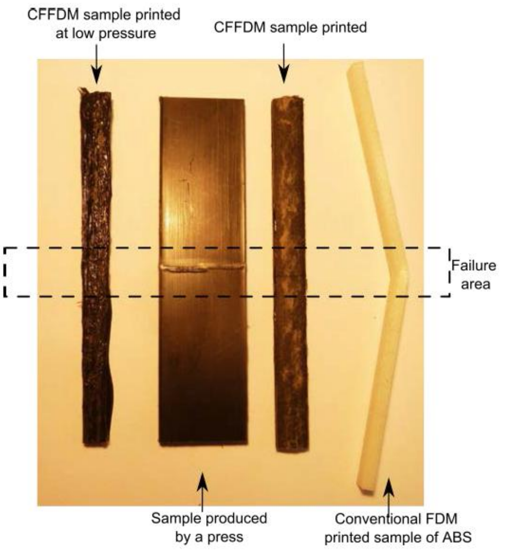


Figure 10: Tested samples and failure area

The current design features a glider that is spring actuated to exert bonding pressure to the newly added material. A simple free body diagram is given in Figure 9. The glider is assumed to have no significant friction and is represented as a roller wheel.

As can be seen from Figure 9, the force on the spring is dependant from the friction force inside the heating channel. Since the friction force is dependent on heater temperature and extrusion speed, it is not possible to use a spring for a constant and known consolidation force in this case. In the worst case, when the friction in the heater channel is very high, the spring loaded guiding element will raise, and no bonding will occur at all.

This phenomena will not only yield an irregular consolidation force and unpredictable bonding, but will consequently cause a deviation in degree of flattening of the printed traces. Over several layers, this will cause a difference in the dimensions of the CAD drawing and the produced part. In Figure 10 the irregular height of the left sample can be seen.

To obtain engineered end dimensions and calculate a reliable E-modulus, this phenomena is not desired. One way to cancel this is an infinitely stiff spring. The other way to avoid influence of heater channel resistance on consolidation force is filament actuation.

#### *1.2.2.4 Tape shape selection*

The tape used in the research has dimensions of 5 x 0.5 mm, and 30% E-glass fibre in a PP matrix. For the use in Fibre Reinforced Fused Deposition Modelling it yields several disadvantages. The most important being that the machine becomes very similar to an AFP machine, with the same limits regarding to tow steering and gaps (see Figure 12). Printing small radii is not possible with a rectangular cross section. This would lose a significant part of the flexibility of the FDM process.

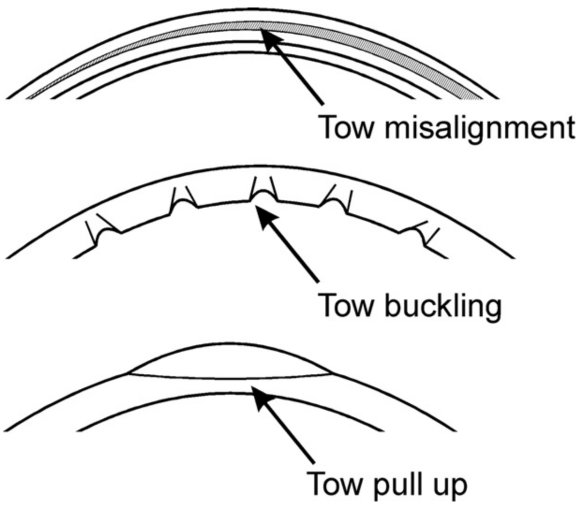


Figure 11: Overview of the most common tow steering defects[5]

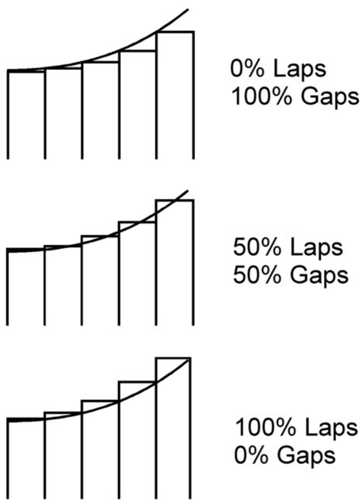


Figure 12: Illustration of laps and gaps during AFP layup [5]

#### *1.2.2.5 Calculation of flexural properties.*

The used tape for the study has mechanical properties that are given in Figure 13 [3].

| Material | Tensile strength (MPa | Tensile modulus (GPa) | | Flexural strength (MPa) | | Flexural modulus (GPa) | | Fibre mass fraction (%) | Fibre volume fraction (%) |
|---|---|---|---|---|---|---|---|---|---|
| | Av. | Av. | SD | Av. | SD | Av. | SD | Av. | Av. |
| GF/PP tape | >424 | 21.4 | 1.5 | 329 | 30 | 16.8 | 1.5 | 54.8 | 30.0 |
| Av. - Average | SD - Standard deviation | | | | | | | | |

Figure 13: Mechanical properties of used tape of Comp Tape Lda (ISO 527-5 and ISO14125)[3]

The used calculation for the Young's Modulus is only valid for linear beams with a constant cross section. It contains the height of the beam to the third power:

$$E_f = \frac{L^3}{4bh^3}\left(\frac{\Delta F}{\Delta s}\right)$$

where $\Delta F/\Delta s$ is the slope of the load – deflection curve.

It is stated in the report that the sides of the tested samples are sanded smooth, but the irregular height (see Figure 10) is not changed. In order to achieve a height h for the formula "*the difference between the outer surfaces is taken as a thickness, the value is overestimated leading to an underestimation of the stiffness.*" The achieved result for the flexural modulus after the three point bending tests is determined to be 18GPa. This result is compared in the report with an analytically defined tensile modulus of 24.7GPa.

As can be seen in Figure 13, the given data from Comp Tape Lda shows a lower flexural modulus than the achieved underestimated value of T.A. de Bruijn. The main explanation for this is that a significant part of the matrix material is lost during the process, leading to a higher volume fraction of the E-glass.

As a result of this, the obtained value for the flexural modulus does not qualify the bonding between printed layers, but is merely an indication for the fibre fraction.

It is therefore desired for future bending tests that leakage of matrix material is quantified, so that the volume fraction of matrix and reinforcement can be adjusted. This could be done by weighing printed samples of specified dimensions to obtain the average density of the material.

### 1.2.3 Conclusions of research phase 1

Based on the findings of the review a new heater block will be designed. It is stated that pushing the tape through a conductive heating channel is not possible in general. This conclusion is rejected because it is based on an incorrect interpretation of an experiment. A series of tests are done in the initial phase of the current research to check if it is possible under certain conditions to push fibre reinforced feed material through a heated channel. They are described in Attachment 2. This has major advantages above pulling the tape, which are described in Attachment 1. The outcome of the performed tests prove that pushing fibre reinforced material through a heated channel is possible.

To obtain end products without deviation from engineered dimensions, two options are regarded feasible as a addition to the designed prototype:
- Actuation of the feed material, so the friction force in the channel is cancelled out.
- A stiff connection of the slider so it is position based controlled, instead of force based.

The choice for a feed material with a square cross section of 0.5 mm x 5 mm limits the possible movements of the printer, especially with printing small radii. Before designing a new heater block, a selection for new feed material must be done first. A circular shaped tape is preferred, since it would allow printing in all directions with the same effort. This is seen as a valuable property of the FDM process.

## 1.3 Research goal

This sub chapter describes the goal of the current thesis research. In the next sub chapter the requirements of expected outcome are explained.

### 1.3.1 Research goal

The goal of this research to further define the process that combines Fused Deposition Modelling with continuous fibre reinforced feed material. This combines the freedom of forming of the FDM process, with the strength/weight ratio of continuous fibre reinforced end products. One of the main focuses will be to create a process that can be used to convert solid models in real products without human intervention. This includes the pre-processing of CAD models into useable machine code, and of course a machine that can understand the code and can print the instructions in continuous fibre reinforced plastic. The process needs to distinguish itself from Automated Fibre Placement processes with respect to the achieved product specifications, which are specified in the next sub chapter. The process needs to be able to produce products with similar free shaping characteristics of the FDM process but with mechanical properties of composites. Samples of printed material will be tested according to the ISO14125 [16] standard to determine this .

The development of a system that supports multiple extruders for fibre reinforced, non-fibre reinforced polymers and support material, would be ideal. The support material could replace the mandrel that is used in ATL techniques to lay the tape on. In this way even curved surfaces can be placed with fibre reinforced plastic. The nozzle with the matrix material could give products a smooth surface and fine detail, where the nozzle with fibre reinforced plastic could improve the mechanical characteristics. Such a machine could be combined with a tool that calculates the ideal fibre orientation depending on product loads. This is however expected to be too time consuming for one Masters research, and the current study focuses therefore on the process of placing fibre reinforced filaments only.

The application of this production method can be consumer products, high end sport products, medical applications and structural industrial applications. The field of application is outside the scope of the study, and is only limited by the imagination of the reader. The market potential of fibre reinforced FDM processes is researched in more detail by T.A. de Bruijn [3].

### 1.3.2 Requirements

The requirements of the study are explained and listed in this sub chapter. A distinction is made between requirements that concern the overall process and those which concern quantified and measurable specifications on the produced end products.

**Process requirements**

1. *Achievement of proper bonding between printed layers*

Bonding of newly printed traces onto the product are of utmost importance to achieve the desired material strength and stiffness. Non consolidated products are likely to fail under relative small loads due to shear stress between- and delaminating of the layers. The bonding will be tested in a microscopic study on the cross sectional surfaces of manufactured parts.

2. *Minimal course length: 10 mm/ minimal radius of curvature: 10 mm*

To obtain a added value in the market of automated composite manufacturing methods, the minimal course length needs to be much smaller than what currently is achieved with AFP systems, which can achieve 50 mm[5]. 10 mm is chosen as a reasonable improvement. Current AFP systems can apply tow steering with a radius of approximately 50 mm[5]. A minimal radius of 10 mm is chosen to be a reasonable added value, which makes the production method suitable for a whole range of products that are too small or complex for AFP systems.

**Machine requirements**

3. *Compatibility with STL and Gcode files*

Commonly used file types for CNC machines and 3D printer pre processors are Surface Tessellation Language (*.STL) files. These consists of a code that only describes the surfaces of a solid. All CAD programs have the option to export files in this format. Many programs are written to convert this file type into specific machine code (*.Gcode), which can be interpreted by CNC machines and 3D printers. Several of these programs are open source, which opens the option to adapt them or write additional code to convert STL files into special Gcode with machine specific instructions without reinventing everything from scratch. Both of the STL and Gcode file formats are widely supported by a large online community, making fibre reinforced filament printing easy to pick up by large group. It will make the developed solutions suitable for future development.

4. *Autonomous operation during manufacturing*

The process of printing should be totally automatic after the user uploads the machine instructions and presses the start button. The printer needs to be able to start and stop a printed trace on itself, without human interaction. The printer or the Gcode processor needs to identify end points of printed traces, and have the hardware to cut the continuous fibres at such points.

## 1.4 Report Outline

The outline of the report is based on the design steps that are made to create a 3D printer that is able to print fibre reinforced material. Based on the evaluation of research phase 1, the system layout of such a printer changes from Figure 5 to Figure 14. When the figure is read from the left to the right, the outline of this report is seen.

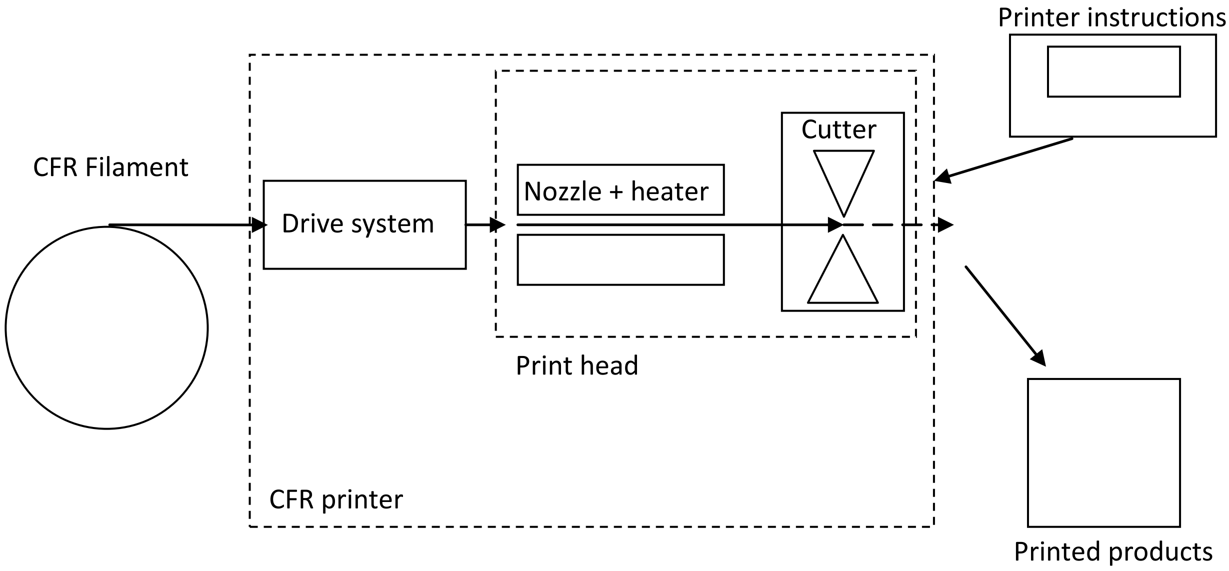


Figure 14: Schematic overview components

The first step is the selection of a suitable feed material. This selection defines a large part of the rest of the mechanical design. Also it influences the minimal printed radius that can be achieved. The material selection is described in Chapter 2. Since it is found that off shelf fibre reinforced filament is not available, a process to create it is designed.

Moving further to the left, the boundaries of the printer are encountered. The selection of the printer frame is made on which the developed prototype should work. Then the design of the printing nozzle with heater and filament drive system done. These topics are covered in Chapter 3.

When the line of the filament is followed further, the cutter design is encountered. This design is described in Chapter 4. After these steps, the designed printer is mechanically ready to print and cut fibre reinforced filaments.

The next important thing to do is the automation of the printing process. The printer needs to be adapted so it understands how to operate the newly added cutting feature. Then the program that communicates with the printer needs to understand when to give the printer the command to do the cutting. This automation is described in Chapter 5. After these steps, the printer is ready to create products.

These products are described in Chapter 6. The achieved minimal dimensions and tolerances are described. Then a look inside the products is taken with a microscope, to see if the printed lines are well connected. At last the products are subjected to destructive bending tests, to determine the mechanical properties.

The conclusions about the designed machine, the developed process and the end products are given in Chapter 7. Further improvements on the design and recommendations for further research are discussed.

# 2 Feed material

The material that will be used during the printing process is discussed in this chapter. The first sub chapter will discuss the criteria and selection of feed material. The second sub chapter describes the required pre-processing of the selected material and the generation of a design that for fills that function. Then the achieved results and conclusions about the process are given.

## 2.1 Selection of feed material

Before selecting a material, the criteria are mentioned in the first sub chapter. Then a small group of possible feed materials is given, and based on the criteria a selection is made.

### 2.1.1 Criteria

The set of criteria for the feed material of the continuous fibre reinforced FDM process are listed and explained below.

1. *Thermoplastic matrix material*

To be used in a common FDM process, a thermoplastic matrix material is required. This can be heated above its melting point in the print head, and pressed onto existing layers to bond and cool down. Generally used materials for the FDM process are preferred, such as ABS, PLA and Nylon. They have low thermal expansion coefficient (~70µm/m·K) and processing temperature (180-220 °C). Polypropylene is also an option, but is not seen very often in FDM because of its higher thermal expansion coefficient (100-200 µm/m·K) which causes warping. Besides that it tends to smear at its processing temperature, making it more difficult to print details.

2. *Fibre reinforcement*

Preferred is an prefabricated continuous tape or filament, where carbon or glass fibres are already bonded to the matrix material. A higher volume fraction is expected to be more difficult to process, since less bonding material is present and less lubrication from the melted matrix is obtained in the heating channel . To keep similarity between the developed process and the FDM process, the maximal desired volume fraction the fibres is $50\%_v$.

3. *Circular cross section*

A circular cross section of the feed material is required. Its symmetry allows printing in every direction without the need of a rotating print head. The printer will still resemble a common FDM printer , with the same freedom of movement. Further it has the following benefits:

- Nozzle and guidance can be made from one piece each with a turning machine, allowing for smooth transitions and surfaces to minimize buckling or blocking of fibres.
- The fraction surface area / volume of the heating channel is as small as possible, reducing friction during process.
- Tolerances on dimensions are expected to be lower than for square shaped filaments (tapes), since they are created by pultrusion and do not need to be slit.

4. *Small diameter*

The diameter of the filament should be as small as possible, since the cross sectional area will remain the same during the printing process. The diameter thus influences the resolution of the printer. A smaller diameter is expected to allow for smaller printable radii, since tow steering defects will decrease with smaller trace width [5].

### 2.1.2 Selection

Below a few options are given. Because thermoplastic continuous fibre reinforced filament is not available on the market, other solutions are investigated that require some extend of pre-processing.

| Option | Availability | Pre processing | Example |
|---|---|---|---|
| Continuous fibre reinforced filament | None | None required | - |
| Small tape | Moderate | Flat to round | Tape produced by CompTape BV[15] |
| Comingled yarn | Good | Consolidation | TwinTex [14] |

Figure 15: Options for feed material

As can be seen from Figure 15 pre-processing of feed material seems necessary, since prefabricated continuous fibre filament is not available.

Because of limited time for the research only two options are regarded. The first is the tape that is used by T.A. de Bruijn. It is produced by CompTape BV [15]. It has dimensions of 5 x 0.5 mm and a 54.8 m% E-glass content. Pre-processing would consist of reshaping the tape to round filament. The achieved diameter would be 1.78 mm.

The other is a comingled yarn of E-glass and Polypropylene filaments, TWINTEX® RPP60N265. It is manufactured by FiberGlass Industries [14]. It has a linear mass of 1870 Tex [gr/km], and a 60 m% E-glass content. After consolidation of the PP and glass fibres, a diameter of 1.26 mm can be achieved.

The available options are both based on a polypropylene matrix which are not favourable for FDM processes. Since no other option was available within the a reasonable time for decision one of the options is selected. Since the pre-processing would approximately be the same for both types (pultrusion), the diameter of the produced filament is taken as a reason to select the TwinTex comingled yarn to use as feed material.

## 2.2 Pre-processing of feed material

Since the selected feed material is a very flexible, rope like material, a setup is made to pre-process the comingled TwinTex® yarns into a solid fibre reinforced filament. This makes the feed material easier to transport throughout the printing process. The design for this is described in the next sub chapters.

### 2.2.1 Function identification

The process of shaping commingled yarns into solid filament can be divided in five functions.

- Shaping
- Heating
- Transport of filament through mould
- Heating control
- Transport control

For first three functions, a separate design is made that can be connected together. If a certain sub design does not satisfy, it is easily interchanged for an improved version. The final sub designs are a result of several iterations. Only the last versions are described in the next sub chapters. The control system for heating and transportation is discussed in Chapter 2.2.1.5.

#### *2.2.1.1 Pultrusion mould (shaping)*

To consolidate the TwinTex comingled yarns into a solid filament, pultrusion is the only option. First the consolidated diameter needs to be calculated. This is done with the formula

$$D = 2 \cdot \sqrt{\frac{TEX}{10^3 \rho \pi}}$$

where

D = the diameter of the consolidated yarns

TEX = the linear mass of the yarns, 1870Tex (gr/km)[14]

ρ = the density of the yarns, 1.5kg/$m^3$[14]

This yields a diameter of the consolidated filament of 1.26mm. A brass bolt (M10) is used as pultrusion mould for its thermal conductive properties. A hole of ø1.3mm machined in its centre to form the moulding channel. The slight deviation of the filament diameter and the channel diameter results in a surface difference f:

$$f = \frac{A_{nozzle}}{A_{filament}} - 1$$

of 6.5%. Because of the given precision of the density ρ of the yarns, it could very well be a rounded number. This could mean that the real density can be between 1.45 and 1.549999 kg/$m_3$. This would yield a difference in surface between 2.9% - 10.02%. The amount of air inclusions in the filament must be examined to see if a nozzle diameter of 1.3mm yields good results. A different size for drilling might yield some problems, since these sizes are not available on the market .

A PTFE guidance with a cambered entrance is then used to guide the yarns into the mould. Connection of the guidance to the mould is done with 3 bolts. A cross section of the mould is given in Figure 16.

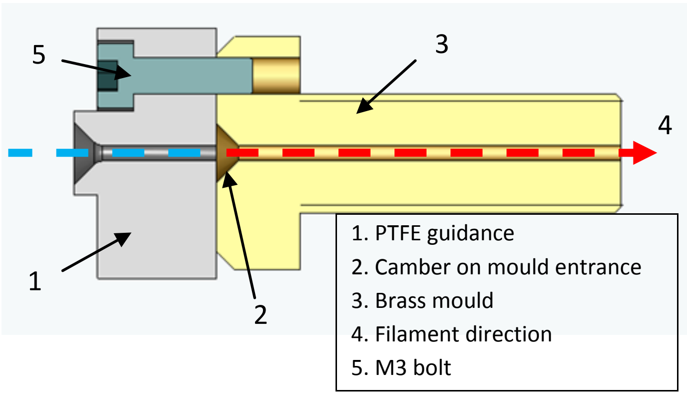


Figure 16: Cross section of pultrusion mould

Figure 17: Half fabricated pultrusion mould

### 2.2.1.2 Heater

To heat the described pultrusion mould, a block of aluminium with four heating resistors (6R8/3W) is used. A threaded hole is made in the centre to fit the brass nozzle. Three bars of PEEK are surrounding the block to minimise thermal losses to the frame. Temperature measurements are done between two resistors, 2 mm away from the brass mould. This location ensures that the measured temperature will never be lower than the temperature in the mould channel. Thermal compound kit is used to increase thermal conductivity between the different parts. Drawings are given in Figure 18 -Figure 20. The built system is given in Figure 21.

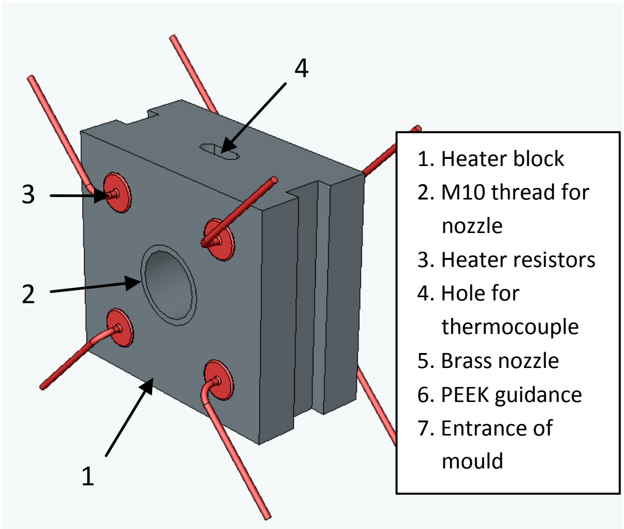


Figure 18: Heater block

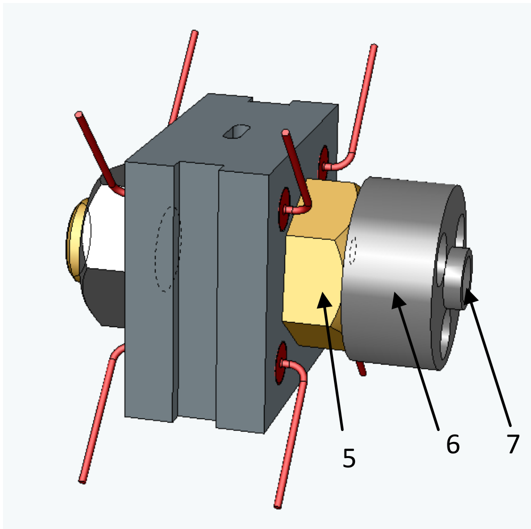


Figure 19: Heater block and pultrusion mould

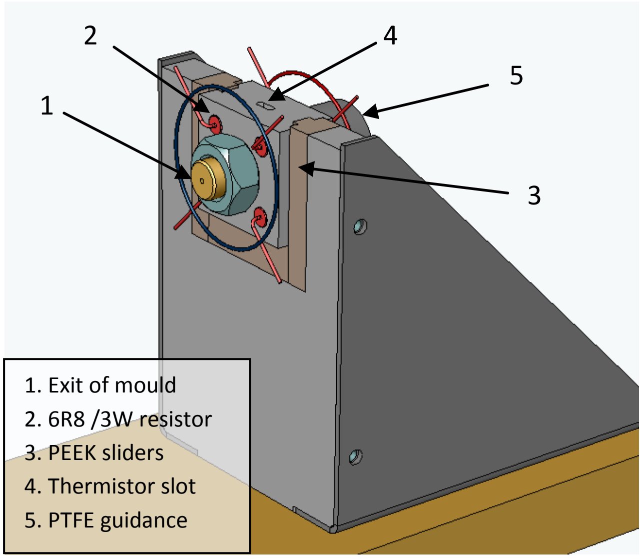


**Figure 20: Drawing of pultrusion setup**

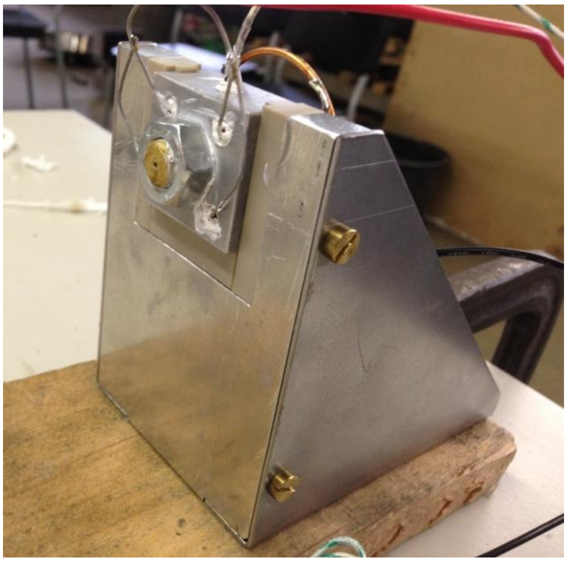

**Figure 21: Built pultrusion setup**

### 2.2.1.3 *Transport of filament*

The TwinTex comingled yarns need to be transported through the heated mould. Since pushing of the loose fibres is not possible, a drive system for pulling the consolidated filament is designed.

#### 2.2.1.3.1 Criteria for pull system

The criteria for selecting a good drive system are:
- that it does not damage the E-glass fibres in the filament
- that it has no slip between drive system and filament.

#### 2.2.1.3.2 Selection of technology pull system

Conceptual drive mechanisms for filaments are taken from T.A. de Bruijn and given in Figure 22 [3].

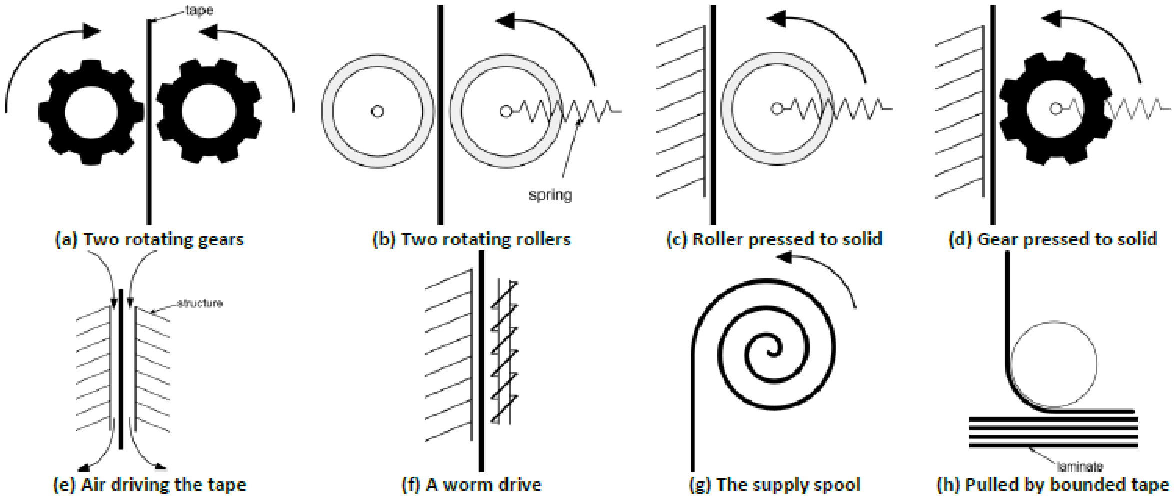


Figure 22: Conceptual drive mechanisms [3]

A variation on the two rotating gears is commonly seen in FDM printers to drive the filament (see Figure 23). All concepts with sharp teeth for extra grip (Figure 22.a,d,f) are however rejected for the first criteria. All concepts with undefined transport speed are rejected for the second reason (Figure 22.e,g). The pull option by bounded tape (Figure 22.h) is not applicable for this situation. The two rotating rollers appear to be the best solution.

### 2.2.1.4 *Design of pull mechanism*

To overcome the problem of a small contact area and low grip, a large diameter for the drive wheel is chosen and the filament is wound three quarters around the wheel before it is clamped. To further enhance the grip, a small groove is designed in the wheel to increase the contact area. This smooth groove is a solution that is commonly seen in MIG/MAG welding machines for driving the welding wire (Figure 24).

Figure 23: Common drive wheel for FDM printers

Figure 24: Common grooved drive wheel for MIG/MAG welding wire

A geared stepper motor (Nema 17, 0,44Nm, gear ratio 13:1) is chosen to directly drive the wheel for its simplicity to control. The diameter of the wheel is chosen to be 95 mm. This experimentally determined to be 20% bigger than the radius where the solid filament will buckle under pure bending. At a speed of 5mm/s, the motor starts to stall. The required force to pull the filament through the mould is therefore loosely defined to be 10N - 100N, depending on the speed (0.5 – 5mm/s). A drawing of the system is given in Figure 25, the actual built system is given in Figure 26.

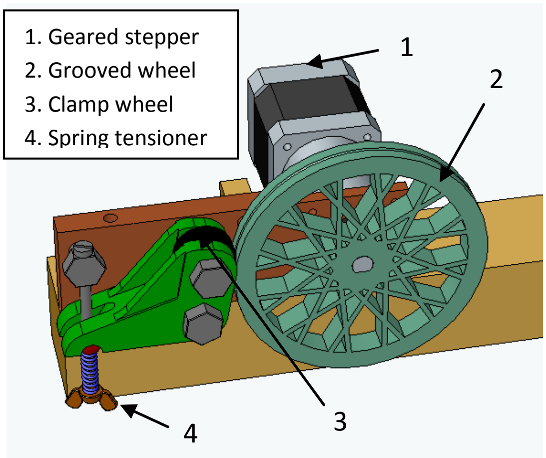


Figure 25: Drawing of pull system

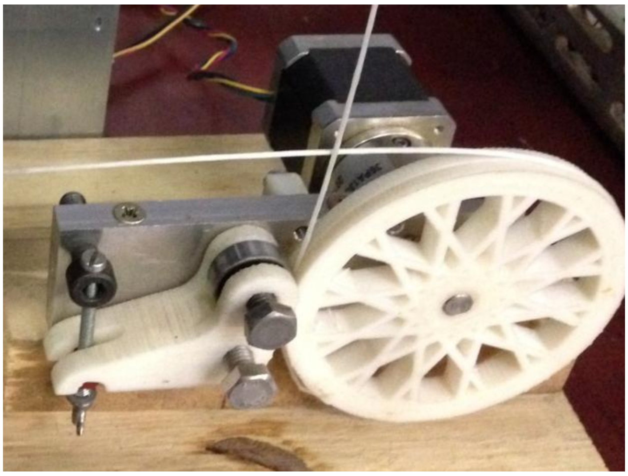

Figure 26: Built version of pull system

#### 2.2.1.5 Temperature/actuation control

For temperature and speed control an Arduino is used. This is an open source hardware board, with an Atmega processor. A lot of documentation can be found online [17], and since it has an USB interface, software iterations can be easily uploaded without the need for an additional programmer device. Required programming is very similar to C++. In the first part of this chapter the electronics are described, in the second part the working of the written program. The code of the program is included with the files of report. The circuit for the electronics can be found in Attachment 4.

#### 2.2.1.6 Electronics

An Arduino Uno R3 is used to read the serial data from a thermocouple amplifier board (MAX 31855) and control a power mosfet (IRLZ34N) which switches four parallel connected 6.8Ω/3W resistors at

12V. The power dissipation in each of the resistors is 21W when switched on, which exceeds specification of 3W. This is however specified for a continuous power consumption without temperature control. The resistors will then break eventually because of the temperature exceeding their limit. In the case with temperature control this will not happen, and the 21W dissipation is not a problem.  The mosfet is switched by the Arduino with Pulse Width Modulation (PWM) at a frequency of 120Hz. Since the width of each pulse is configurable from 0 (off) to 255 (100% duty cycle), the power to the resistor (and thus the temperature) can be regulated accurately.

The stepper motor is connected to a stepper driver board (A4988) which can be controlled by the logic 5V of the Arduino.

To make alterations of setpoints and pultrusion speeds easy, a display and two rotary knobs are added. The display shows the current temperature (T [°C]), the internal temperature of amplifier chip (Ta[°C]), and the setpoint temperature (Ts[°C]) (Figure 27). The knobs are used to set the desired temperature and speed from 0 to 220 $^{0}$C and 0 – 50 mm/s respectively. The temperature can be logged in real-time on the computer to test the settings of the control system (Figure 28).

The setup is powered by a computer PSU of 340W which offers a convenient level of 12V (max 18A) for the heating circuit and the Arduino. The connected shields are powered by the onboard voltage regulator (5V) of the Arduino.


Figure 27: Display layout of Arduino controller

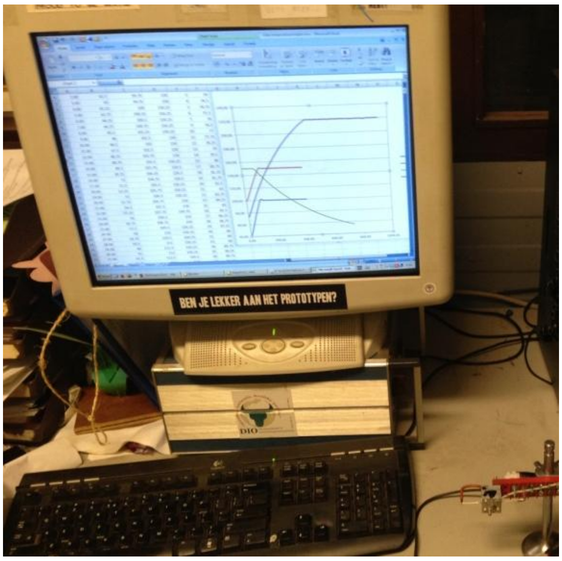


Figure 28: Data plotting of temperature with different parameters and setpoints

### *2.2.1.7 Program*

Several programs are tested on the Arduino. One with a simple on/off regulation (bang-bang control). When the measured temperature is higher than the setpoint, the program switches the temperature off. If the temperature is lower than the setpoint, the program switches the power resistor fully on. The frequency of this control is approximately 5Hz. In systems with a lot of thermal mass, and a long distance between sensor and heat source, this will result in a high overshoot. In the current system, where the sensor is placed between the resistors and the aluminium block is relatively small, the overshoot is relatively small (~1 $^{0}$C)

An improved program is written with a PID controller to minimise this overshoot. The parameters of the PID are designed to be overdamped, so overshoot will not occur. A big disadvantage is that such a system is much slower in response. Heating this system from ambient temperature to printing temperature takes almost two times longer than the program that uses simply an simple bang-bang control. To prevent this, an improved program is written that uses bang-bang control when the error |Tc-Ts| > 5 $^{o}$C, and very conservative overdamped parameters when the error becomes smaller than 5 $^{o}$C. The adaptive PID controller gives an overshoot of 0.75 $^{o}$C. The extruder temperature with the different control systems is given in Figure 7.

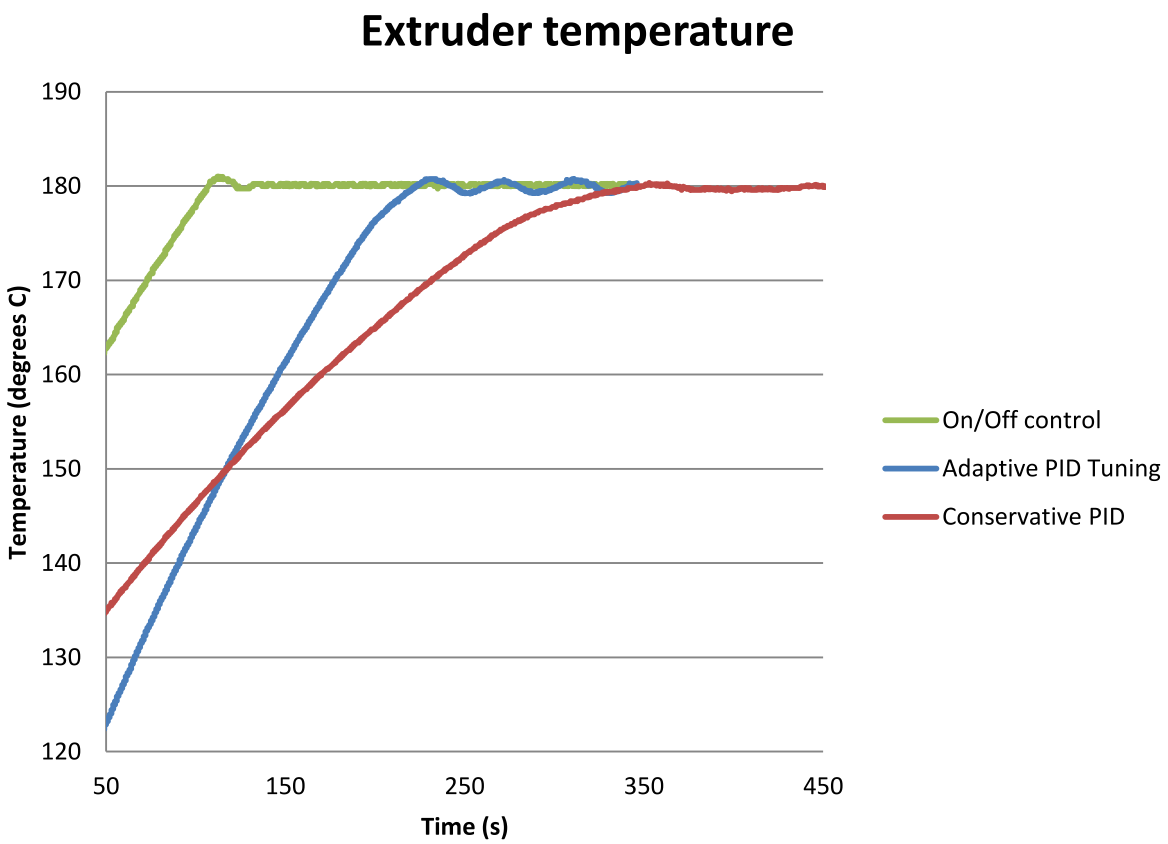


**Figure 29: Data plot of extruder temperature with different control systems without line smoothing**

From Figure 29 can be seen that both the simple On/Off and PID control systems give an error of less than 1$^{o}$C (with Ts = 180). The adaptive PID control gives an error of less than 0.25 °C (Ts=180). It is expected that the Adaptive PID control is more flexible to use in other systems, since it can be tuned to a higher degree than the On/Off system.

### 2.2.2 Final design

A drawing of the total system is given in Figure 30, a picture of the built system is given in Figure 31. A bicycle wheel (ø600mm) with a small motor is used to spool the produced filament.

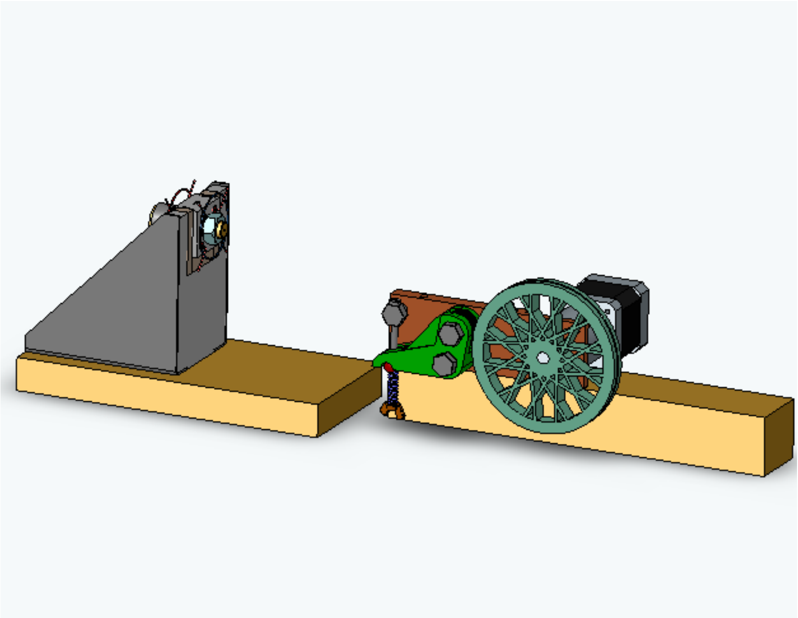

Figure 30: Drawing of pultrusion setup

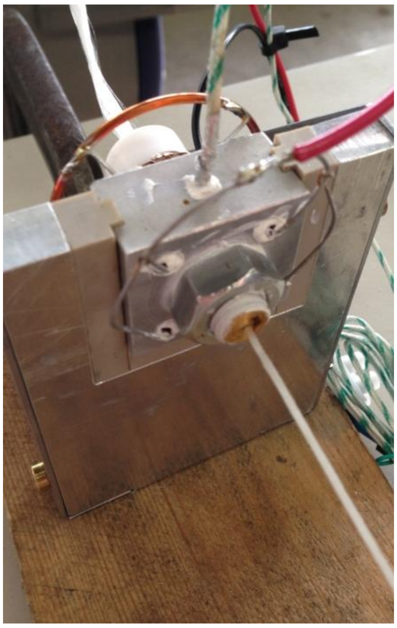

Figure 31: Pultrusion nozzle

#### *2.2.2.1 Starting production*

Starting of production is a challenge, since the TwinTex® yarns cannot be pushed through the system. A separate starting nozzle is created, with PTFE liner inside. A short portion of the yarns (appr. 50mm) can be manually consolidated with a butane lighter, and then pushed through the starting nozzle. At the exit it can be pulled for a convenient length of  approximately 200 mm. Then the filament is removed from the start nozzle by pulling it backwards, the start nozzle is replaced by the production nozzle in the heater block, and the consolidated length of the filament is pushed through the production nozzle without problems.

#### *2.2.2.2 Notes on the design*

Some observations done during several experiments that influence quality of the produced filament are given in a short list below. These can be used as a reference when reproducing the setup.

- The connection between PTFE guidance and brass mould is not sufficient to prevent some leaking of the PP matrix material. This is caused by stress relaxation in the PTFE. Tightening of the three bolts will stop the leaking for some time but deforms the guidance. An improved sealing/clamping is recommended. The pultrusion stepper motor is capable of delivering a force in the filament of approximately 100N. The pressure in the mould channel can therefore reach up to 100N/channel area = 100/1.3E-6 = 75.3 MPa. The current connection of PTFE and brass nozzle is not capable of holding that pressure.
- The alignment of the PTFE guidance and brass mould is of utmost importance in the setup. Small misalignments will cause fibres to buckle, resulting in a blocked mould channel after a few meters of production (See Figure 51). This phenomena can be identified by the surface

quality of the produced filament, which will be non smooth with protruding glass fibres. Transporting filament will require increasing force, and a slight scraping sound can be heard.

- The chamfer mould entrance(See Figure 16) is equally important. Non chamfered entrances will yield the same problems as non-alignment. The chamfered edges are sanded smooth with fine sanding paper (P1500). The chamfer must be very small (approximately 0.1 x 0.1 mm x 45°) to avoid too much pressure to build between the guidance and the brass mould. In the current setup, this causes leaking, as described above.
- Buckling of consolidated filament as a result of pure bending occurs at an empirically determined radius of approximately 40 mm. The drive wheel for filament transport through the mould has a radius of 45 mm. This is too close to the critical radius and some buckling spots occur during the process (appr. 0.25/m).
- Buckling of the filament can occur during storage on the spool for several reasons.
    - *Stress relaxation*
      After a couple of days, buckling initiates on a spool of 300mm diameter. The reason is probably the tension that is induced on the glass fibre during the cooling of the consolidated matrix. After spooling, the tensile and compressive stresses at the inner and outer diameter in the matrix material of a filament relax, yielding a higher compressive force on the fibres at the inside of the winding than before relaxation. This phenomenon has stopped with spooling on a diameter of 600 mm (bicycle wheel rim).
    - *Non tight winding*
      If the filament is not wound tightly around the storage spool, it tends to form a polygon shape around the spool rather than a circular shape. This phenomenon has stopped with introducing a small motor to drive the wheel with a slip coupling. The motor originates from the platform of a microwave. It has therefore no preference for direction at start-up. It is noted several times that also during production the motor can reverse its rotation.

## 2.3 Filament Quality

To confirm the quality of the filament, a microscopic study is done to check the geometry and prevalence of air inclusions in cross sections. The procedure of creating the samples is described in the next sub chapter. Then pictures of the results are listed and a conclusion is given in the last sub chapter. The occurring leakage of the pultrusion mould seem to increase with extrusion speed. This is further determined for  several printed samples and can be found in Chapter 6.2.

### 2.3.1 Procedure

Since the pultrusion process has only two variables, these are varied for the test samples. The temperature of the nozzle is varied from 180°C to 210°C with steps of 10°C. For each temperature the pultrusion speed is varied from 0.5 to 3 mm/min with steps of 0.5mm/min. Short lengths of the obtained 24 samples are inserted in an holder and embedded in epoxy. After 24 hours of curing, the epoxy with filaments is cut in half with a diamond saw and sanded with increasing P-number (P500 to P 4000) and polished to obtain a clear view on the cross sectional area. A picture of the filament samples in the holder is given in Figure 32, a picture of the samples after polishing the cross section is given in Figure 33.

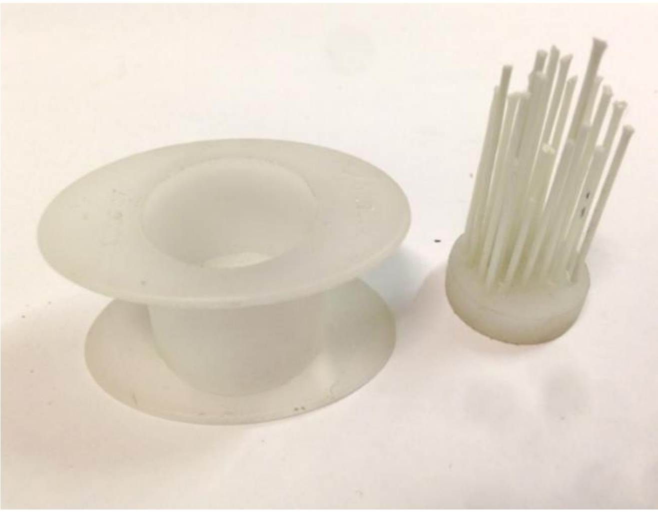

Figure 32: Samples of filament in holder

Figure 33: Embedded and polished samples

### 2.3.2 Results

One of the obtained images is given in Figure 34. Small air voids can be seen, together with dull spots and irregularities in the polished surface.

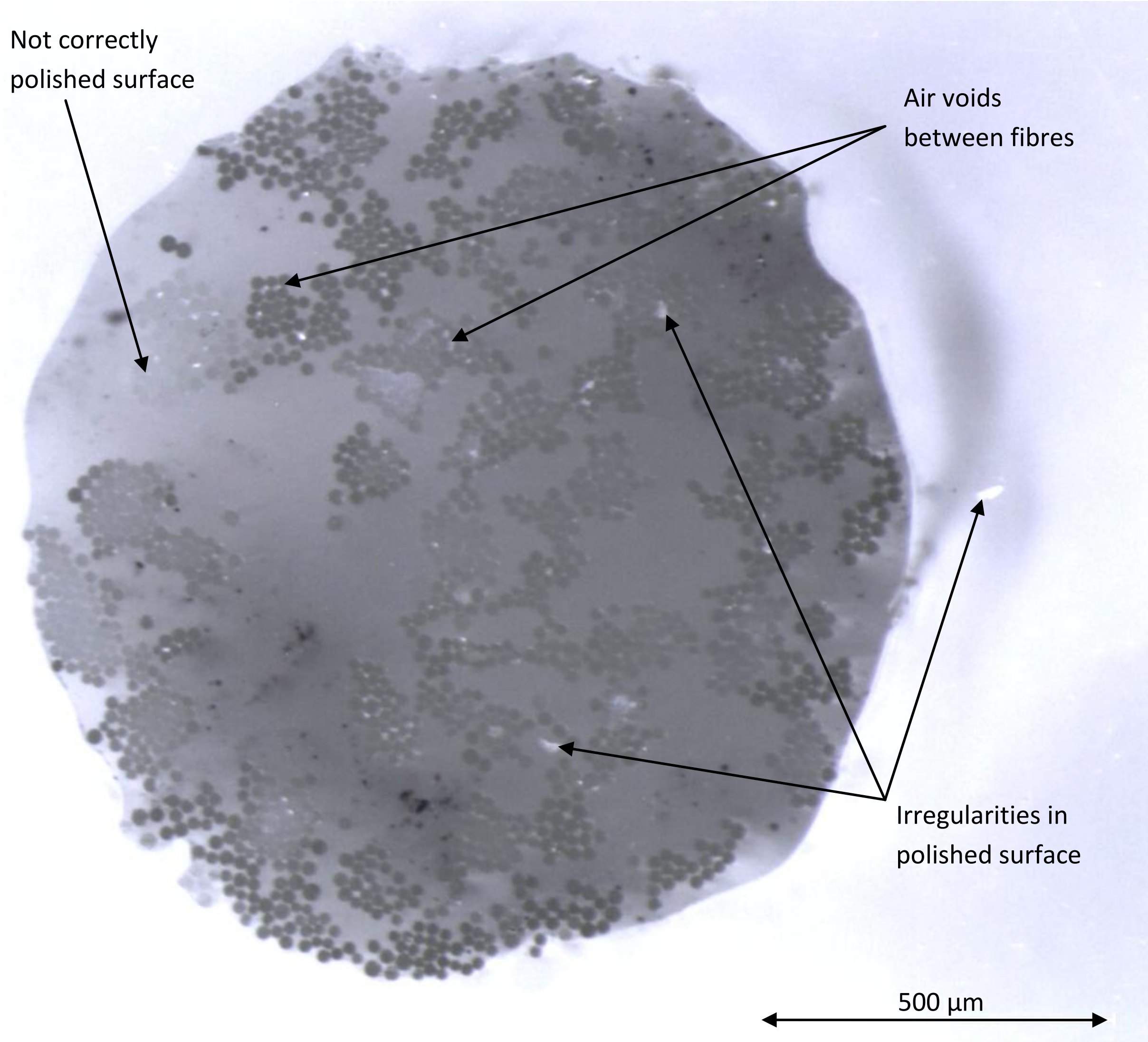


**Figure 34: Cross section of filament produced at 1mm/s @ 200°C**

The microscopic images (10 times optically magnified) of the samples are given in Table 1. An evaluation on several observations is given below. The images can be found with the enclosed files with this report.

| | 180°C | 190°C | 200°C | 210°C |
|---|---|---|---|---|
| **0.5 mm/s** | 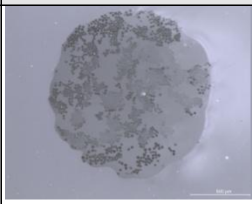 | 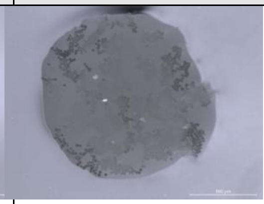 | 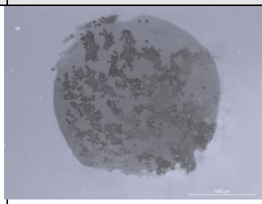 | 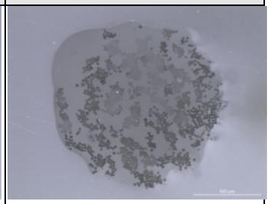 |
| **1.0 mm/s** | 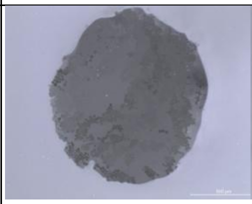 | 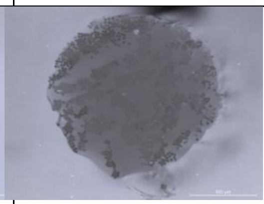 | 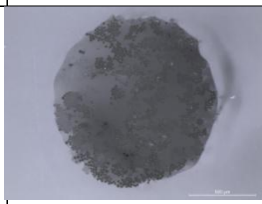 | 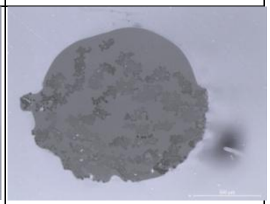 |
| **1.5 mm/s** | 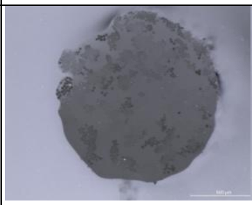 | 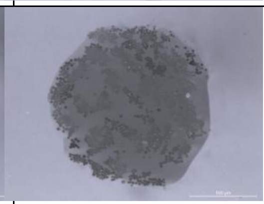 | 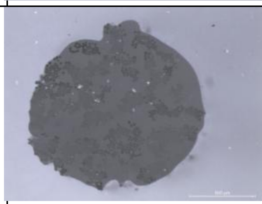 | 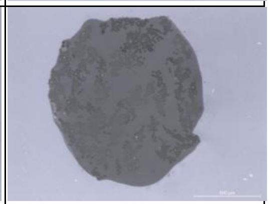 |
| **2.0 mm/s** | 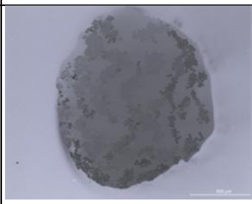 | 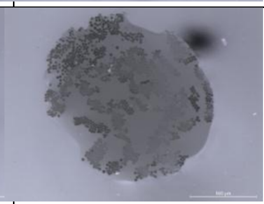 | 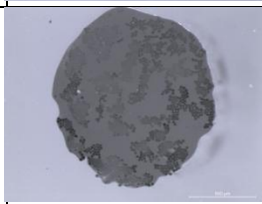 | 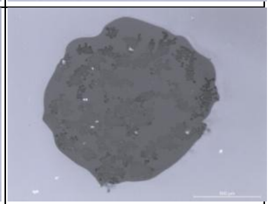 |
| **2.5 mm/s** | 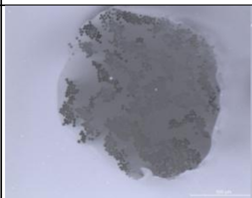 | 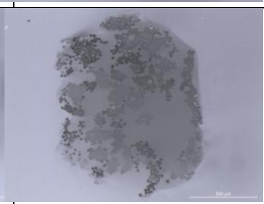 | 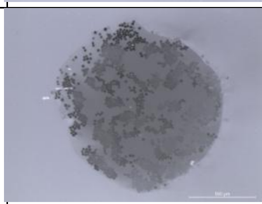 | 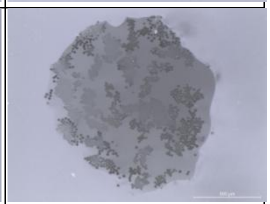 |
| **3.0 mm/s** | 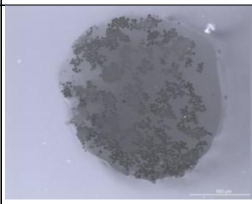 | 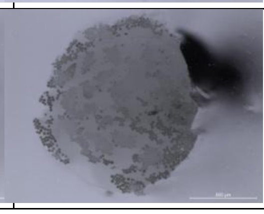 | 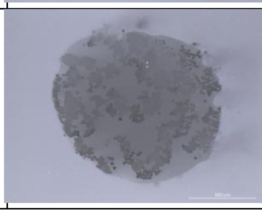 | 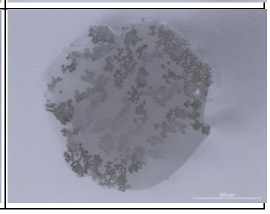 |

Table 1: Magnified cross sections of filament samples

***Fibre distribution***

It can be noted that samples printed at high temperature with low pultrusion speeds tend to have an uneven distribution of fibres with on one side a spot of mainly matrix material. This is most probably caused by the fact that fibres are not pulled exactly in line with the extruder. At high temperatures, the yarn does not have much friction through the nozzle. This makes the tension in the filament very low, so that it does not follow a straight line from mould exit to pulling wheel. The slack filament can be seen in Figure 35. This might cause the fibres to be pulled to the upper side, leaving more matrix material on the lower side.

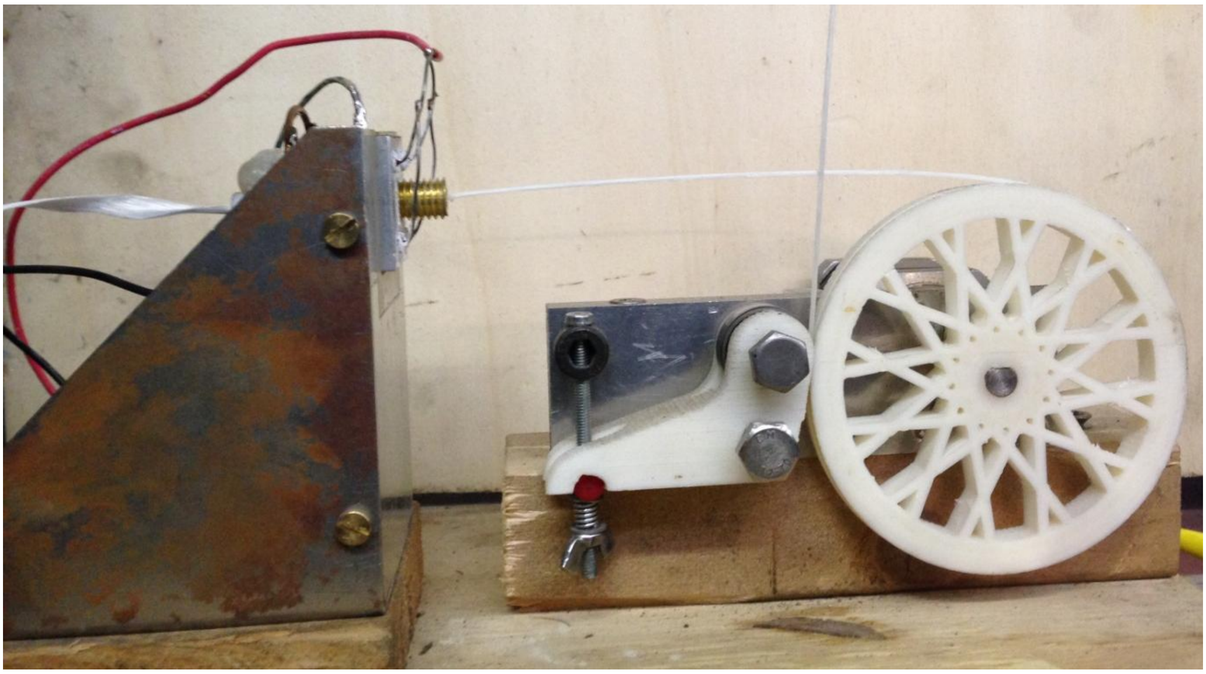

Figure 35: Pultrusion at 0.5mm/s @ 210°C

***Outer shape***

From Table 1 can also be seen that a higher pultrusion temperature tends to result in a more irregular outer shape of the filament with more protrusions. This is most likely caused by a longer solidification time of the filament after the mould. Fibres will have more freedom to move back to a less compressed state after they are forced in position by the mould.

***Air voids***

For all of the samples, small air voids are present in the cross section. They are mainly seen between clusters of fibres. No clear relation is seen between air inclusions and extrusion speed and temperature. No further analysis is done to quantify the area of the air voids, since the quality of the polished sample surface was poor and the light conditions were not the same for each image. For the sample printed at 200°C and 1mm/s  an enlarged picture is given in Figure 34.

### 2.3.3 Conclusion on filament quality

Small air voids occur in all samples without remarkable relation with pultrusion speed or temperature. They are mainly found between fibres in clustered groups. They are not expected to influence the printing process to a high degree since the matrix is heated again during printing and the fibres will have another opportunity to bond with the matrix.

At a temperature of 200°C a filament can be created that is expected to be suitable for the printing process. The speed of the pultrusion is not limited by observations from the microscopic study. In practice it is found that leaking of matrix material increases with increasing pultrusion speed. For the production of filament for the printing processes, the speed was set to 2mm/s to avoid too much leaking. From the microscopic images can be concluded that this will yield filament with a good surface quality and fibre distribution.

## 2.4 Conclusion

From the limited selection of possible feed materials for a continuous fibre reinforced filament printer, the comingled yarn TWINTEX® RPP60N265 is chosen. Compared to the other options, this yarn offered the smallest diameter of 1.26mm after consolidation. This is expected to allow for smaller printable radii with less tow steering defects.

A process is developed for pultrusion of the commingled yarn to consolidate it into a solid filament. The process is automated to a high degree, with adjustable pultrusion speed and mould temperature. Produced filament is wound on a storage spool of ø600mm, which is powered by a small motor. It is noticed that the nozzle of the pultrusion setup is leaking polypropylene, which could be improved. The filament is therefore expected to have a slightly lower volume fraction of reinforcement fibres.

The quality of the produced filament is expected to be good. Some small air voids are detected during the microscopic study, but these are not dominantly present and are not expected to influence the printing process.

# 3 Design of a CFRF printer head

This chapter describes the design of the printer head for the continuous fibre reinforced filament printing process. In the first sub chapter the functions of the printing head are given per subject. Each design is then discussed with its belonging functions in the sub sequent chapters. The selection of the printer frame is included in this chapter, since it is connected (physically and functionally) with the printing head and affects the performance. These designs are combined into the detail design. At the end of this chapter the performance of the design with respect to the requirements is discussed. The cutting system is described in the next chapter.

## 3.1 Function identification

The functions of the printing head are given in Table 2. They are divided in four different subjects which are described in the next sub chapters.

| Subject | Functions | Control system | Defines | Dependant on |
|---|---|---|---|---|
| **Spatial movement** | Moving printing head | Movement control | x, y, z, $v_{print}$ , a | T, $k_{frame}$ |
| **Printing head** | Heating filament | Heating control | T | |
| | Placing/consolidate filament | | - | x, y, z, $k_{frame}$ |
| **Filament transport system** | Filament transport | Speed control filament | - | $v_{print}$ |

Table 2: Overview of functions of printing head

## 3.2 Spatial movement

The design of a system to move the printing head is outside the scope of this research. For that reason an existing 3D printer is selected for spatial movement. The selection criteria for the printer are given in the first sub chapter. The selection of an existing printer is discussed in the last sub chapter.

### 3.2.1 Criteria

The criteria for the printer main frame are listed.

*1. Stiffness of the frame*

A consolidation force is required to add new layers onto the print. The printer frame needs to be stiff enough so it will not deflect under this force. An indication of the required consolidation pressure is taken from specifications of ATL processes, and ranges between 1.4 MPa [5] to 3.6MPa [6]. The printer nozzle is assumed to have a circular area to exert this pressure with a diameter of 4 mm. This nozzle design is further discussed in Chapter 3.3. A schematic bottom view of the print nozzle is given in Figure 37. The coloured area is used for consolidation, which is estimated to be <55% of the total area, or $< 7mm^2$. A pressure of 1.4MPa to 3.6MPa on this surface yields a reacting force of 9.8N to 25.2N. It is however expected that the consolidation pressure for an FDM process is much lower than for ATL processes. With ATL processes the consolidation force is exerted on the solid outer surface of the tape, since it is only heated at the contact area. During the FDM process the pressure is exerted on the melted polymer. A very high consolidation pressure will press the melted matrix away instead of bonding it to the previous layer.

The exertion of consolidation pressure can only be influenced by  the selected layer thickness t. The smaller t, the more force is required to flatten the printed trace to a larger width w. Since the printer frame is not infinitely stiff, the consolidation force $F_c$ is achieved by deflection of the frame. The resulting force exerted by the filament on the printer head is given as $F_f$. More deflection of the printer frame yields a higher consolidation force, resulting in a flatter layer. This is schematically given in Figure 36, where $x_n$ is the difference in ideal printed thickness (n*t) and the achieved thickness $T_n$ after n layers.

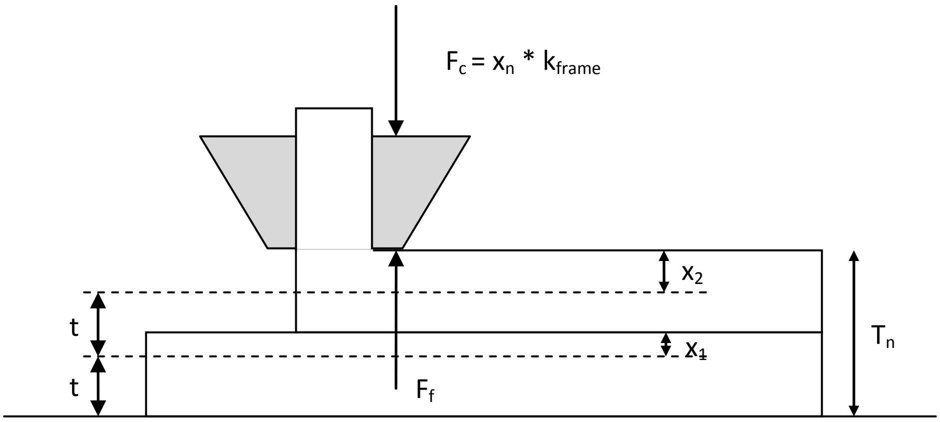


Figure 36: Schematic view layer thickness

Since the consolidation force increases with a larger deflection $x_n$, and the printed trace becomes flatter with increasing consolidation force, the process is stable and $x_n$ converges to a limit. The result will be an constant error $x_n$ after a certain number of layers. Only the first printed layers are affected by the stiffness of the frame. The main criteria for the printer frame is therefore that the stiffness is the same on each location on the print bed and as high as possible.

*2. Possibility to adapt printer firmware*
To add the function of cutting continuous fibres, the firmware of the used printer must be adapted. This is not possible with commercial printers, so only printers with open source firmware are regarded. The printer needs to have the option to communicate with external hardware such as the cutter.

*3. Budget*
The budget of this research was lower than the price of the cheapest available 3D printer. Purchasing a new printer was not an option for this reason.

### 3.2.2 Selection of 3D printer

With respect to the last criterion, only two options remain feasible. The first being the Fab@Home printer, used in the earlier research of T.A. de Bruijn[11]. The second option was a RepRap I3 printer owned by the Working Group on Development Techniques (WOT)[18].

The Fab@Home printer is a design of the Cornell University started in 2006. Currently there is no support or documentation about the firmware anymore, and the website contains mostly dead links. Further it lacks support for the most common CNC file format (*.gcode) and uses its own non documented format. At last the print platform is only supported on one side, resulting in a decreasing stiffness towards the other side. T.A. de Bruijn reported this to yield a variable consolidation force in his setup [3]. Measurement of the stiffness is not obtained.

The RepRap I3 has good maintained and documented open source firmware of which the source code is available and adaptable.  and .gcode file format support. The build platform is spring supported on its four edges, resulting in a more continuous stiffness between printing head and build platform. The stiffness of the frame is measured by inserting a spring with known stiffness (27.5N/m) between nozzle and bed. The uncompressed length of the spring is 30mm. First the bed is levelled, and the nozzle is calibrated. Then nozzle is lifted 30mm above print bed, and is then lowered 10mm with the spring in between. The measured distance from the bed is then 20.5mm, yielding an overall frame stiffness of

$$k_{frame} = \frac{F}{d} = \frac{27.5 \times 9.5 \times 10^{-3}}{0.5 \times 10^{-3}} = 522.5\, N/m$$

For reasons of simplicity, the stiffness is taken as a constant for small deflections (<0.5mm). No significant differences are found for the stiffness on different spots of the print bed.

The RepRap has eight unused I/O pins onboard, which can be used to communicate with external hardware.

For the above mentioned reasons, the RepRap I3 is compliant with the requirements and selected for this research.

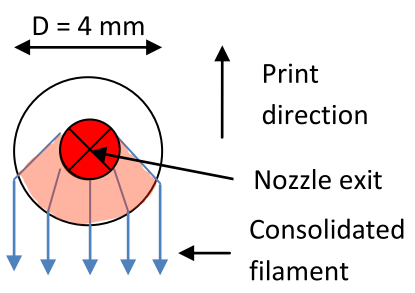


Figure 37: Bottom view of nozzle with filament direction


Figure 38: RepRap Prusa I3

## 3.3 Design of the printing head

The design of the printing head is described in this chapter. The first step in this iterative process is the decision for the location of the drive system for the filament. The two options are pulling the filament after the heating stage, or pushing the filament before the heating stage. The design of the printer nozzle, heater and cutter are totally dependent on that decision.

Pushing of the filament through the heater has major advantages. This further elaborated in Attachment 1. The first step is to determine if such a system would be possible without damaging the fibres or clogging the heater channel. Several small prototypes are built to test this, which are described in Attachment 2. A picture of two tests is given in Figure 39 and Figure 40. The outcome of these tests prove that pushing of filament through a heater is possible without clogging the heater channel or damaging the filament.

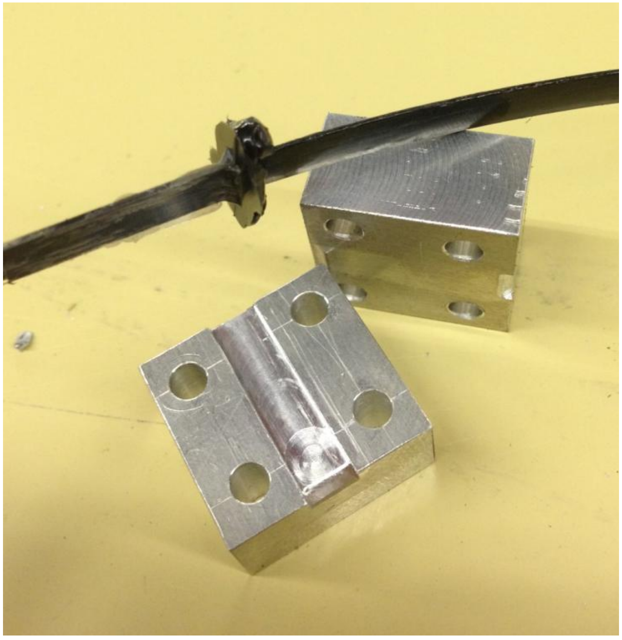

**Figure 39: Test with manual pushing filament through heater**

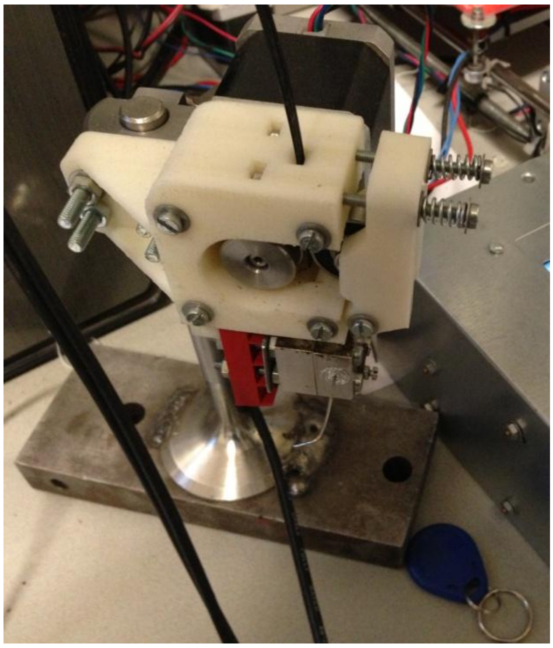

**Figure 40: Motorized pushing of filament through heater**

Based on this outcome the functions of the printing head are given in Table 2. Each function yields its own sub design and is described in the next sub chapters.

| Subject | Functions | control system | defines | dependant on |
|---|---|---|---|---|
| **Printing head** | | | | |
| | Heating filament | Heating control | T | |
| | Placing/consolidate (melted) filament | | - | x, y, z, $k_{frame}$ |

Table 3: Functions of the printing head

### 3.3.1 Placing and consolidation of filament

A cross section of the nozzle is given in Figure 41.

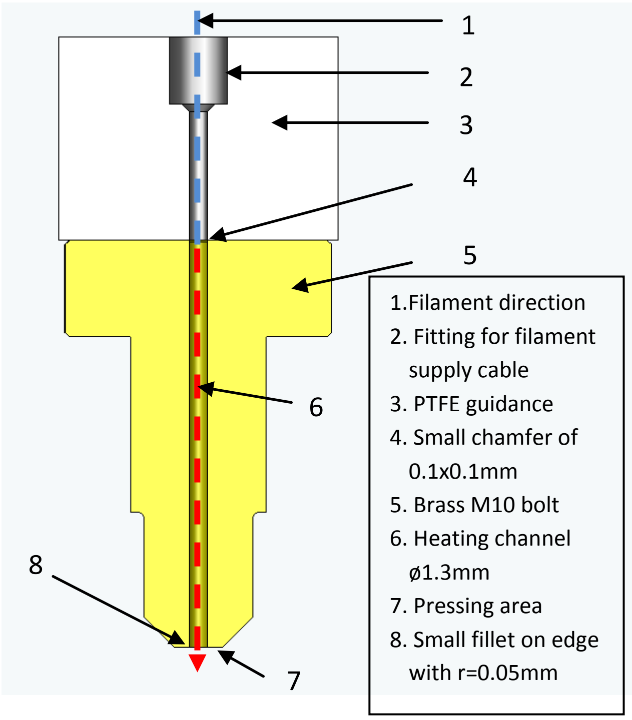


Figure 41: Cross section of nozzle

The placement of filament is done by a heated nozzle, which is very similar to the mould that is used for the pultrusion process (See Chapter 2.2.1.1). It is made from a brass M10 bolt, with a PTFE guidance at the entrance. The channel through the nozzle and the guidance have the same diameter of the consolidated filament, 1.3mm. The exit of the nozzle is chamfered to act as a slider for consolidating the filament onto the print.

### 3.3.2 Heating of filament

Heating of the nozzle is done by two resistors of 6.8Ω/3W through an aluminium block. The block has a hole with M10 thread to fit the nozzle. The block is connected to the frame by PEEK spacers to avoid heat transfer. A cross section of the heater block is given in Figure 42 and Figure 43.

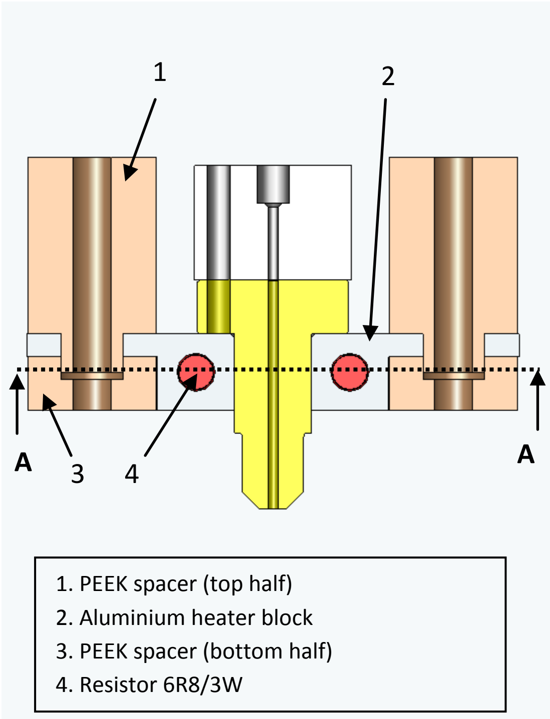


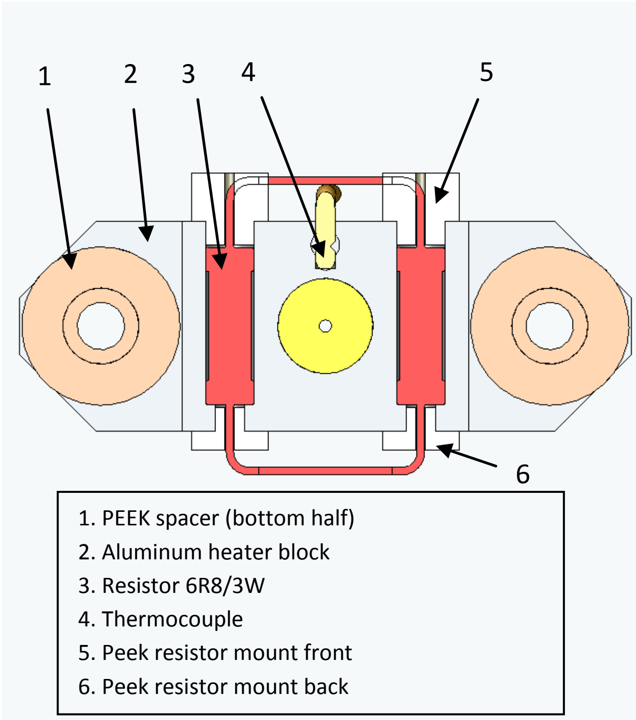


**Figure 42: Cross section print head**

**Figure 43: Cross section A-A print head**

The frame on which the heater with nozzle is mounted is FDM printed from ABS. Mounting holes are compatible with the standard RepRap printing head, so it can easily be interchanged. A drawing of the setup and the actual built printing head are given in Figure 44 and Figure 45 respectively.

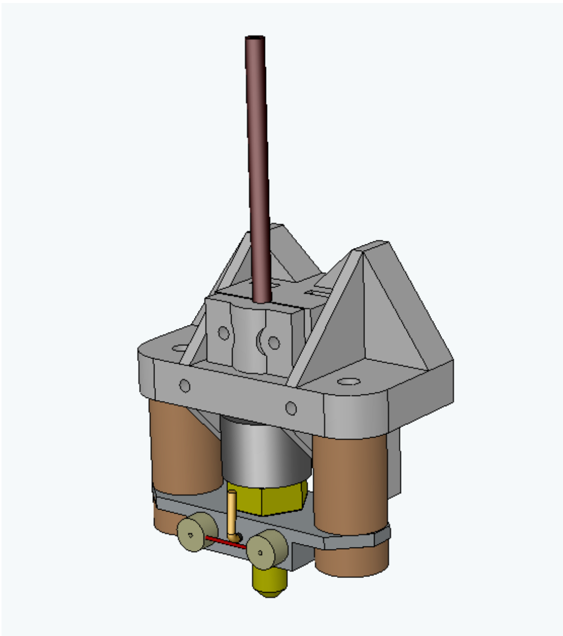

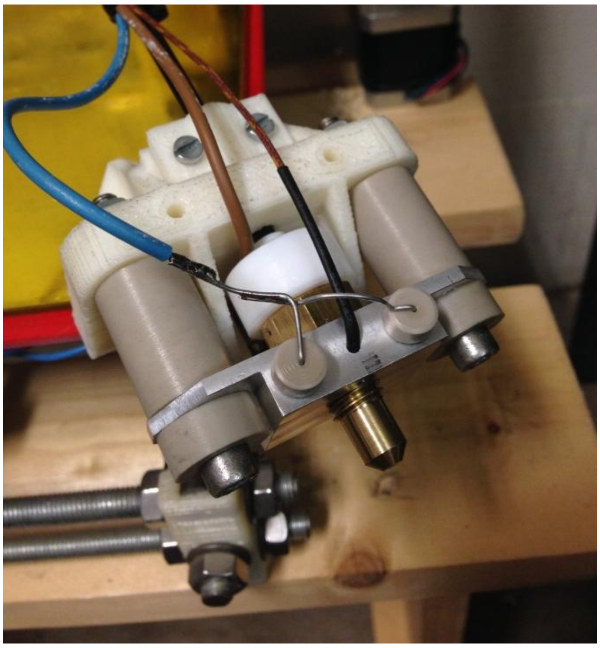

**Figure 44: Drawing of print head**

**Figure 45: Built printing head**

## 3.4 Filament transport system

This chapter describes the design of the drive system that feeds the consolidated filament to the printer head. To avoid the weight of the drive system on the printing head, a cable system is selected. The drive system can then be mounted apart from the printer. A 90 mm long PTFE lined Shimano index shifting cable is used. It has a internal diameter of 2mm, and does not elongate under tensile loads.

The force required to push the filament through the nozzle is estimated after several experiments to be approximately 5N, depending on the speed. This is much lower than the force for the pultrusion process. A simple stepper motor is used to drive a grooved wheel (ø16mm). The groove is made with an angle of 60°, and a depth of 1.3 mm. A ABEC 9 ball bearing (608-2RS) is used to press the filament to the drive wheel. The force can be adjusted with a spring tensioner. A drawing of the system is given in Figure 46, the built system is given in Figure 47.

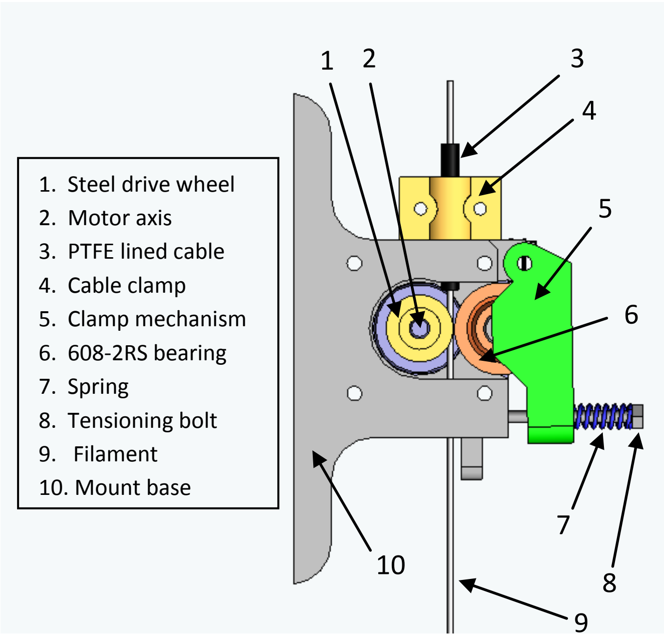


Figure 46: Drawing of filament transport system

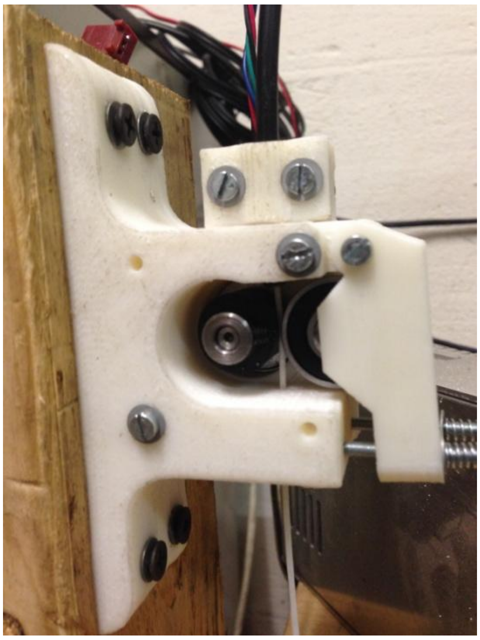

Figure 47: Built system for filament transport

## 3.5 Total design

The described hardware from the previous sub chapter is with the control system of Chapter 2.2.1.5 and normal printer firmware already capable of putting traces of filament on the print bed. The code for printing must be created manually, since normally created gcode files are not directly compatible for continuous fibre reinforced filament. Bonding between layers appears to be sufficient, since manually breaking of printed samples do not show interlaminar shear fracture. An extended study on physical characteristics of several printed samples is done in Chapter 6. A picture of the printer is given in Figure 48.

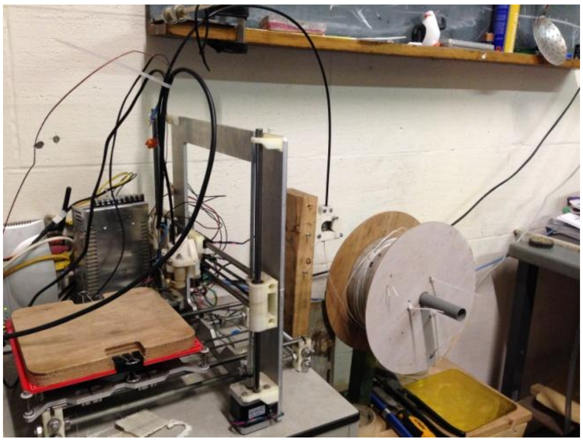

Figure 48: RepRap Prusa I3 with CFRF head

Figure 49: Printed samples with continuous fibres without cutting

### 3.5.1 Evaluation of design

A few remarks are given on the created design after completion of several test parts. They are summarised below.

- Two printed samples are given in Figure 49. It can be noted that small radii (r=2.55mm) are possible to print, but yield interesting tow steering defects which are generally not seen in ATL processes[5]. The fibres rotate around the length axis of the filament. While doing so, they protrude slightly out of the printed surface.
- The connection of the PTFE guidance and brass nozzle is not leakage proof. This is because the PTFE is too weak to bolt tightly on the brass. An improved clamping between these two parts is created with a metal ring (See Figure 52), but this did only decrease the rate of leaking. A picture of leaking is given in Figure 50, where the guidance is removed. The fibre fraction in the printed parts is therefore slightly higher than the specified fraction for the commingled yarn of the manufacturer.
- If the hole alignment of the PTFE guidance and the brass nozzle is not accurately manufactured, fibres tend to crack at the transition area. A picture of a removed filament is given in Figure 51. Damaged fibres can be seen at the transition area of guidance and nozzle. The best way to align the two parts is tightening them with a drill stem of the nominal diameter (1.3mm) inside.

Figure 50: Leaking of guidance-nozzle connection

Figure 51: Damaging of fibres due to misalignment

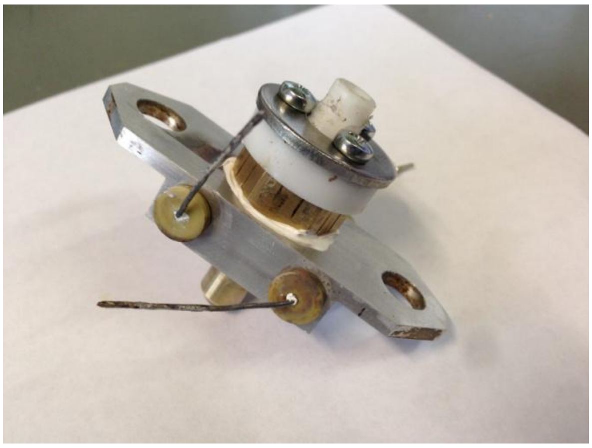

Figure 52: Improvement of nozzle design

## 3.6 Conclusions

During the research it is shown that pushing of the fibre reinforced filament through a heated nozzle is a feasible option for the CFRF printing process.

A working nozzle, designed for printing filament with fibre reinforcement, has been created during the research described in this chapter. Printing with the nozzle is successfully done and some test parts are printed. The printed samples appear to be consolidated, but further tests will be done after designing the cutter and appropriate software. Manually typing Gcode files is quite labour intensive, so only a few products are created during this stage.

Leaking of matrix material occurs during printing at the connection of the hot nozzle and the guidance. This is caused by deformation of the PTFE element, which becomes weaker at temperatures around 200°C. An improvement on the clamping has been designed (See Figure 52), which decreased the leaking of polypropylene, but it has not stopped totally. The amount of leakage will be evaluated in Chapter 6.2.

# 4 Design of cutting mechanism

This chapter describes the design of the cutting mechanism for continuous fibre reinforced filament. First the specific requirements for this sub design are given. The next sub chapter describes a number of options for the cutting mechanism and the selection. Then the final design is discussed, including the mechanic, electronic and software design. At the end of this chapter a conclusion is given with respect to the requirements.

## 4.1 Requirements

The cutting mechanism will be placed after the heated nozzle. The requirements of the cutting mechanism are discussed below.

*Total segregation of fibres.*
All the fibres in the filament need to be cut in order for the print head to move to a new spot. When some fibres remain intact, the print head will remain bonded to the print, the stepper motors will slip and the head will lose its calibrated position.

*Flush cut*
The cutting device must be able to cut directly at the surface of the print. No rest volume is allowed to remain on the print after cutting. This would influence the height and compression of the next layer.

*Lifetime*
The lifetime of the cutter setup needs to be a reasonable time span. It is estimated that a lifetime of 10.000 cuts before maintenance is sufficient. With an average cut length of 100mm, it will work for 1km of filament, or be used to print 1.870kg of composite material. This is estimated to be sufficient for the current study.

*Communication interface*
Communication between the printer firmware and the cutter software is required, in order to fulfil the overall requirement of the system being capable of autonomous production.

*Budget*
The budget of the cutting mechanism is approximately 100 euro.

## 4.2 Selection of technology

This sub chapter describes the selection for the type of cutting technology to be used, and how it can be actuated. The next sub chapter will discuss the design of the cutter.

### 4.2.1 Cutting mechanisms

Several options to cut the glass fibre filament are given in the overview below. The advantages and disadvantages are discussed. In the next sub chapter a selection for the cutting technology is made.

**1. Ultrasonic knife**
This technique utilises sharp carbide blades that oscillate with a frequency between 20kHz and 40kHz and an amplitude around 50 µm. A variety of materials can be cut with a relative small cutting force and almost no sticking to the blade. This is the most preferred option, and is widely used in ATL

machines to cut carbon and glass fibre reinforced tapes. An example of a ultrasonic cutting hand device from manufacturer SonoTec is given in Figure 53.

**2. Automatic composite scissors**
Motorised scissors are widely used to cut fibre reinforced fabrics in manual layup processes. They have special treated cutting blades to avoid wear by the hard reinforcement fibres. Blades overlap during cutting like normal scissors.

**3. Wire cutter**
Several manual cutters are suitable for glass fibre reinforced materials. They have blades that do not overlap during cutting, which allows them to cut close on a surface (flush cut). They can be automated with an actuator. Many cutters are available that have no specifications about the hardness of the blades.

**4. Laser**
A focussed laser can be used to cut the filament. It does not require physical contact which is regarded as a benefit.

**5. Grinding disc**
A fast spinning grinding disc can be used to cut filaments, but will easily be polluted by the melted thermoplastic matrix.

Figure 53: Ultra sonic cutter SF-8541RR by SonoTec

Figure 54: Wire cutter TRE-03-NB by Piergiacomi

### 4.2.2 Selection of cutting mechanism

The mentioned cutting mechanisms are evaluated with the requirements. Apart from the price, the ultrasonic cutter seems to be the best option. It can produce a flush cut, without material sticking to the blade or pressing hard against the material. However, prices range from 500€ and are therefore outside the budget.

This is also the case for a >50W laser. Further the laser will leave burned residue at the cut ends and produce unhealthy gasses. These need to be filtered or abducted, increasing the costs. At last all kinds of eye protection needs to be installed. A laser is for that reason not preferred.

The automated scissors are not selected to use since they cannot cut close to flat surface, the minimal distance is one time the blade thickness. They are mainly designed for cutting woven fabrics, where a flush cut is not important. Further they have the tendency to push thick material out of the scissors because of the relative large angle between the blades during cutting.

A simple wire cutter is the preferred option that falls within the budget. It can produce a flush cut and will not push material out of the blades since they approach each other with a relative small angle. A cheap electronic wire cutter is chosen, produced by Piergiagcomi (See Figure 54). Specifications of the hardening and/or tempering are not supplied, but the steel is hardened to a high degree. Drilling in the metal is therefore not possible.

## 4.3 Actuation

The selected cutter needs to be actuated in two directions. First it needs to be moved to the right position under the nozzle, secondly the cutter needs to be closed in order to cut. Since the cutter is located at the printing head, an important design factor is the weight. First the actuation of the cutter is discussed. Then the movement to the correct position is described.

### 4.3.1 Cutting

First a few measurements are done to estimate the required torque to operate the cutter. This is done by fixing one end in a vice, and placing an increasing weight on a specified location of the other half, up to the point where an inserted filament is cut. For two specified locations of filament between the blades the results are given in Figure 55.

| Location filament from centre | Location of applied weight from centre | Weight | Displacement of weight | Cutting force on blades | Torque |
|---|---|---|---|---|---|
| 12 mm | 80 mm | 1.50 kg | 8.7 mm | 98 N | 1.18 N·m |
| 15 mm | 80 mm | 1.80 kg | 6.9 mm | 94 N | 1.41 N·m |

Figure 55: Measured cutting force and torque

Based on the required torque, several ways to actuate the cutter are given in the next sub chapter

#### *4.3.1.1 Actuation mechanism for cutting*

A short overview of actuation mechanisms for the cutting tool are given in the list below.

**1. Motor with eccentric**

A large slow rotating motor can be used with an eccentric to create a tensioning force. This construction is not necessarily built on the printing head. The force can be transported by a Bowden cable to the head with the cutter

**2. Solenoid**

A solenoid can be used to exert the required force on the cutter. This type of actuator can easily be operated with a PWM signal, allowing to change the exerted force. Also the exerted work can be dosed by adjusting the duration of the signal. The weight of a solenoid might be too high for direct mounting on the print head, since it contains a lot of copper wire and a soft iron core. Suitable solenoids weigh around 200 grams.

**3. Servo motor with eccentric**
Servo motors are generally very lightweight, since they use a very large gear ratio. An advantage is the included closed loop control system with position feedback, so minimal control is required to operate it. Suitable servo motors weigh around 90 grams.

#### 4.3.1.2 Selection of cutting actuator
The first option with a large motor with an eccentric might work well. An option would be to use a car shield wiper motor, which has already a gearbox included and does rotate at a suitable speed. It is however difficult to dose the exerted force. A spring tensioned Bowden cable could be used, but it will snap the blades too hard against each other when the filament is cut. Another option is a position control system, but this is relative difficult to design and would ask for more electronics. This option is therefore not selected.

Both the servo motor and the solenoid are expected to perform well on the cutting mechanism. The solenoid is slightly more difficult to control than the servo motor, since it needs additional electronics components. Further is the solenoid slightly heavier, since it contains a large metal core and a lot of copper wire. For that reason a servo motor is selected to operate the cutter. The selected motor is the TowerPro MG995 and has a maximum torque of 98N·cm. It has metal gears and ball bearings on the outgoing axis and weighs 55 grams.

#### 4.3.1.3 Design of actuation system
The design for a cutting actuation system with a servo motor is given in Figure 56. It features a small arm on the motor. Between the motor arm and the cutter arm a link is inserted.

The arm on the motor axis is 8mm, and the distance from the cutter axis is 90mm. The resulting cutting torque is calculated to be 11N·m, which is more than enough to cut the filament. However, after a test cycle of 250 cuts, the servo stopped working. It appeared that a position controlled system was not necessarily the best option. The servo could easily be controlled to a position further than the closed position of the cutter, resulting in a very high load on the motor axle. This has probably contributed to the short lifetime of the servo.

Figure 56: Servo motor for cutting (TowerPro MG995)

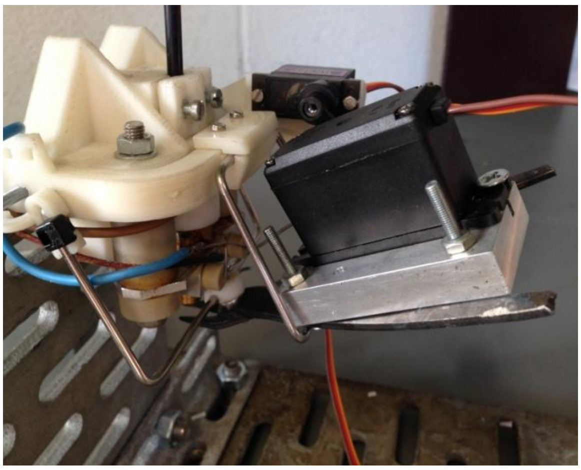

Figure 57: Test setup 1 with servo cutting

To avoid this to happen again with a different servo motor, the option with a solenoid is built. It is slightly heavier (181gr), but has no parts that wear easily. If the solenoid turns out to be too heavy for the printing head, it can always be used in combination with a Bowden cable. The selected solenoid is an Intertec ITS-LZ 2560-Z-6VDC (order nr:503148 at Conrad.nl). The characteristics are given in Figure 58. When powered on 12V DC, the 20W curve is applicable. The solenoid is mounted on the cutter at a 90mm distance from its hinge point, so it can apply a cutting moment ranging from 0.7N·m (blades open) to 1.9 N·m (blades closed). The solenoid mount and the connection to the hinge is welded onto the cutter. Only one half of the cutter is moving, the other half is connected to the movement mechanism. Since machining in the hardened steel of the cutter was not possible, two pieces of metal are welded onto it. One is for mounting the solenoid, the other metal is designed for the connection with the printer head. A drawing is given in Figure 59.

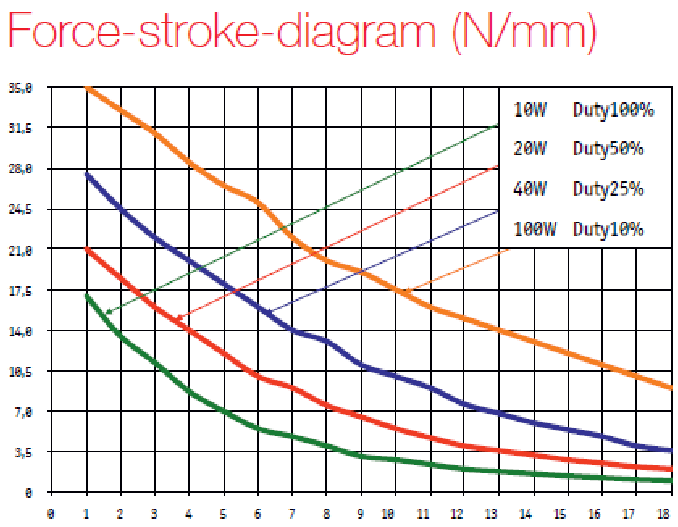


Figure 58: Characteristics of solenoid ITS-LZ 2560-Z-6VDC

Figure 59: Drawing of solenoid mounting

### 4.3.2 Movement

The designed movement mechanism is based on a parallel system, with unequal arm lengths. This causes the weight of the solenoid to remain on the same height (See Figure 60). The movement of the cutter does not require much force for that reason. A small 14 gram servo motor (TowerPro MG90S) with a maximum torque of 22N·cm is selected to move the mechanism for its ability to be position controlled. All the components are assembled on a frame that can be easily placed on- and removed from the existing printing head (See Figure 61).

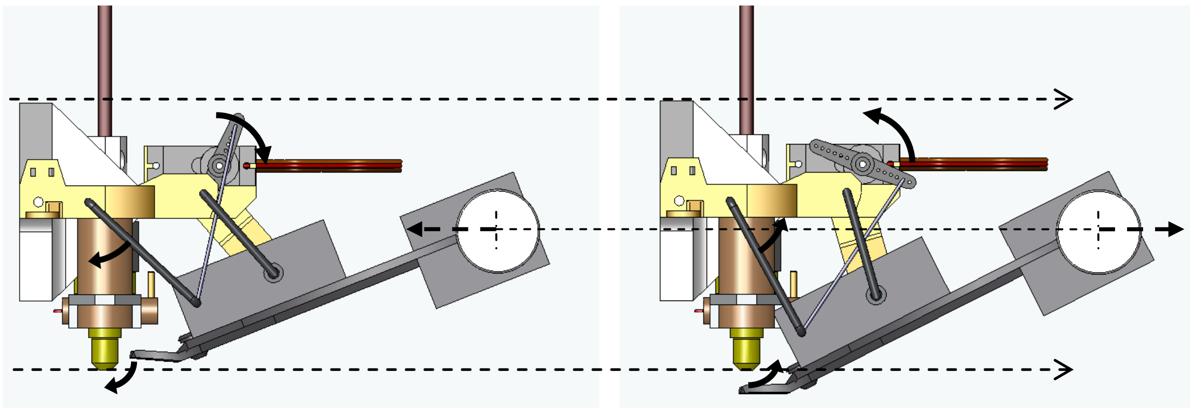

Figure 60: Movement of cutter (up and down position)

To ensure that the cutter is moved to the exact right position under the printing nozzle, left and right positioning can be adjusted with a bolt. A higher and lower position under the nozzle can be adjusted by the motor. A drawing of the printing head with included cutter is given in Figure 61. For a better understanding of the shape of the cutting mechanism, please see the SolidWorks files included with this report.

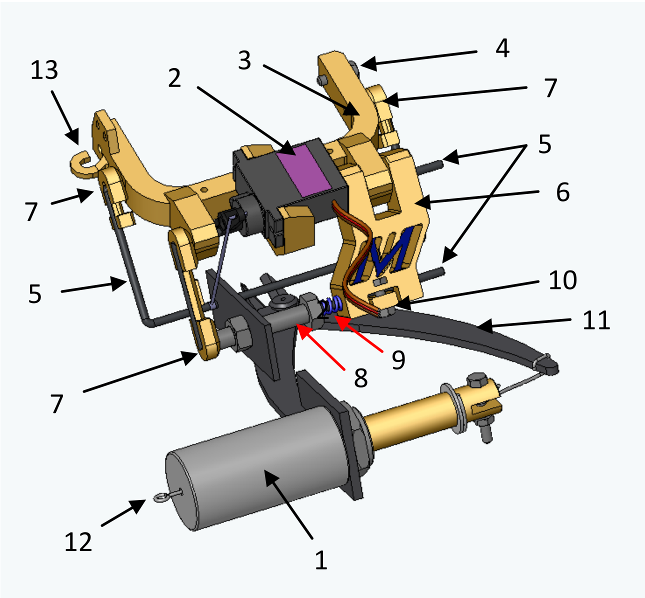

1. Solenoid (Intertec ITS-LZ 2560-Z-6VDC)
2. Servo (TowerPro MG90S)
3. ABS frame
4. Press connection to print head
5. Stainless steel arm
6. ABS arm
7. ABS corner spacer
8. Left/Right adjustment bolt
9. Spring tensioner
10. Integrated arm clamp
11. Wire cutter (TRE-03-NB)
12. Solenoid opening limiter
13. Integrated cable clamp

Figure 61: Drawing of cutter assembly

## 4.4 Final design

The built cutter is given in Figure 62. A drawing of the print head with cutter is given in Figure 63. A repetitive test is performed with 250 cycles of extruding and cutting. No decrease in performance is noticed during this test.

The print head including the cutter can be mounted on the RepRap I3, and simple shapes can be printed. The cutter can make a flush cut on the printed surface.

Operation of the cutter initially done by pausing the printing process and manually push a button to actuate the solenoid. A more advanced control system and its electronics are described in the next chapter.  Some notes on the installation and operation are given in the next sub chapter.

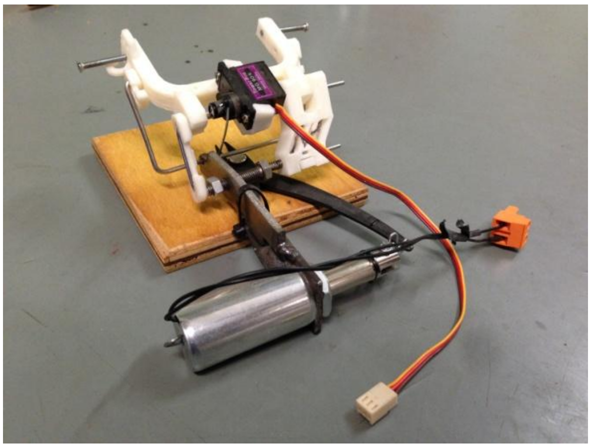

Figure 62: Built cutter assembly

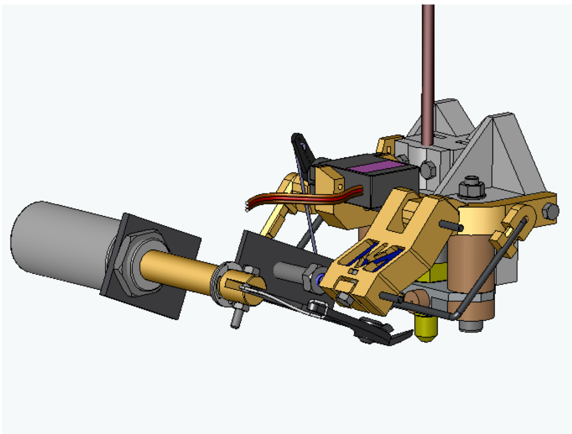

Figure 63: Drawing of print head with cutter

### 4.4.1 Evaluation of cutter design

Some remarks can be made on the design that are important for correct functioning. They are listed below.

- The solenoid is powerful enough to actuate the cutter, as can be deducted from Figure 58. During a test setup with 250 cycles, it performed well. After installation on the RepRap frame, longer and thinner cables were used to power the solenoid, and total dissection of fibres was not possible anymore. After measuring, a voltage drop of 3.1V was measured over the cabling and especially the traces on the circuit board and Arduino. This is a relative large portion of the supplied 12V. The cables were replaced and traces on the circuit board resoldered with AWG 18 copper wire, which solved the problem. The measured voltage over the solenoid during action is 10.8V, which is sufficient for cutting.
- After several cutting actions without filament between the blades of the cutter (to solve the previous issue), another problem arose. Without any significant resistance, the blades are bouncing very fast onto each other, causing them to become blunt very fast. Cutting with dull blades requires a significant higher force, which the solenoid could not deliver. The blades were easily sharpened with a wet grinding stone. The initial sharpness of the blades is not achieved, but cutting was possible again. Measurements on the required cutting force are performed by clamping one handle in the vice, inserting a piece of filament in the cutter and raise a weight on the other handle. The amount of weight at which the filament is cut is given in Table 4 for the three scenarios.

| **Location filament from centre** | **Location of applied weight from centre** | **Weight** | **Displacement of weight** | **Cutting force on blades** | **Torque** |
|---|---|---|---|---|---|
| ***Initially*** | | | | | |
| 12 mm | 80 mm | 1.50 kg | 8.7 mm | 98 N | 1.18 N·m |
| 15 mm | 80 mm | 1.80 kg | 6.9 mm | 94 N | 1.41 N·m |
| ***After cutting without filament*** | | | | | |
| 12 mm | 80 mm | 1.8 kg | 8.7 mm | 118 N | 1.41 N·m |
| 15 mm | 80 mm | 3.0 kg | 6.9 mm | 157 N | 2.35 N·m |

| *After sharpening* | | | | | |
|---|---|---|---|---|---|
| 12 mm | 80 mm | 1.7 kg | 8.7 mm | 111 N | 1.33 N·m |
| 15 mm | 80 mm | 2.0 kg | 6.9 mm | 105 N | 1.57 N·m |

Table 4: Measured cutting force and torque before and after sharpening

## 4.5 Conclusion

In this chapter a cutting mechanism is designed that performs good on glass fibre reinforced filament. The requirements of Chapter 4.1 are met. Total segregation of fibres is achieved for over 1000 times during tests and sample printing, without showing any signs of decreases performance. It is noted that operation of the cutter without filament between the blades will reduce the sharpness significantly because of the high speed that is achieved without resistance.

A flush cut on the surface of the print is achieved, so that next layers can be placed without problems. The budget of 100 euro is easily met. The main costs are the solenoid (15€), the servo motor (7.59€) and the wire cutter (4.85€).

Before printing of complex shapes is possible, a control system needs to be designed which automates the cutting operation. This is described in the next chapter.

# 5 Control system design

With the complete hardware, as described in the previous chapters, three steps remain before glass fibre reinforced 3D printing can be realised without manual interference. The cutter needs electronic components to operate, and a program to understand communication with the existing printer. This is described in the first sub chapter. Then the printer firmware needs to be adapted, so it can understand cutting commands in the Gcode files. This is shortly described in the second sub chapter. Then a Gcode generator needs to be created or adapted, so it can detect where to insert cutting commands in the code that is send to the printer. Further the extrusion speed needs to be matched with the movement speed in the Gcode file. This is described in the last sub chapter.

## 5.1 Cutter control system

The base for the control of the cutter is an Atmega 328P-PU on board of an Arduino Uno. This is not strictly necessary, since the RepRap printer is also equipped with an Atmega chip onboard, which has free I/O pins. The choice for a different microcontroller makes it however very easy to perform stand alone tests and to upload different versions of cutter firmware, without uploading the extensive printer firmware each time. A schematic of the electrical circuit is given in Figure 64.

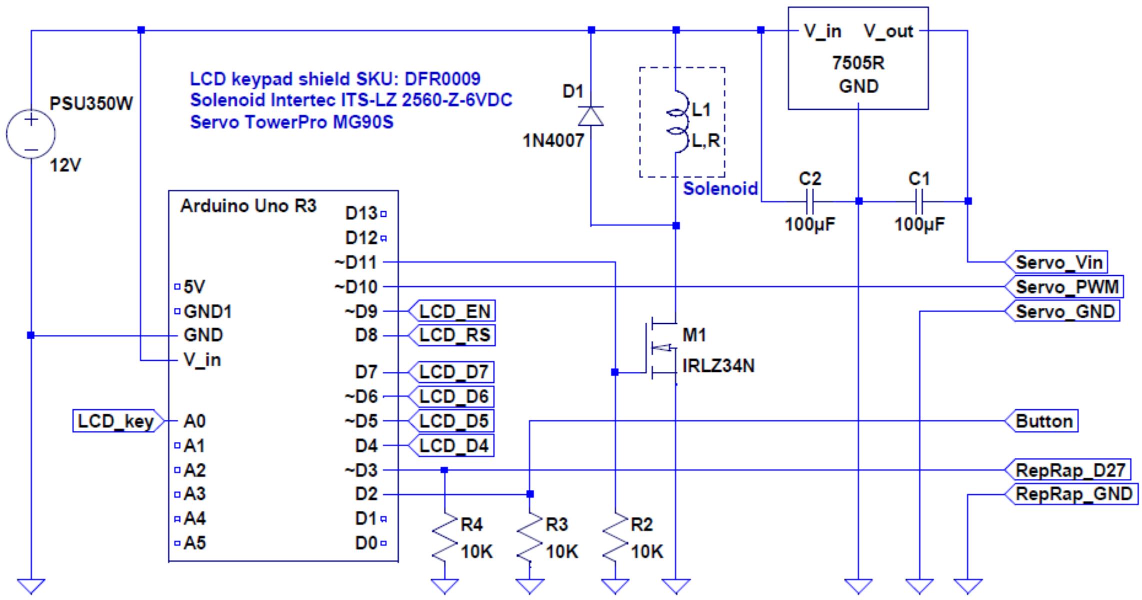


Figure 64: Circuit of cutting mechanism

The actuation of the solenoid is done by power mosfet M1, which can be operated by a logic 5V signal from the Arduino. It can handle the current drawn by the solenoid (approximately 2.5A) easily. A push button is added on port D2 to manually control the cutting action. The servo motor is controlled by a Pulse Width Modulation (PWM) signal, which comes directly from the Arduino (D10). The 5V power for the servo is supplied by a 7805 voltage regulator directly from the 12V input, to avoid overloading the internal Arduino regulator. A display shield with 5 buttons is added, so several variables can be changed and stored in the EEPROM of the Arduino without the need of an external computer. Communication with the RepRap 3D printer is done through port D3, which is set to poll the state of the port with a 1KHz frequency. When a HIGH signal is registered (5V) for longer than 50ms, the software in the Arduino starts the cutting routine. First the servo rotates so that the cutter blades are below the print head. Then the solenoid is actuated for a specified time so the filament is cut. At last the servo rotates back so that the cutter is moved away from the print head . The lower and upper position and the duration of the pulse to the solenoid are configurable through the buttons of the LCD keypad shield. These values are stored in the EEPROM of the Atmega, so they are retained when the power source is disconnected.

The firmware of the printer needs to be programmed to make one of its external I/O pins high when a cutting command is encountered in the Gcode file. This is described in the next chapter. The code for the Arduino is enclosed with the files with this report.

## 5.2 Adaptation of printer Firmware

This sub chapter describes a few modifications to the RepRap printer software.

The current software installed on the printer is Marlin, which is maintained on GitHub [19]. The heart of the printer is a Sanguinololu 1.3a board, equipped with a Atmega 644P microcontroller. Required modifications are that the printer recognizes a new machine code (Mcode) in the Gcode file to start the cutting sequence by putting a signal on one of the extension I/O pins. The sequence of actions to perform between printing two separated lines are: Print line – Move print head up – Send signal to actuate cutter mechanism – Wait for cutting – Retract excess filament – Move print head down – Print line. To maintain flexibility in the behaviour of the printer, all the steps are done in normal Gcode, except the signalling to the cutter mechanism. For this a special function is made that is called when the code M352 is encountered in a Gcode file. The printer will then raise one of the extension pins to 5V. That pin is connected to the cutter control system, which is described in the previous sub chapter. The ground (0V) of both systems needs to be connected as well to achieve similar voltage levels on both systems. The steps of the modifications can be found in Attachment 3.

With the described modifications on the printer firmware, the printer can already understand the cutting command. It will then activate the cutting electronics, which operate the solenoid. The last step that remains is to automatically insert the cutting command in the Gcode during generation. This is described in the next sub chapter.

## 5.3 Gcode generation

In this sub chapter the required alterations for the printer instructions are described. First the normal steps to create this file are described. The typical steps from a CAD model to an instruction file for a 3D printer are listed below.

1. Creation of Surface Tessellation Language (*.STL) file from the designed solid from any CAD program. This file only describes the outside surfaces of the created solids with coordinates of nodes in a triangulated mesh.
2. The described solid of the STL file then needs to be sliced in horizontal layers of the desired printing layer height. Each layer is then converted to linear pathways (traces) that the printer can follow to fill the layer. Each trace has a start and end point and attributes of temperature, velocity and extruded length. Each trace has its own line in a so called Gcode file.

The requirements for the adapted Gcode for the fibre reinforced filament printer are given in the first sub chapter. Two steps are undertaken to print products with only fibre reinforced material in an automated way. The first is a script that runs directly after Gcode creation in Slic3r, a commonly used open source program [20]. This script can be used to process CAD files into printable Gcode with cutting commands. This script is discussed in the second sub chapter. The second script is a way to automatically create printable Gcode for beams that will be used to test the mechanical properties in Chapter 6. This script is discussed in the third sub chapter.

### 5.3.1 Requirements for the Gcode

Ideally, reinforcement fibres in the printed product are aligned in the direction of the main stresses that are imposed. Fibres would only be placed as reinforcement, and the main volume of the product would consist out of the matrix material. This would demand a new way of slicing, where this information can be processed. This is out of the scope of the research because it would be very time consuming. Two steps are taken in this research to print products solely for reinforced material. The requirements for the Gcode are listed below.

**Print speed dependency**

A drawing of the printing process is given in Figure 65.

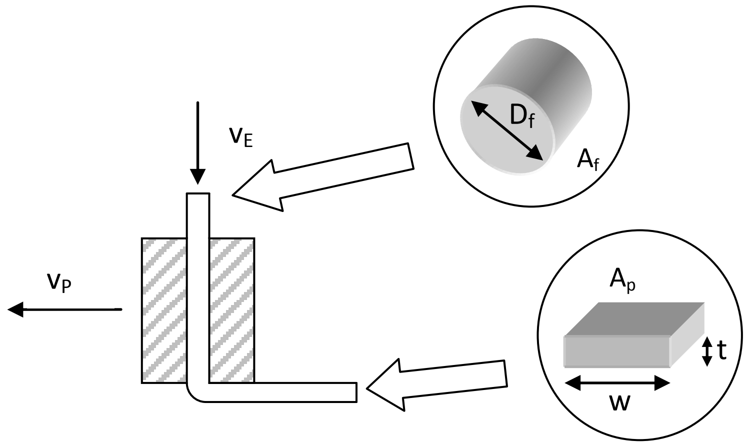


Figure 65: Drawing of print process

Since the glass fibres in the filament cannot be elongated during the printing process, a print speed $v_p$ that equals the extrusion speed $v_E$ is required. This means that the cross sectional area of the ingoing filament equals the cross sectional area of the printed trace. This leads to:

$A_f = A_p$

When w >> t, the printed trace will be flattened in a high degree and a perfect rectangle is assumed. Solved for the width of a printed trace, this leads to:

$$w = \frac{\pi D_f^2}{4t}$$

For a given layer height t of 0.5mm and a diameter D of 1.3mm this yields a trace width w of 2.65mm.

**Insertion of cutting command**

The adapted Gcode also needs to support the cutting before it can move to a new position. Before the actual cutting command 'M352' can be inserted, the print head needs to be lifted to make space for the cutter. To do so without pulling at the filament, the printer needs to extrude in the same speed. The cutting command can then be sent to the cutter electronics, while the printer waits for the cutting to be done. Then the printer needs to retract the extruded filament from the upward move, move down and continue printing. The Gcode for this set of instructions is given below.

```
;CUTTING COMMAND
G91                ; set to relative positioning for all axes
M92 E40            ; calibrate Extruder for upward movement
G1 Z6.5 E6.5 F90   ; lift z while extruding same amount
M352               ; actual cutting command
G4 P6000           ; wait six seconds
G1 E-6.5           ; retract E
G1 Z-6.5           ; lower Z
G90                ; set positioning back to absolute coordinates
;END CUTTING COMMAND
```

### 5.3.2 Script to convert common Gcode

This sub chapter describes a script that is developed to convert an existing Gcode file into adapted Gcode for the current printer. The language for the script is chosen to be Python, to facilitate integration in many open source slicing programs, among which is Slic3r. This is a commonly used program to create Gcode from surface tessellation files. The script accepts a regular Gcode file as input, and gives a converted Gcode file as output. The two main steps are explained below.

***Extrusion speed correction***

The settings for printer configuration are quite extensive in Slic3r. Line width, layer height, infill pattern, etc. However, all configurations will yield automatic calculated extrusion rates that are calculated on required volume to print, which makes total sense for an FDM printer. This means that the extrusion speed is most probably not equal to the movement speed of the print head. Even if the settings for the width, height and extrusion amount are balanced to each other, Slic3r will create Gcode based on volume conservation. This means that it can extrude additional material to fill gaps and interstices between two traces. To remove this and get an extrusion speed that equals the movement speed at all times, the following steps are taken.
The first step in the Python script is to read the Gcode file in, and create vectors for all movements of the printer head. For each printing move, the length of the vector is calculated. This length is then inserted in the in the extrusion command. An example of this conversion step is given below.

| Line | Gcode before conversion | Interpretation |
|---|---|---|
| 1 | G1 X10 Y10 F500 | Move to x= 10mm, y= 10mm with speed 500 |
| 2 | G1 X20 Y10 E9 | Print move to x = 20mm, y= 10mm while extruding 9 mm |
| **Line** | **Gcode after conversion** | **Interpretation** |
| 1 | G1 X10 Y10 F500 | Move to x= 10mm, y= 10mm with speed 500 |
| 2 | G1 X20 Y10 E10 | Print move to x = 20mm , y= 10mm while extruding 10 mm |

This correction of speed is found to work quite well, but only when the printed width and layer height are given as a fixed value in Slic3r. If they are not correctly calculated, the printer will extrude not enough or too much volume to fill in an object after this operation. The relations between extrusion speed, layer height and extruded width are given in Chapter 5.3.1.

***Insert cutting command***

The script also detects where to cut the filament, based on movement pattern from the Gcode file. The criteria for when to insert this command are listed below.

- *Minimal length to go*
  If the printer starts a new print move, the script checks the length to go (according to all criteria). If the length to the next cutting position is smaller the minimal length, it will ignore the line and move to the next position without printing. From empirical testing, 6 mm is found to be printable.
- *Minimal angle*
  The script checks the angle between two connected print traces. If this angle is smaller than the minimal angle, it will insert a cutting command. The minimal angle is set to 120 degrees.
- *Minimal radius*
  Since standard Slic3r Gcode files consists of linear lines only, curves are divided in multiple straight lines. If the lines are short enough, two of those connected lines can have an angle larger than the defined minimal angle. Printing these small radii will however still cause tow steering defects. The script checks for that reason the radius of a rounded corner. If this radius is larger than 6mm, steering defects are found to be minimal. If the radius is larger, the script inserts a cutting command.

Print traces of one layer of a test Gcode file (a wheel) are given in Figure 65. The converted pattern after running the script is given in Figure 66. Green lines are representing non print moves, printed lines are given in black. Blue dots represent the cutting positions.

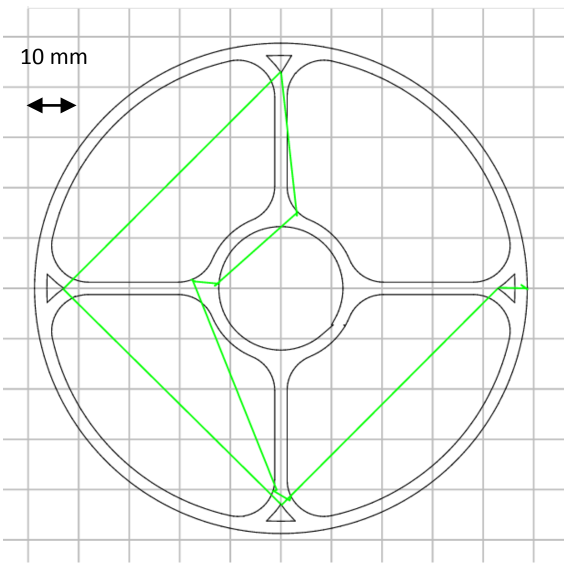


Figure 65: Print traces original Gcode (one layer)

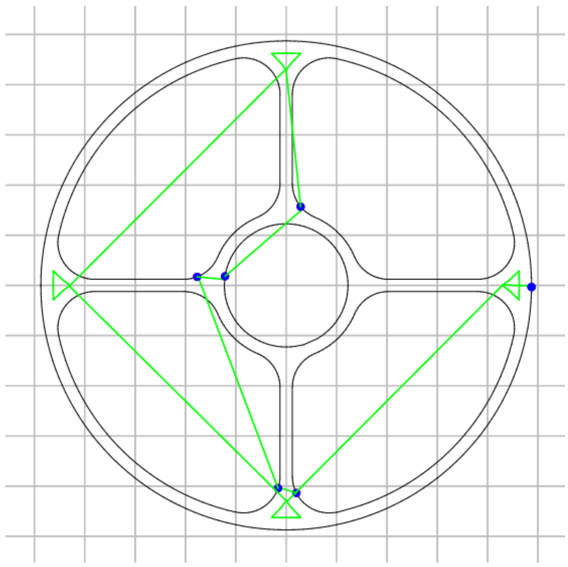

Figure 66: Print traces converted Gcode (one layer)

The full code of the script is included with the files of the report.

### 5.3.3 Script to create test beams

A Python script is written to create Gcode files for simple beams. They are used to obtain test results for bending tests (as described in Chapter 6.4). This script gives full control over all settings such as orientation of printed lines, trace width, layer height and distance between traces. Input for the script are the dimensions of the test beam and the layer height. The script calculates the trace width with the given layer height, assuming  volume conservation. The script can be found with the included files of this report.

# 6 Printed products

To obtain data of the printer specifications, and the properties and quality of the printed products, several tests are performed. The first sub chapter describes the specifications of the printer and the tolerance on the printed samples. The second sub chapter describes the effects of leaked matrix material during pultrusion and printing. Then several samples are studied with a microscope, to see if the printed traces are correctly connected and bonded. This is described in the third sub chapter. The fourth sub chapter describes 3 point bending tests. Obtained data is then compared with given data of the manufacturer. At the end of this chapter an evaluation and conclusion is given about the obtained data during the tests.

## 6.1 Geometric tests

This sub chapter describes the features of the developed printer. The minimal printable dimensions are discussed, together with the accuracy.

***Minimal radius and course length***

From experiments it is determined that a course length of 6 mm is achievable without problems (See Figure 67). A 180° corner with a radius of 2.55 mm is achievable (See Figure 49). The filament will protrude slightly out of the surface of the material. At a radius of 20mm this is not occurring. The fibres in the filament are rotating around the filament length axis during printing of the radius. This causes the matrix material to be squeezed to the outer sides of the printed trace. A microscopic image of this tow steering defect is given in Figure 68 (12.5X) where a printed curve (r = 20mm, t = 0.5mm) is coloured with black ink to show the fibre alignment.

Figure 67: Printed rectangle 6x6x2mm

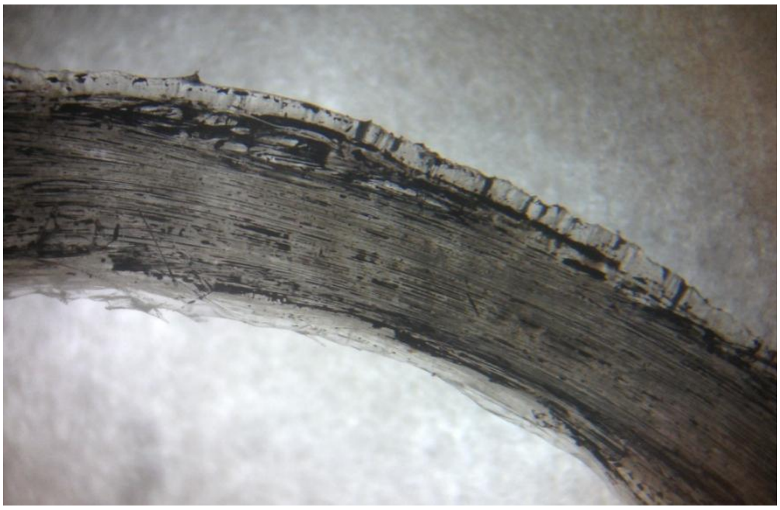

Figure 68: Magnified (12.5x) image of radius (r=20, t=0.5mm)

***Width deviation***

For all printed products, the width is slightly larger than the input parameters for the printer. The difference is mainly caused by printed filament that is squeezed out of the print at the sides. For that reason it is determined by the compression force, and thus the printed layer height. A wavy pattern can be seen on the sides of the printed specimen in Figure 69. Without sanding, the additional width is approximately 1 mm at each side for a printed layer height of 0.5mm. In the middle of a printed area, the lines are fit in space nicely. For that reason it is expected to yield no problems when using two extruders, where one is printing reinforced filament, and one is only printing matrix material.

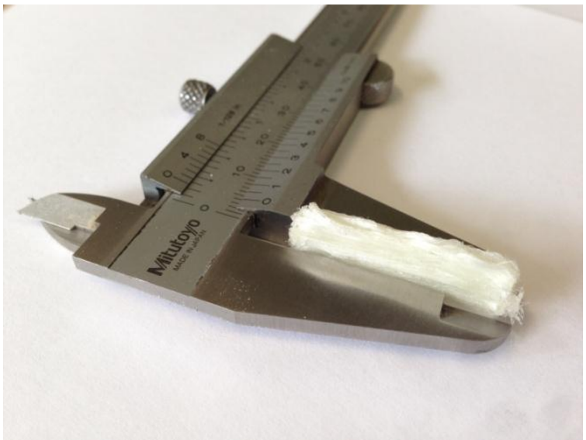

Figure 69: Wavy pattern on upstanding side

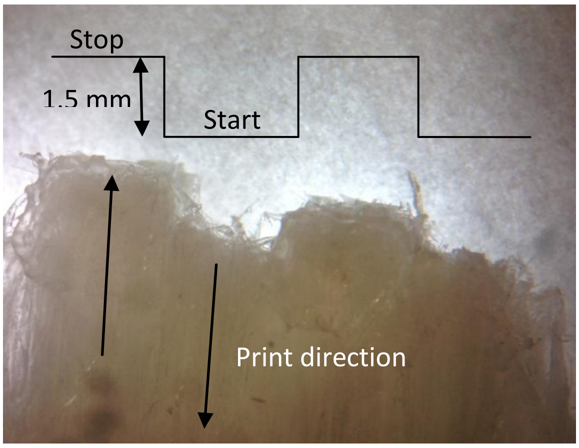


Figure 70: Start - stop behaviour

***Height deviation***

The height of the printed products deviate slightly from the input height. For a layer height of 0.5mm and a product height of 3mm, a deviation of 0.3mm is measured in the middle of a printed surface. Two factors influence this deviation. The first is the levelling of the print bed. This is done according to a general procedure with a paper, as described on the RepRap wiki [21]. It is expected to be accurate within 0.05mm.
The main cause for the height deviation is the stiffness of the printer frame. When the nozzle exerts pressure on the bed, it tends to move slightly upwards because of a low stiffness. Since the stiffness of the frame-nozzle connection is known to be 522.5N/m (see Chapter 3.2.2), a deviation of 0.3 mm implies a force on the printing head of approximately 0.16N. With an estimated surface for consolidation of 7mm$^2$ (See Figure 37) the consolidation pressure during printing is estimated to be 22.8KPa. This is much lower than the lowest reported consolidation pressure of 3.6Mpa for ATL processes [5].

After a few layers, the printer frame will be pre tensioned due to the height deviation. A more stiff printer frame will therefore mainly improve the compression of the first layers.

***Length deviation***

At starting and stopping a small error occurs. Lines in one print direction are shifted with approximately 1.5 mm with respect to lines printed in reversed direction. This can be seen in Figure 70, where a four-trace object is given. The length of each line (when protruding fibres are mildly removed) are matching the input length. This phenomena is mainly caused by a simplification of the created Gcode. The error resulting from that is schematically given in Figure 71, and is close to the diameter of the used filament. It can easily be solved with a new start and end condition in the Gcode generator.

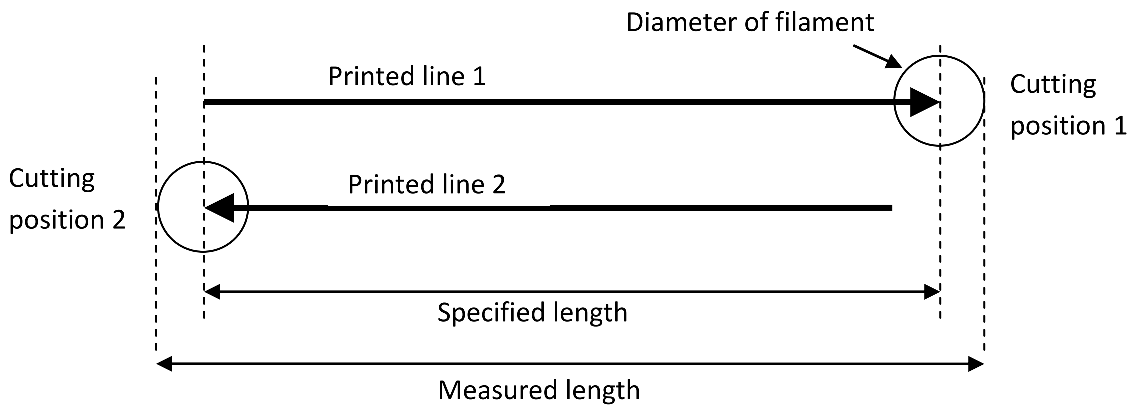


Figure 71: Deviation in print length

***Volume deviation***

Because of the width and height deviation, a larger volume is obtained than expected. The exact volume increase is hard to specify, because the sides of the samples can be somehow irregular. After a bit of sanding, to remove the irregularities and obtain a smooth surface, the printed volume is measured. This is covered in the next chapter, where the mass properties of the samples are evaluated.

### 6.1.1 Conclusion on geometry.

A good forming freedom is achieved with the current setup. Small radii and lengths of respectively 20 and 6 mm are printed without problems.

However, the width and height of the printed samples deviate from ideal width and height with approximately 2 mm and 0.3 mm on printed products of 10 mm by 3 mm. This leads to a higher volume of the printed products than ideally would be filled by the printed material only. The remaining space is therefore expected to be filled with air voids. This will be identified in Chapter 6.3.

## 6.2 Mass properties printed samples

In this sub chapter the mass properties of the printed samples are evaluated. This is important, since some of the matrix material has leaked away during the pultrusion and printing process. Weight measurements are done to quantify the amount of leaked material. The volume fraction of the glass fibres is recalculated in the end of this sub chapter. The used samples for the weight measurements are described in the first sub chapter. The first 8 samples will also be used in the study of the microscopic images.

### 6.2.1 Sample creation

Three variables are expected to have a significant influence on the quality of the printed samples. The temperature, printing velocity and layer height. A higher temperature is lowering the viscosity of the matrix material, making it more easy to press through the nozzle. On the other hand, it will make the bonding pressure lower, since a lower force is required to flatten the filament onto the existing layer. The layer height is expected to have a major influence. This determines in large extend how much pressure will be exerted to press the new line onto the existing print.

A temperature of 200°C, a layer thickness of 0.5mm and a print speed of 60mm/min is taken as the middle point. From there the temperature is varied to 190°C and 210°C. Then the speed is changed to 30mm/min and 120mm/min. At last the layer thickness is changed to 0.4 and 0.6 mm. The steps of the process are given in Figure 72.

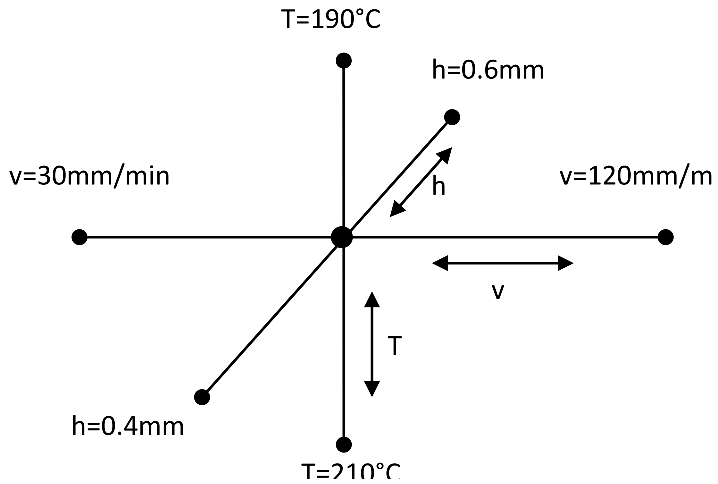


Centre: v = 60mm/min, h = 0.5mm , T = 200°C

Figure 72: Varied process parameters for samples

The specifications of the printed samples are given in Table 5. The 'specifications' of the printed samples are the inserted dimensions in the Gcode beam generator. The 'printed dimensions' are the real printed dimensions, based on a round number of lines and layers. This is automatically calculated by the generator. The ideal weight is calculated according to the given material properties of the comingled yarns of 1870 Tex (gr/km). For each printed sample the weight is measured in a balance to determine the amount of leaked material and the remaining fibre fraction in the product. Further the slightly sanded dimensions of the samples are measured, and the increase of volume is given in the table.

| Nr. | Specifications [Temp @ lxbxh @ layer height @ print speed] | Printed dimensions lxbxh [mm] | Used length of filament [mm] | Measured weight [gr] | Difference [$\%_m$] | Measured volume increase [%] |
|---|---|---|---|---|---|---|
| 1 | 210°C @ 30x10x3 @0.5 mm @ F60 [mm/min] | 30 x 9.98 x 3.0 | 720 | 1.26550 | 6.009 | 3.51 |
| 2 | 200°C @ 30x10x3 @0.5 mm @ F60 [mm/min] | 30 x 9.98 x 3.0 | 720 | 1.26900 | 5.749 | 9.22 |
| 3 | 190°C @ 30x10x3 @0.5 mm @ F60 [mm/min] | 30 x 9.98 x 3.0 | 720 | 1.24830 | 7.286 | -0.20 |
| 4 | 200°C @ 30x10x3 @0.5 mm @F120 [mm/min] | 30 x 9.98 x 3.0 | 720 | 1.25500 | 6.788 | -0.20 |
| 5 | 200°C @ 30x10x3 @0.5 mm @F30 [mm/min] | 30 x 9.98 x 3.0 | 720 | 1.34630 | 0.007 | 10.11 |
| 6 | 200°C @ 30x10x3 @0.4 mm @F60 [mm/min] | 30 x 9.35 x 3.2 | 720 | 1.32100 | 1.887 | 22.88 |

| | | | | | | |
|---|---|---|---|---|---|---|
| 7 | 200°C @ 30x10x3 @0.6 mm @F60 [mm/min] | 30 x 10.39 x 3.0 | 750 | 1.39250 | 0.713 | 7.32 |
| 8 | 200°C @ 30x10x3 @0.8 mm @F60 [mm/min] | 30 x 9.35 x 3.2 | 720 | 1.30820 | 2.837 | 32.04 |
| 9 | 200°C @ 70x10x3 @0.5 mm @F90 (sample 5) | 70 x 9.96 x 3.0 | 1680 | 2.96720 | 5.551 | |
| 10 | 200°C @ 70x14x4 @0.5 mm @F90 (sample 6) | 70 x 14.96 x 4.0 | 3360 | 5.93680 | 5.513 | |

Table 5: Samples for microscopic study

### 6.2.2 Determination of leakage

After measuring the actual weight of the samples, the missing volume fraction of matrix material is calculated according to

$$f_{missing} = \frac{\left(L_{printed} \times TEX \cdot 10^{-6} - m_{measured}\right)}{\rho_{PP}} \frac{1}{V_{extruded}}$$

with

$$V_{extruded} = \frac{L_{printed} \times TEX \cdot 10^{-6}}{\rho_{TwinTex}}$$

where

$f_{missing}$ is the volume fraction of the leaked material with respect to the extruded volume,
$L_{printed}$ is the extruded length of the filament for a sample in m,
TEX is the linear mass of TwinTex, 1780 Tex (gr/km),
$m_{measured}$ is the measured mass of the sample in kg,
$\rho_{pp}$ is the density of the pp matrix material, 909 kg/m$^3$,
$\rho_{TwinTex}$ is the density of the comingled yarn TwinTex, 1500kg/m$^3$.

The results of the missing fraction of matrix material are given in Figure 73.

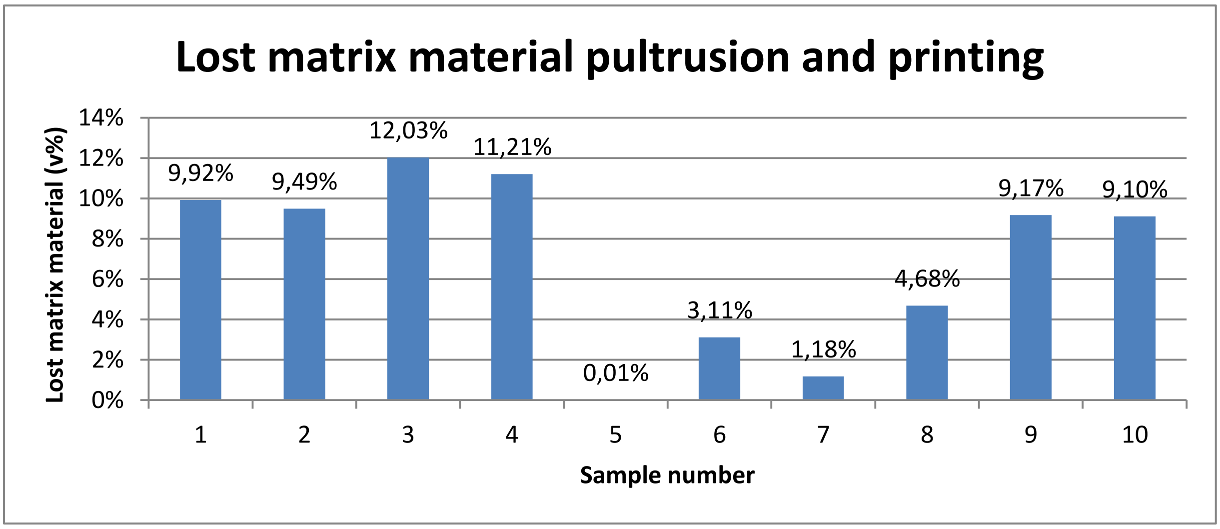


Figure 73: Lost matrix material during process

### 6.2.3 Determination of air voids

The expected amount volume fraction of air voids can be geometrically estimated based on the measured printed volume and the expected volume, where

$$f_{volume} = \frac{V_{measured}}{V_{ideal}} - 1$$

with

$$V_{ideal} = V_{print} - V_{leak}$$

where

$f_{volume}$ = Increased volume fraction
$V_{measured}$ = Measured volume of slightly sanded specimen
$V_{ideal}$ = Ideal volume of printed product
$V_{print}$ = Extruded volume by printer
$V_{leak}$ = Leaked volume during process

The results of the additional volume based on the formula above is plotted for the first eight samples in Figure 74. As can be seen, this volume increase is slightly larger than the measured volume increase of Table 5, since the lost matrix material is discounted in the calculation of $V_{ideal}$.

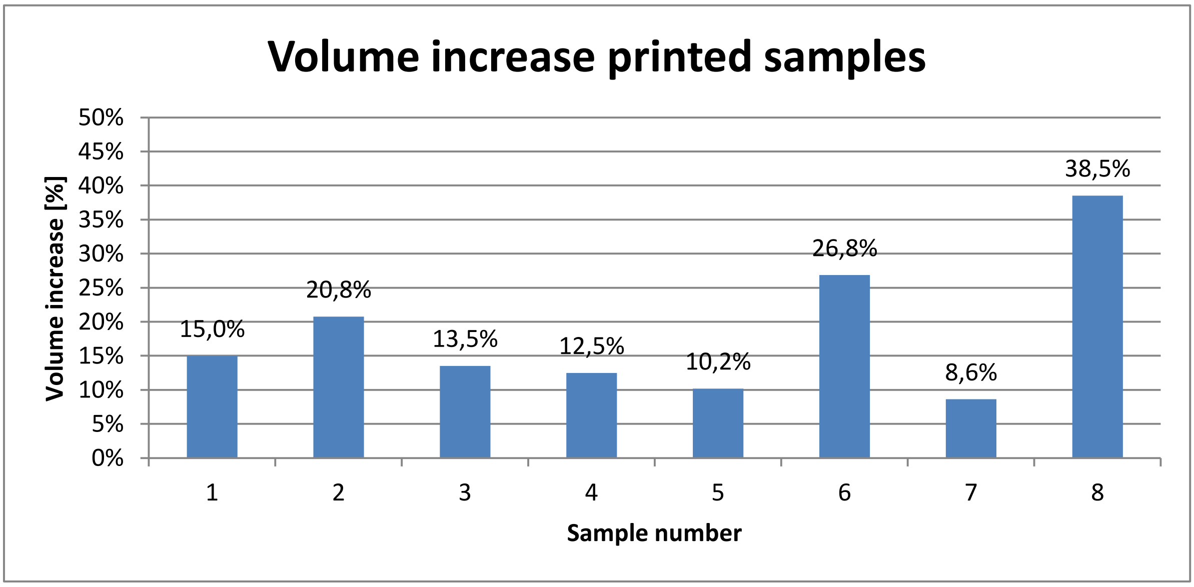


Figure 74: Volume increase printed samples

The average volume increase for all samples is 18.24%. This is expected to be seen in the images of the cross sections, studied in Chapter 6.3. The reliability of the measured sample dimensions is low for the samples with a large volume increase. They have a more irregular surface, which means that it is difficult to measure width and height.

### 6.2.4 Influence of leakage on flexural modulus

From the graph in Figure 73 can be seen that the printed sample 5 appears to have a very low loss of material. This is assumed to be caused by an error in the weighing procedure, since the filament for each sample comes from the same batch. For all printing temperatures of 200°C at a layer height of

0.5mm and a print speed of >60 mm/s, the results are very close. For this group, the average of the percentages is 10.15%$_{(v)}$. It is assumed that this is a reliable assumption for the printed test beams for the three point bending test, which are printed with similar process parameters. The average mass fraction of fibres in the specimen is raised from 60%$_m$ to 63.9%$_m$ and the volume fraction has increased from 34%$_m$ to 37.8%$_m$ by the loss of matrix material. The influence of the fibre volume fraction on the flexural modulus can be calculated with the rule of mixture according to

$$E_{composite} = fE_f + (1-f)E_m$$

where

| | |
|---|---|
| $E_{composite}$ | is the flexural modulus, |
| f | is the volume fraction of the fibres |
| $E_f$ and $E_m$ | are the flexural moduli of the fibres and the matrix material respectively. |

The flexural modulus of the TwinTex material with 60 volume percent E-glass is 26.5GPa according to the manufacturer. The flexural modulus of the PP matrix material is assumed to be 1.52GPa[22]. The modulus of the E-glass is then calculated with the rule of mixture to be 75GPa.

The new flexural modulus of the material after the loss of matrix material is then calculated with

$$E_{new} = 0.378 \times 75 + (1 - 0.378) \times 1.5 = 29.33\ GPa$$

This is an increase of 10.7% with respect to the value of the original material. The printed test beam properties will be compared with this value for the flexural modulus in Chapter 6.4. The increased volume during printing (see Figure 74) is not taken into account for the recalculation of the flexural modulus. The recalculated value is a standard that would be achievable when printing with the given material was done perfectly bonded. Achieved deviations from this value specify therefore the printing process.

## 6.3 Air voids and bonding printed samples

The process to check several samples for air inclusions with microscopic images from cross sections are described in the next sub chapters. Air inclusions influence the bonding between printed layers in a high degree.

The first sub chapter describes the process of preparing the samples for the microscopic images. In the second sub chapter the results of the study are evaluated and compared with the measured volume increase of Chapter 6.2.3.

### 6.3.1 Process of microscope study

To check the bonding between the layers, the samples of Table 5 are prepared for a microscopic study. Each sample is cut in half with a diamond saw and embedded in epoxy. After hardening of about 24 hours, the epoxy at the location of the cross section is sanded (up to P6000) and polished. Microscopic pictures of the cross sections are taken at optical magnifications of 1, 2.5 and 5 times. To be able to quantify the cross sectional area,  the fraction of fibres and the fraction of air voids, a program for analysis of scientific multidimensional image data (ImageJ) is used[23]. The results are given in the next sub chapter.

### 6.3.2 Results and evaluation of microscope study

The evaluation of the microscopic images is done with the open source program ImageJ, which is a powerful tool for analysing microscopic images[23]. It can detect hue, saturation and brightness differences in the images, and select regions with specified boundaries. In this study is used to detect air voids in the cross sections of the samples, which are visually separated by their brightness. This is somehow subjective, since there are brightness differences in the matrix material. For that reason two measurements are taken. The first being the minimal amount of air voids. Only the very clear white spots are regarded here. The second measurement is the maximum estimation. The lighter spots in the matrix material are included as well. The surface of the detected air voids is compared with the surface of the cross section to obtain their volume percentage. An image of sample 2 is given in Figure 75. The same image is processed for minimal and maximal estimations in Figure 76 and Figure 77, where coloured areas are inserted for the air entrapments.

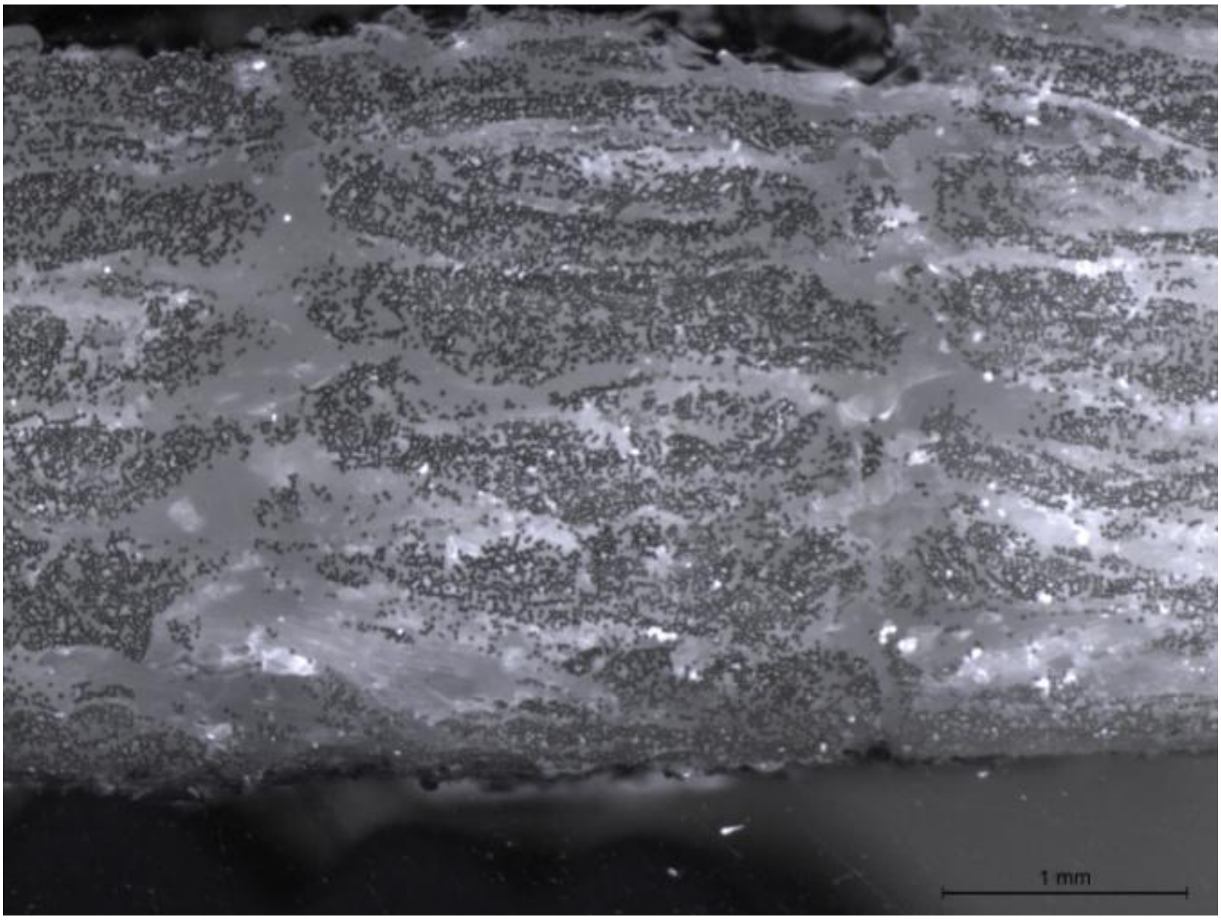


Figure 75: Cross section of sample 2

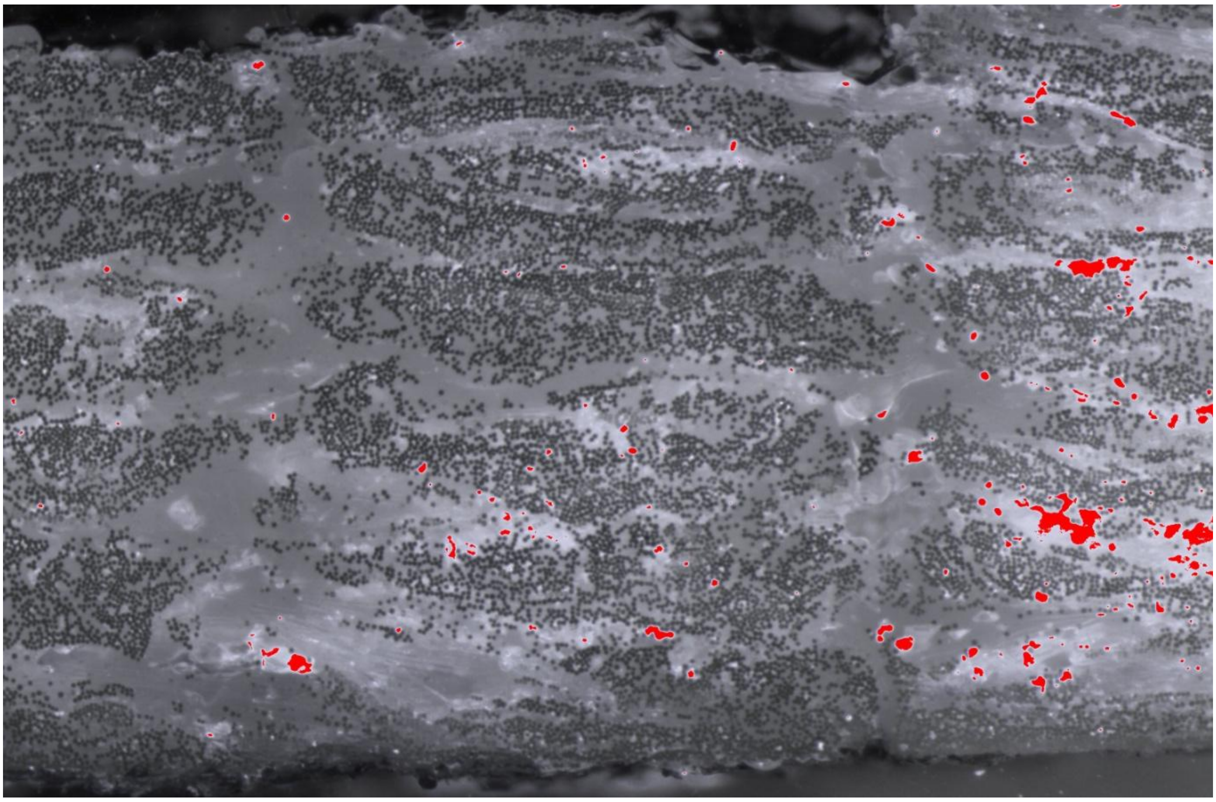

**Figure 76: Processed image of sample 2 with minimal estimation (0.9% air voids)**

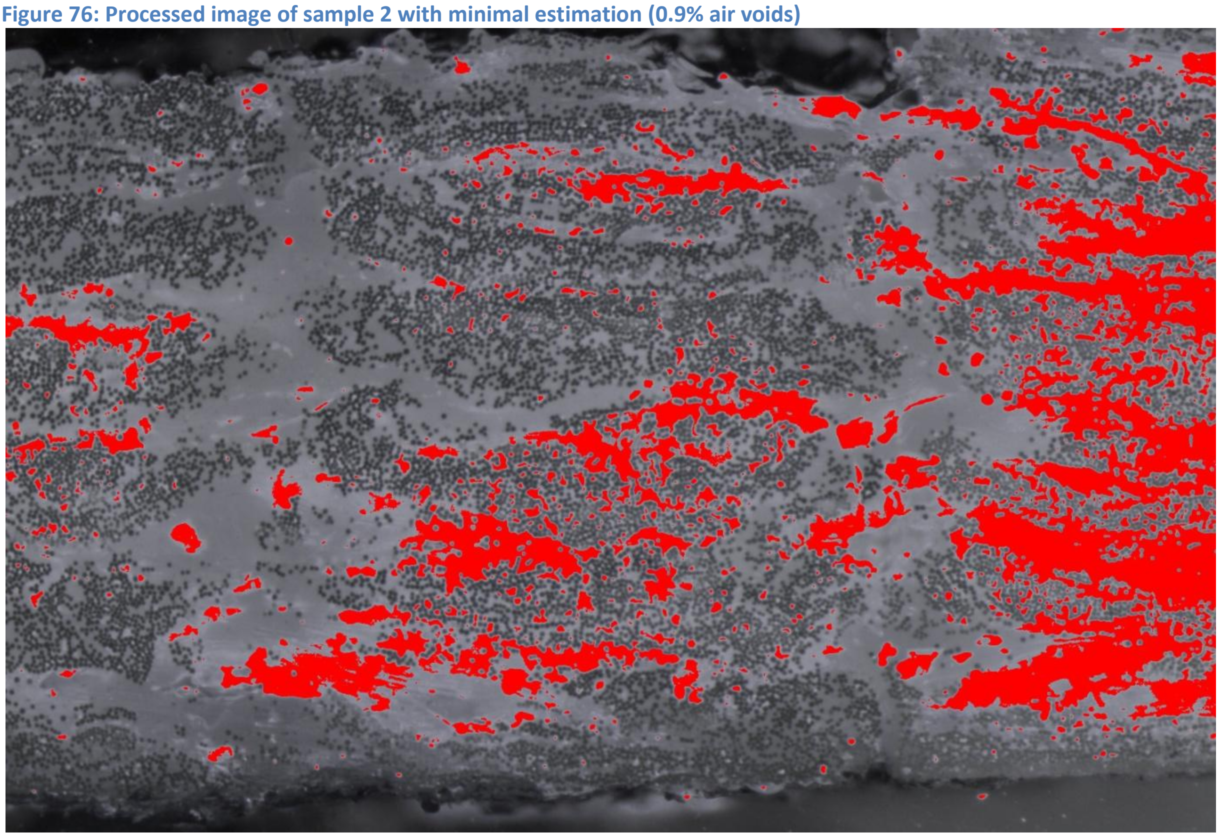

**Figure 77: Processed image of sample 2 with maximal estimation (16.2% air voids)**

As can be seen from the images, the real amount air voids is difficult to estimate based on the images. This is partly because of the light conditions during the recording of the images, and partly because some parts of the images was unusable because of an insufficient polished surface. It is however certain that the actual amount is in between the minimal and maximal estimations.

The resulting minimal and maximal air void concentration based on the analysis is given in Figure 78.

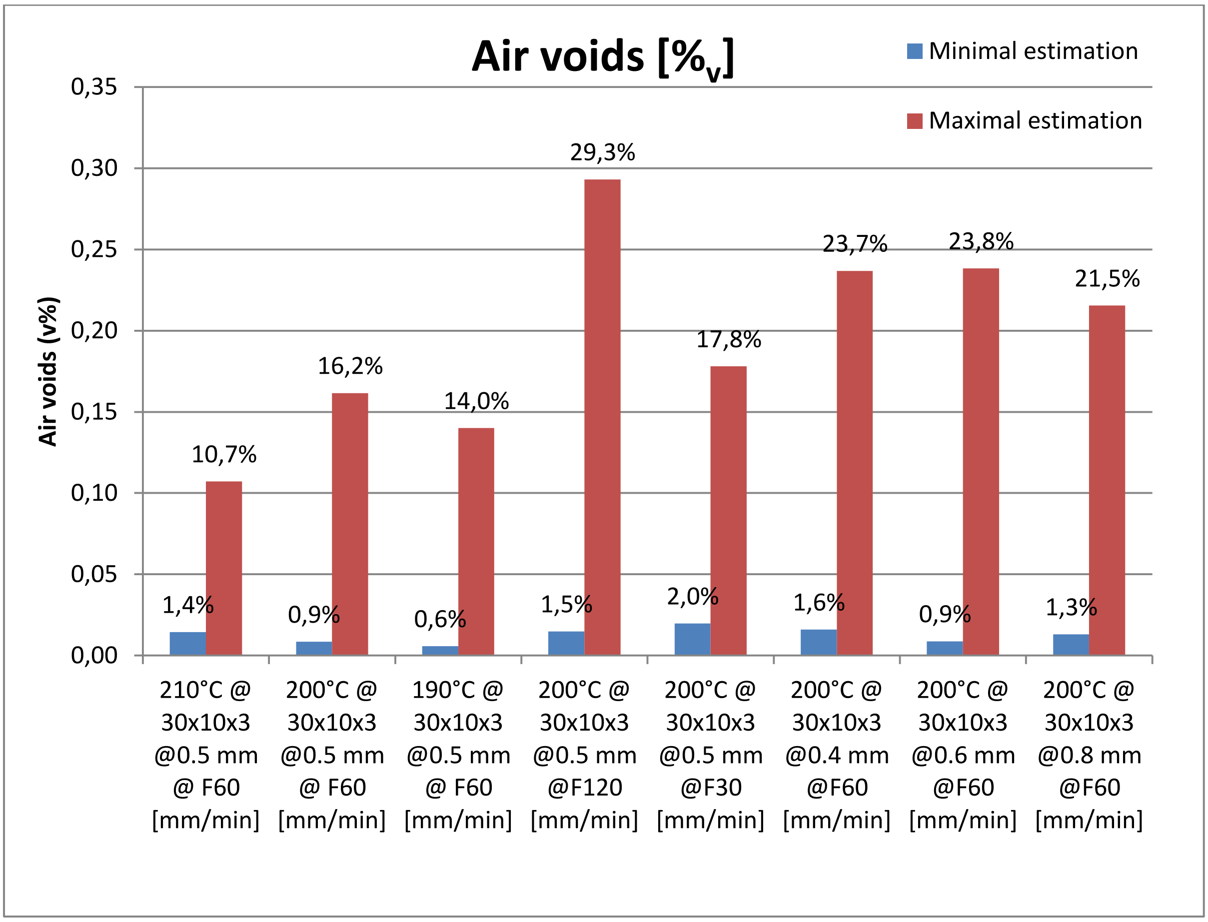


**Figure 78: Percentage of air voids in samples**

Based on Figure 78 it can be stated that the analysis based on the microscopic images is not very reliable, since it depends highly on user interpretation. The minimal average of found air voids is 1.15%, the average maximum is 19.36%. For that reason it cannot be used to establish correlations between process parameters. Since the maximal estimated value is close to the geometrical defined fraction of air voids (see Chapter 6.2.3), this is probably the most reliable result. A new study with a larger sample size and improved microscopic images is however advised to obtain possible relations. Generally printed ABS specimen are found to have an air void content ranging around 10% (See Figure 79).

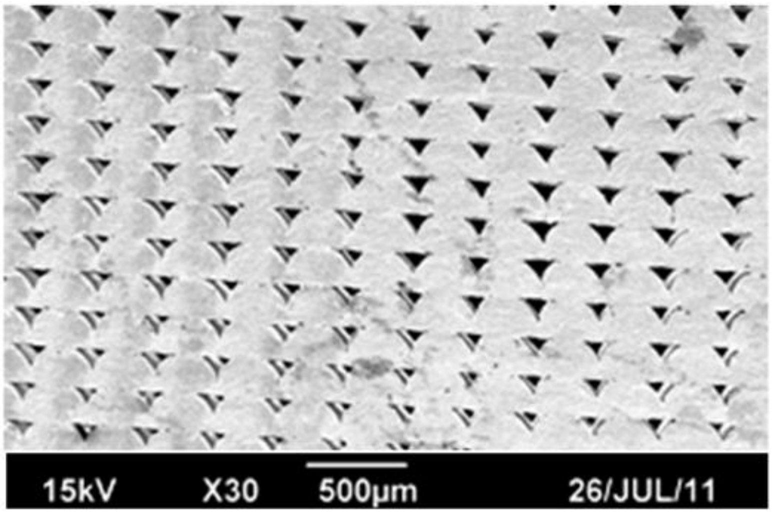


Figure 79: SEM image of air voids in unidirectional FDM printed ABS[24]

Some interesting phenomena can be seen for the current study. A horizontal bonding and a vertical bonding surface is created during printing. For both bondings, air entrapments occur more often at the sides of the printed specimen, where material can easily be pushed away. The bonding areas are schematically represented in Figure 80, where a cross section of a sample is given perpendicular to the printed direction. A few notions on the bondings are made in the following sub chapters.

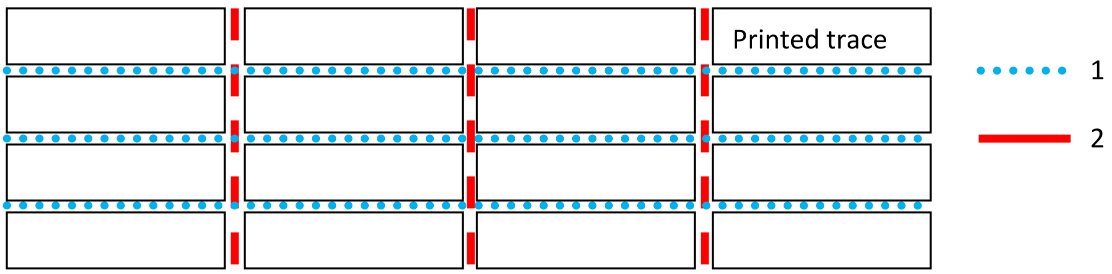


Figure 80: Distinct regions of air voids in cross sections

#### *6.3.2.1 Air voids region 1*

The bonding between horizontal layers show a relative small portion of air voids for printed samples at a layer height of 0.5mm. An example of this is given in Figure 81.

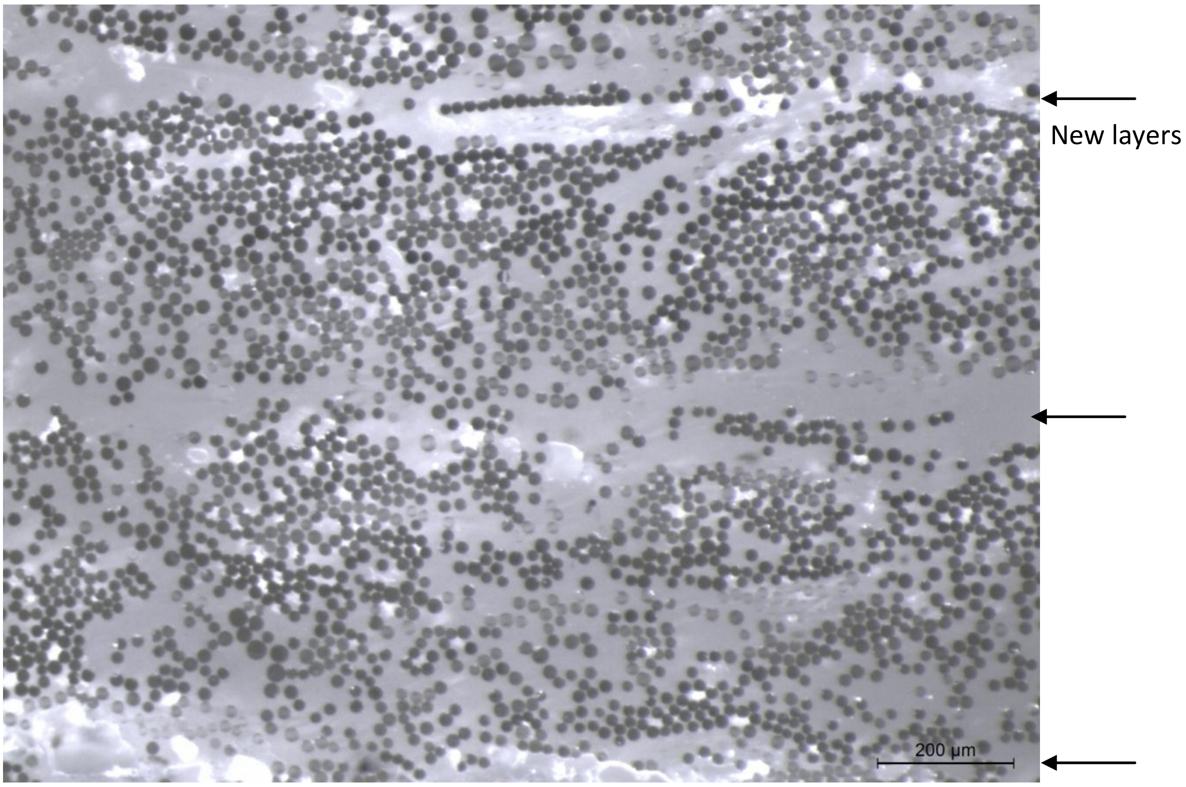


Figure 81: Horizontal bonding of sample 1 (layer height 0.5mm)

It appears that the consolidation force could be higher to decrease these air voids between the layers.

#### 6.3.2.2 Air voids region 2

The connection between the vertical sides of each layer shows the most air inclusions. An example from sample 4 is given in Figure 82. This would suggest that a higher pressure was required to flatten the filament and press the material to the sides.

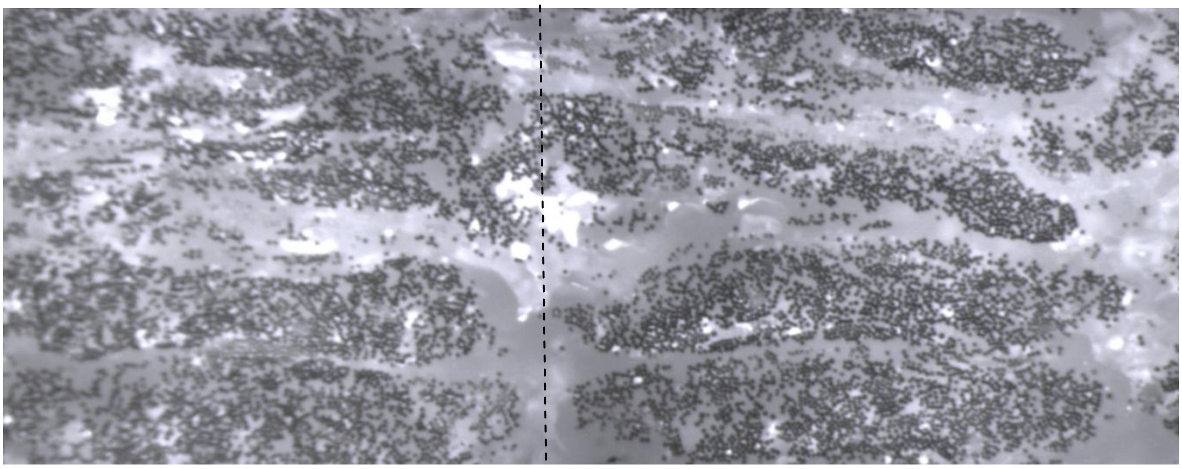

Figure 82: Gaps between vertical bonding areas of sample 4 (layer height 0.5mm)

This is checked for sample 6, where the layer height was reduced from 0.5 to 0.4mm. The filament is flattened to a higher degree, causing a higher consolidation force. An image of this sample is given in Figure 83.

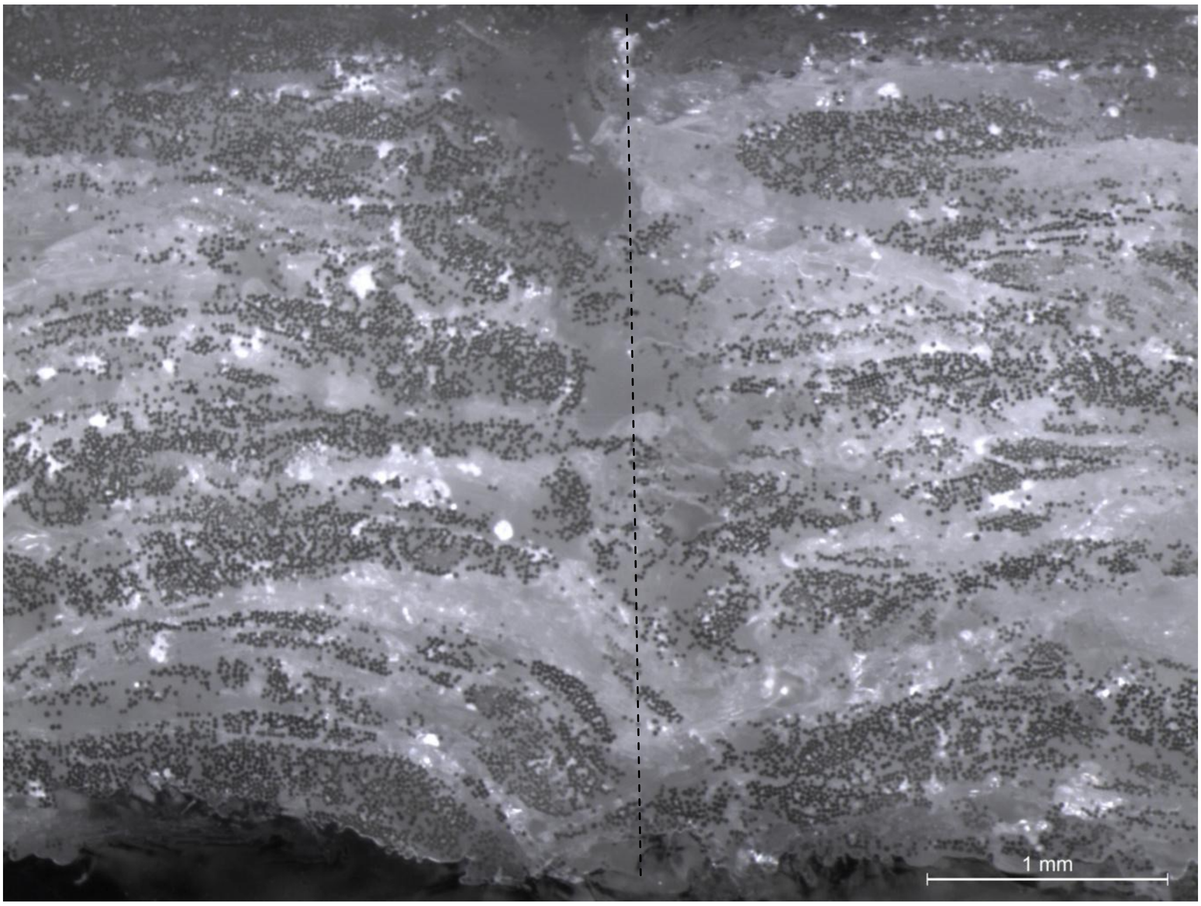

Figure 83: Sample 6 with reduced layer height of 0.4 mm

From Figure 83 can be seen that the vertical bonding has improved by the higher consolidation pressure. However, relative more air voids are found between the horizontal surfaces. The stacking of the printed traces has become very rough and irregular. This is caused by two reasons. First is the resistance of the fibres against flattening. This causes them to move back to a less compressed state while the matrix material is still melted. This creates a rough surface with protruding fibres on which it is much more difficult to print a new well bonded layer. This could be improved by a design that exerts pressure during the solidifcitation of the materix material. Secondly, the vertical gaps seen in Figure 82 are not present in Figure 83 because they are filled with matrix material which is squeezed to the sides. This causes the remaining middle parts to have a lower fraction of matrix material. This decreases the possibilities for good horizontal bonding. A lower printing temperature might cause the fibres to be dragged with the matrix in a higher degree, since the viscosity of the matrix will be higher. This is not significantly noticed in sample 3, printed on a lower temperature of 190°C.

### 6.3.3 Conclusion microscope study

The printed samples are observed to have a certain fraction of air inclusions. The average fraction for all of the studied samples is between 1.5% and 19.36%, depending on user interpretation. It is estimated that the higher bound is a reliable maximum, since all uncertain spots of a cross section are taken as air voids. Relations between process parameters and bonding between the layers cannot reliably established based on the microscopic images since only one cross section is imaged per sample. A new study is advised for further research.

However it is noticed that by smaller layer heights the consolidation pressure has increased, and the layers are flattened to a higher degree. This causes more matrix material to be squeezed to the sides of the printed trace, and a more irregular surface is likely to be achieved by protruding fibres. This seems to cause additional air voids between this layer and the next. To prevent this, consolidation can be done on a larger surface, so that the matrix material solidifies under pressure. This would prevent fibres to protrude out of the surface while the matrix is still melted. It is expected that this would yield smoother surfaces and a decrease in air voids. To obtain a more homogenous print, the temperature could be lowered. This could cause the matrix material to drag more fibres with it during its flow to the sides, decreasing the high matrix fraction at the vertical bondings. This would increase the matrix volume fraction at the horizontal bondings which facilitates the horizontal bondings.

## 6.4 Three point bending tests

In this chapter 3 point bending tests are performed to determine the flexural properties of printed beams. In the first chapter the theoretical values are defined. Then the process parameters and the preparation of the samples are explained. In the last chapter the results of the 3 point bending test are given and evaluated.

### 6.4.1 Material properties

The used material to print the beams for the bending tests is TWINTEX® RPP60B265. The material consists of 60%$_v$ E-glass in a matrix of Polypropylene [14].

According to the manufacturer Fiber Glass Industries, the flexural strength and flexural modulus of processed TWINTEX® RPP60B265 are 580MPa and 26.5GPa respectively according to test specifications of ISO14125 (Figure 84).

TWINTEX® R PP ROVING COMPOSITE MECHANICAL PROPERTIES (after processing)

| TWINTEX® ROVING R PP 60% (265 yield) 1870 tex E-glass based | | | | | |
|---|---|---|---|---|---|
| Mechanical properties at room temperature – UD SAMPLE | | | | | |
| Product | Tensile Properties | | Flexural properties | | |
| Twintex® RPP601870 | Strength at break [MPa] | Modulus [GPa] | Strength at break [MPa] | Modulus [GPa] | Glass Content % |
| | ISO527-5 | | ISO14125 | | ISO1172 |
| Technical datasheet | 760 | 29.5 | 580 | 26.5 | 60 |
| Mfg database | - | - | 698 | 26.7 | 61.3 |
| 04 / 2012 Trials performed on 6 rovings natural & black (60 coupons/test) SRP 17779-17766 | 821±31 | 30.2±0.8 | 607±35 | 27.3±0.6 | 62.8 |

Figure 84: TwinTex RPP601870 mechanical properties [14]

As mentioned in Chapter 6.2.4, the expected flexural modulus for the material are slightly raised by the higher volume fraction of the fibres due to leaking. The expected modulus is determined to be29.33 GPa.

The thermoplastic matrix material only has a flexural modulus ranging from 1.48GPa (copolymer) to 1.55 GPa (homopolymer) [22]. It is not specified type of polymer is used.

### 6.4.2 Process and specimen preparation

To comply with the standards of ISO14125 five specimens for each bending test are required. The dimensions of any test specimen shall nowhere deviate more than 2% from its mean height or 3% from its mean width. Further its cross section must be rectangular without rounded edges. The used dimensions are described below.

***Dimensions***

The test beams are all printed with unidirectional fibres in the length direction of the beam (0°). For this reason they comply with Class III of the ISO standard with standard test dimensions of 60 x 15 x 2 mm. There however chosen to deviate from the standard dimensions. The most interesting outcome of the test is the achieved bonding during the print process. The standard thickness of 2 mm only contains 4 layers when printing at a layer height of 0.5mm. This layer height gives visually good results without protruding filament. Possible deviations of print bed levelling will influence the first layer bonding in a high degree. With four layers, this would influence 1/3 of the bondings between layers. To minimize this influence, a thickness of 3 mm (6 layers) is chosen to be inserted in the Gcode generator (see Chapter 5.3.3).

The width of the specimen is chosen to be 10 mm. This is different from the ISO specification, but is done to save material and time. The inserted width and height are given in Table 6 under 'Given specifications'.

The width and the height are rounded to a whole number of lines and layers in the Gcode generator. The resulting outer dimensions are given under 'Engineered dimensions' in Table 6.

The test beams are sanded (P120) on each surface to remove protruding material. The final measured dimensions  are given in Table 6. These dimensions are accurate within 50µm. The measured volume difference is given in the last column. From here it can be seen that the dimensions of the printed beams is larger than the specified volumetric dimensions. This is not clarified by the presence of air voids, as they are contributing to an average of 1.3 $\%_v$ (See Chapter 6.3.2). Most probably the difference in dimensions is clarified by the rough surfaces of the specimen, even after sanding.

The inserted length in the Gcode generator printed for each test beam is 70 mm. This is cut to a length of 62 mm with a diamond saw and sanded to 60mm.

### 6.4.3 Variables

It is assumed that the process velocity has no major influence on the material properties within the limits of the machine. For that reason a safe production speed of 90mm/min is chosen which is not changed during the production of the samples. The samples are given in Table 6.

Only the production temperature and layer height is varied between different sets of samples (1-4). To specify the process stability, a similar sample (5) to the first set is printed after printing all the other samples. This one is compared with the first set to see deviation that occurred during the process.

To exclude side phenomena of squeezed matrix material, another sample (6) with different dimensions is printed. The outside traces are sanded off so that the same width is obtained as set 1 and 2. A slightly higher flexural modulus is expected for this test sample since disturbances at the outer layers are sanded off.

| Nr. | Given specifications [Temperature @lxbxh @ layer height @ print speed [mm/min]] | Qty | Printed dimensions | Measured dimensions (after sanding) |
|---|---|---|---|---|
| 1. | 200°C @ 70x10x3 @0.5 mm @F90 | 6 | 70 x 9.98 x 3.0 mm | 60 x 10.3 x 3.3 mm |
| 2. | 210°C @ 70x10x3 @0.5 mm @F90 | 5 | 70 x 9.98 x 3.0 mm | 60 x 10.3 x 3.3 mm |
| 3. | 200°C @ 70x10x3 @0.4 mm @F90 | 3 | 70 x 9.35 x 3.2 mm | 60 x 9.3 x 3.7 mm |
| 4. | 200°C @ 70x10x3 @0.6 mm @F90 | 3 | 70 x 10.4 x 3.0 mm | 60 x 11.0 x 3.3 mm |
| 5. | 200°C @ 70x10x3 @0.5 mm @F90 | 1 | 70 x 9.98 x 3.0 mm | 60 x 10.3 x 3.3 mm |
| 6. | 200°C @ 70x14x4 @0.5 mm @F90 | 1 | 70 x 15.0 x 4.0 mm | 60 x 10.3 x 4.2 mm |

Table 6: Printed specimen for 3 point bending test

A picture of correctly printed test beams is given in Figure 85. A set of sanded specimen (before cutting them to length) is given in Figure 86.

Figure 85: Printed test beams 5 and 6

Figure 86: Test beams sanded to correct dimensions (set 1)

**Notes on the printed specimen**

The last two samples of test Nr. 1 were corrupted by a blocked nozzle. It caused the filament to be extruded with irregular speeds. This can be seen in Figure 87 by a rough and wavy surface. They are however sanded to the same dimensions and will probably yield a lower flexural modulus.

During printing the third set of specimen it is seen that the traces at the lowest layer failed to connect. A bottom view of one of this test beams is given in Figure 88. The filament required too much force to be compressed to 0.4mm. This caused the printer head to lift slightly, causing the lower layer to remain higher. From the third layer (out of 8) the print head pre tensioned so much that the traces are connected again.


Figure 87: Test beams 1.5 and 1.6

Figure 88: Voids between traces in set 3

As can be seen from Table 6, the volume of the printed samples is larger than the intended dimensions. This is assumed to result in a lower flexural modulus, since the average volume fraction of the fibres has decreased. This is further discussed in the evaluation of the bending test.

### 6.4.4 Setup of 3 point bending test

The setup of the 3 point bending test is given in Figure 89 [16].

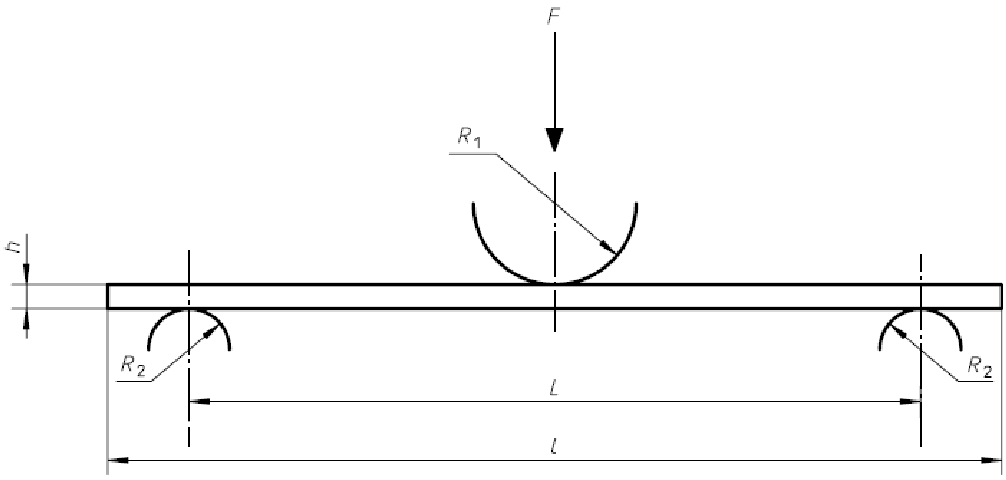


Figure 89: Three point loading arrangement [16]

The span of the supports L is set to 40 mm according to the standard specification for Class III composites. The radius of the support cylinders $R_2$ is 1/16" (ø 3.175mm) and the diameter of the press cylinder $R_1$ is 1/8" (ø6.35mm). As mentioned above, the length of the specimen (l) is 60mm, and the height of the specimen (h) is variable per test (See Table 6). The speed of the press is set to 1mm/min to match the specified speed of

$$v = \frac{\varepsilon' L^2}{6h}$$

where ε' is a strain rate of 0.01/minute [16].

The results for the flexural modulus $E_f$ is calculated according to the formula [16]:

$$E_f = \frac{L^3}{4bh^3}\left(\frac{\Delta F}{\Delta s}\right)$$

where ΔF/Δs is the slope of the load – deflection curve.

The samples are placed in the middle of the machine with their first printed layers facing upward.

### 6.4.5 Results of three point bending test

All the samples failed on compressive stress, as depicted in Figure 90.This yields valid results from the bending test with respect to the flexural properties [16]. An enlarged image of the compressive fracture of sample 1.1 is given in Figure 91.

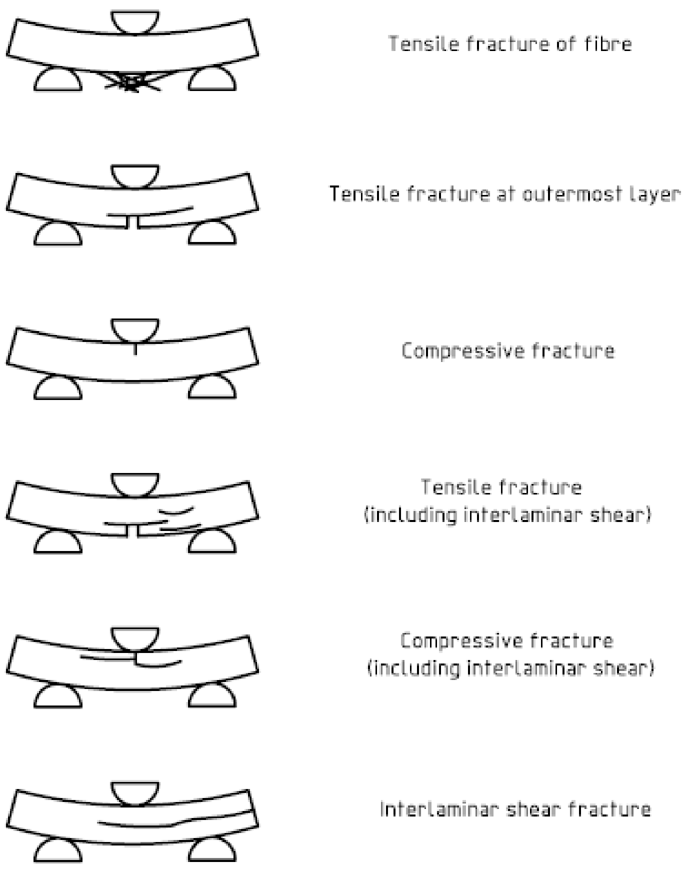


Figure 90: Possible failure modes [16]

Figure 91: Compressive fracture of sample 1.1

For the first set of test beams the results of the three point bending test are given in Figure 92. The plotted results of the other beams are given in Attachment 6.

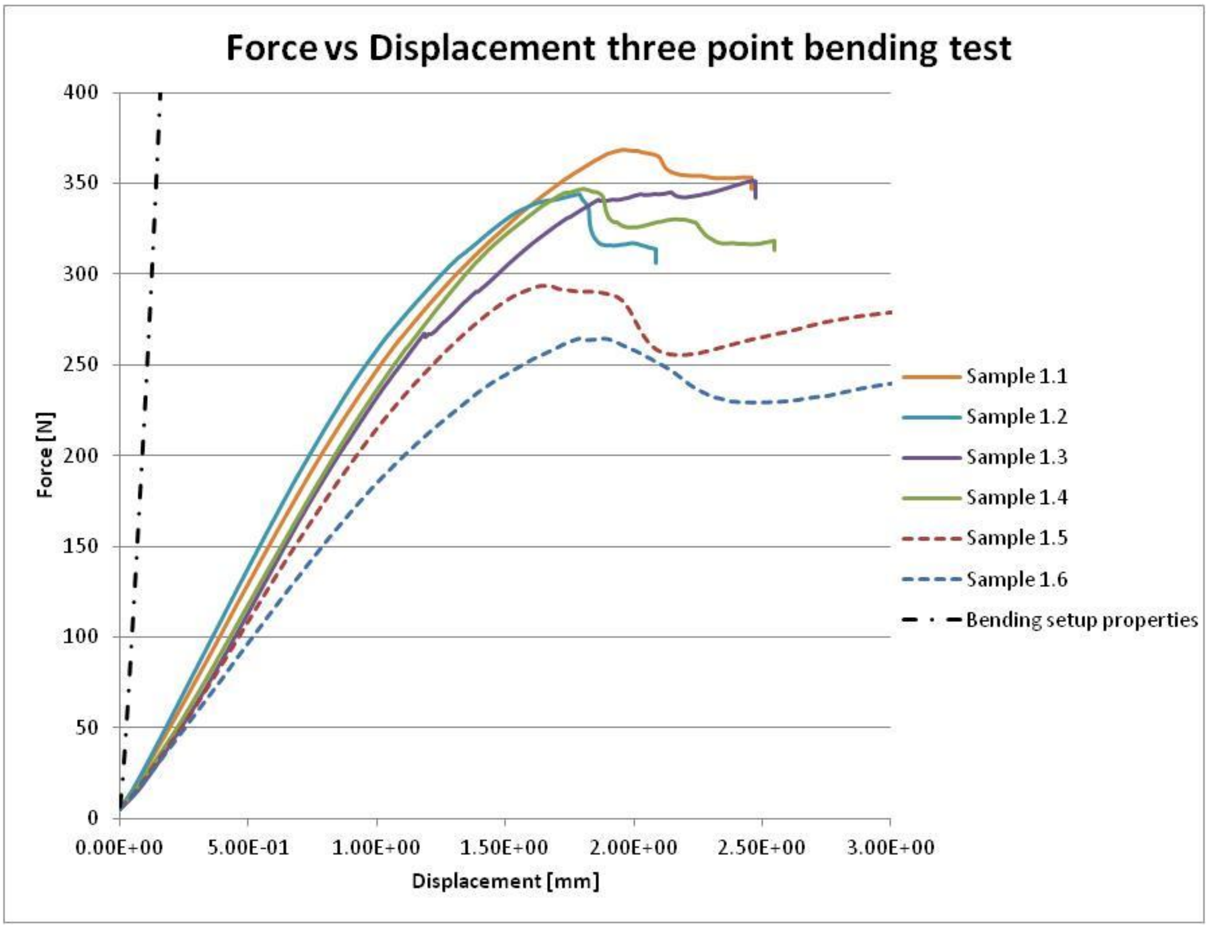


Figure 92: Force - Displacement curve of sample set 1

In Figure 92 the dashed lines belong to the samples that were printed with an obstructed nozzle (See Figure 87). They are excluded from further calculations because of their low quality. To eliminate the influence of the bending setup stiffness on the measurements, a hardened metal piece with a 10 x 10 mm cross section is inserted in the bending setup. The obtained force displacement curve (dash dot line) is regarded as machine compliance, since the hardened metal beam is not expected to be significantly deflected during the test. This will be subtracted from obtained values.

It is noticed that small indents (up to 0.1mm) are made by the press cylinders during the bending tests, which did encourage the failure on the compressive side of the specimen. The presence of air voids in the specimen surfaces at the location of the press cylinders probably increased this phenomena. A shim or cushion between the samples and the press cylinder could have decreased the occurrence compressive fractures [16].

This indentation of the cylinders into the samples has also influence on the obtained stress strain curve. The measured displacement is increased with the depths of the dents. The described manner in ISO14125 to calculate ΔF/Δs gives therefore no satisfactory results. In the norm is described to calculate the slope of the curve between two defined points s' and s'' according to:

$$s' = \frac{\varepsilon_f{}' L^2}{4.7h}$$

$$s'' = \frac{\varepsilon_f{}'' L^2}{4.7h}$$

where $\varepsilon_f'$ and $\varepsilon_f''$ are prescribed values of flexural strain of 0.0005 and 0.0025 respectively. This would yield a slope in the displacement range of 0.05 mm to 0.26 mm. Irregularities in the data due to rough sample surfaces yield a very unreliable result.

To exclude this behaviour, the maximum of the derivate of the force displacement curve is taken with the next steps. First the slope is determined between each data point with:

$$G(n) = \frac{\Delta F(n)}{\Delta s(n)} = \frac{F_n - F_{n-1}}{s_n - s_{n-1}}$$

where n is the current number of the data point. This result is filtered to H(n) according to:

$$H(n) = k \cdot H(n-1) + (1-k) \cdot H(n)$$

where $0 < k < 1$. The larger k, the more emphasis on previous measurements, and the more filtering of sudden jumps in data. To obtain a stable result, k is chosen to be 0.98. The maximum value of the filtered results for $0 < s < 1$ mm is chosen to represent the specimen property $\Delta F/\Delta s$.

The process for sample 1.2 is plotted in Figure 93. The obtained slope is given in Figure 94.

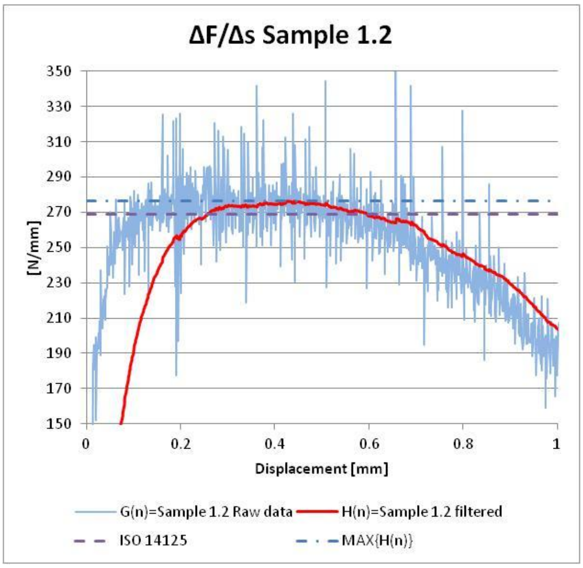


Figure 93: Slope calculation of Force-Displacement sample 1.2

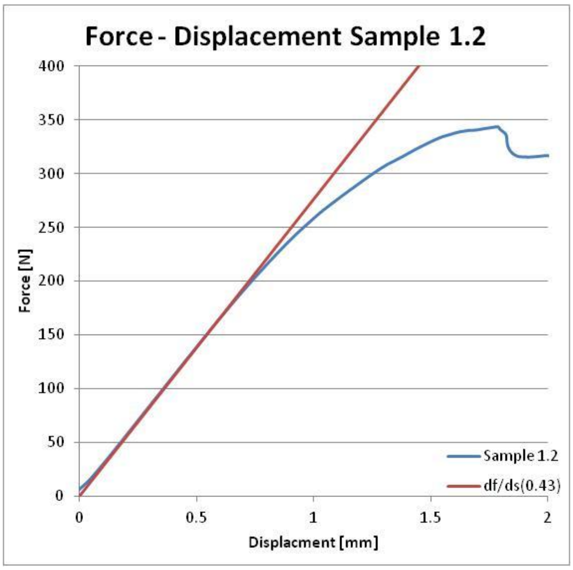


Figure 94: Slope of Force-Displacement sample 1.2

After obtaining the compliance of the specimen, the machine compliance needs to be subtracted from the sample compliance according to

$$\left(\frac{\Delta F}{\Delta s}\right)_{real} = \left[\left(\frac{\Delta F}{\Delta s}\right)_{sample}^{-1} - \left(\frac{\Delta F}{\Delta s}\right)_{machine}^{-1}\right]^{-1}$$

where $(\Delta F/\Delta s)_{machine}$ is taken at the point where F reaches 100N. This is the same force as where most of the samples are evaluated. It is evaluated to be 2.13KN/mm.

The obtained results after the described calculations is given in Table 7 and graphically represented in Figure 95.

| Nr. | Given specifications [Temperature @ layer height @ print speed [mm/min]] | Qty | Sample dimensions | Average flexural modulus [GPa] | Standard deviation [GPa] |
|---|---|---|---|---|---|
| **1.** | 200°C @0.5 mm @F90 | 4 | 70 x 10.3 x 3.3 mm | 13.00 | 0.57 |
| **2.** | 210°C @0.5 mm @F90 | 5 | 70 x 10.3 x 3.3 mm | 12.37 | 0.76 |
| **3.** | 200°C @0.4 mm @F90 | 3 | 70 x 9.3 x 3.7 mm | 13.06 | 0.34 |
| **4.** | 200°C @0.6 mm @F90 | 3 | 70 x 11.0 x 3.3 mm | 11.44 | 0.73 |
| **5.** | 200°C @0.5 mm @F90 | 1 | 70 x 10.3 x 3.3 mm | 13.22 | - |
| **6.** | 200°C @0.5 mm @F90 | 1 | 70 x 10.3 x 4.2 mm | 13.46 | - |
| **7.** | TwinTex material properties (f=34%) | - | - | 26.50 | 0.6 |
| **8.** | TwinTex corrected to fibre fraction (f= 37.8%) | - | - | 29.33 | - |

Table 7: Flexural properties test beams

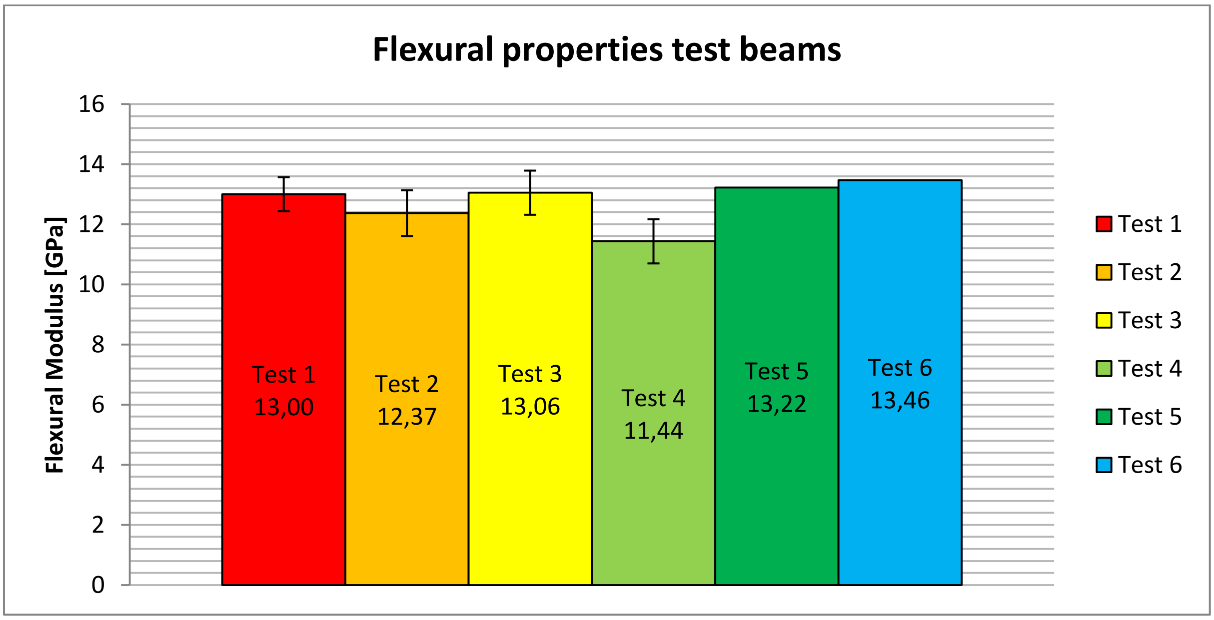


Figure 95: Flexural properties test beams

### 6.4.6 Evaluation on sample differences

As can be seen from Figure 95, the flexural moduli of the test samples are relatively close together. Test set 1 is printed first and yields a flexural modulus of 13GPa. An increased temperature seems to have a negative impact on the flexural modulus (Set 2). This can be explained by a lower viscosity of the matrix material, and thus a lower pressure that can be asserted on it during printing. This could yield a lower bonding pressure. Another reason could be that the glass fibres have more freedom to rearrange after being printed, since the matrix material need a longer time to solidify. This could have caused the fibres to protrude from the printed surface, and decrease bonding with the next layer.

From sample set 1 and 5 can be seen that the process is reliable. Test beam 5 was printed after finishing all the other samples, to check possible changes in the print process with the same input parameters. This does not seem to be the case.

From sample 6 can be concluded that the sides of the specimen have  lower mechanical properties than the centres. The sides of sample 6 are sanded down with approximately 2mm each, to remove the irregularities of squeezed out material.

However, it must be noted that the differences between outcome of the test sets are smaller than the standard deviation of each set. Each conclusion that is made with respect to the process input parameters is therefore not statistically reliable, but more an actual guideline for further research.

### 6.4.7 Evaluation on average flexural modulus

The difference between the flexural moduli supplied by the manufacturer and the averaged test samples shows a large difference. This is given in Figure 96, where both are compared with the corrected modulus, which is calculated for the missing volume fraction of matrix material (See Chapter 6.2.4). This is difference is compared with achieved results for other FDM printed samples from research of Ziemian [24] . In this study the mechanical properties of FDM printed samples made from ABS are subjected to tensile, compression, flexural and impact tests. A flexural modulus for unidirectional printed ABS of 1.594GPa is achieved with a standard deviation of 0.33GPa. This is plotted against the flexural modulus determined by values specified according to the ASTM D790 norm for injection moulded ABS in Figure 97.

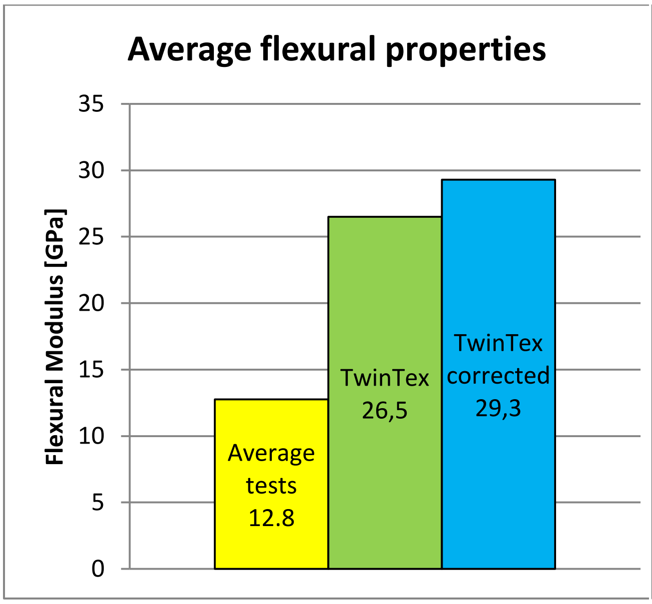


Figure 96: Comparison of average flexural modulus of TwinTex

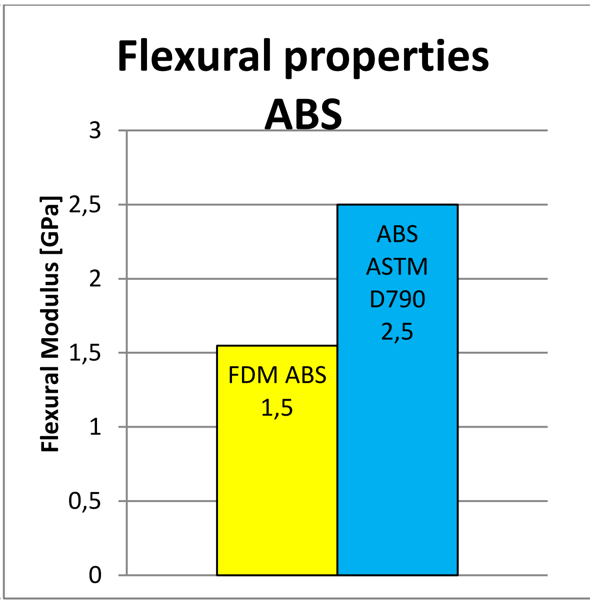


Figure 97: Comparison of ABS (FDM vs. injection moulding)

It is found by Rodríguez that moduli values of ABS printed products by FDM are 11% to 37% lower than injection moulded ABS [25]. For the current test samples with continuous fibre reinforcement, four causes for this behaviour are discussed in the next sub chapters.

#### 6.4.7.1 Influence of air voids

The height and width of the tested samples are on average 18.24% larger than the intended height and width during printing (See Chapter 6.2.3). This is supported by the microscopic evaluation, where a maximum estimation of 19.36% is found (See Chapter 6.3.2).

The influence of air voids on the flexural modulus of consolidated TwinTex is found to be significant in an earlier study of Hagstrand. A negative relation between the air void fraction and the flexural modulus is found, where the modulus decreases by about 1.5% for each 1% of air void content [26]. This found relation is plotted in Figure 98.

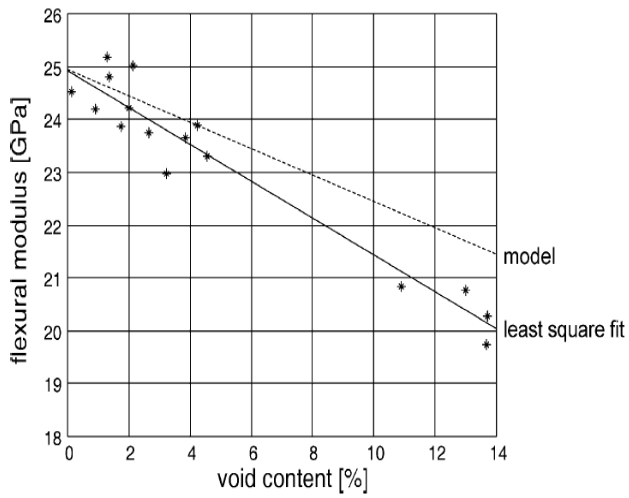


Figure 98: Flexural modulus vs. void content

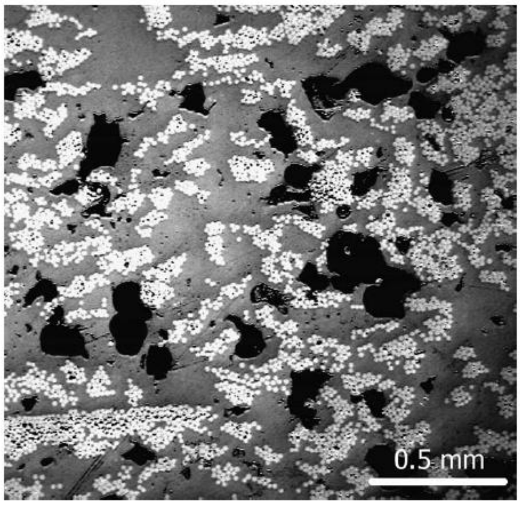


Figure 99: Polished cross-section of sample with an overall void content of 13%

The relation is researched up to 14% of air void content in press consolidated TwinTex. An image from the study with 13% air void content is given in Figure 99. Obviously this relation is not valid up to large extends of voids. If linearity is assumed for up to 19% air voids, the found relation would lower the expected flexural modulus with 28.5% to 18.9 GPa.

As can be seen from Figure 99, the found air voids from the study are concentrated in larger clusters, mainly surrounded by matrix material. In the current results, air voids are also found in between bundles of fibres (See Figure 100). This is expected to decrease the flexural modulus even more, since no proper bonding is achieved between fibres and matrix at those places.

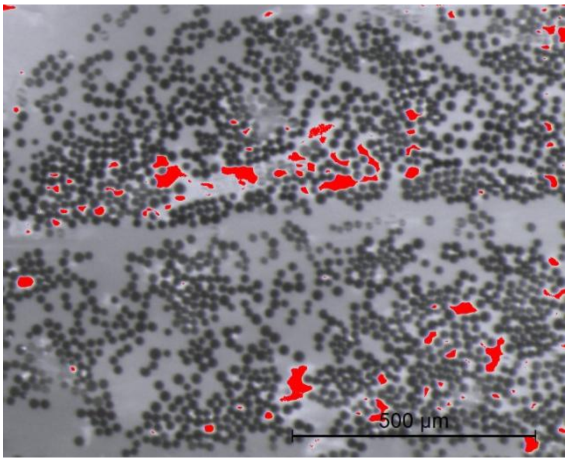


Figure 100: Intra bundle voids (red spots, sample 4)

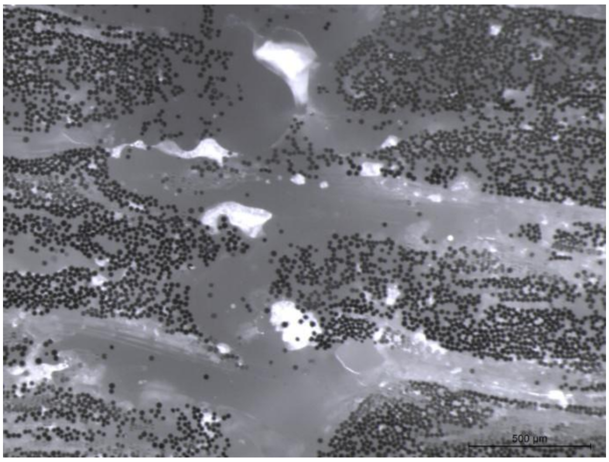

Figure 101: Inter bundle voids (Large white spots, sample 5)

The intra bundle voids are most likely originating from the pultrusion process, whereas the inter bundle voids (See Figure 101) originate from the printing process.

#### 6.4.7.2 Volume increase

Another obvious reason for the lower flexural modulus is the lower average fibre fraction due to the printed air voids. According to the rule of mixtures, an average increase of volume approximately 19% leads to a decrease in fibre fraction of

$$f = \frac{f_{original}}{1 + f_{add}}$$

where

$f_{original}$ = the initial fibre fraction of the material corrected for leaking (0.378)

$f_{add}$ = the added volume fraction during printing (0.19).

This leads to a lower average fibre fraction of 31.8%$_v$. According to the rule of mixtures (See Chapter 6.2.4) , this would yield an expected flexural modulus for the samples of 24.8 GPa. The decrease in the flexural modulus because of a lower fibre fraction is however also covered in the relation discovered by Hagstrand [26], mentioned in the previous sub chapter.

#### 6.4.7.3 Fibre orientation

The specified flexural modulus of the manufacturer is specified according to ISO 14125 for samples with alignment of fibres in length direction. During printing, it can be that a fraction of the fibres are not straight aligned in the printed direction, but are slightly waving through the surface. The flexural modulus will be affected by this phenomena, since the fibres are not loaded longitudinally during the three point bending tests in that case. The flexural modulus is then in a higher degree influenced by the matrix material, which is much lower. For a specific composite ($E_f$ = 82.7GPa, $E_m$ = 2.18GPa) with short fibre lengths (3.2mm), the influence of the mean fibre orientation is given in Figure 102 [27].

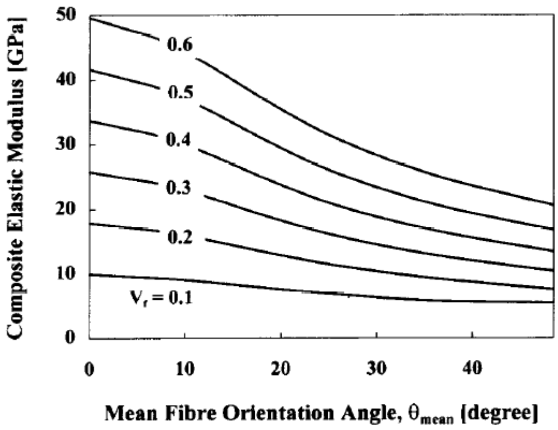


Figure 102: Elastic modulus predicted for various volume fractions $V_f$ [27]

The alignment of the fibres cannot be seen in the studied cross sections in Chapter 6.3.2 since they are perpendicular to the fibres. For that reason the influence cannot be quantified in the current study. A new study for images with parallel cross sections to the fibres would yield more insights in fibre orientation.

#### *6.4.7.4 Broken fibres*

The lower flexural modulus can also be influenced by an amount of broken fibres during the print process. This could be the case due to the sharp bends that the fibres must make when they exit the nozzle. For a mean fibre length of larger than 3.2mm, the length does not influence the flexural properties significantly [27]. The mean fibre length is observed to be longer than 3.2 mm, so this is therefore not identified as a significant cause for the lower flexural modulus.

## 6.5 Conclusion on quality of printed products

Several products are printed with the prototype. Short printable lengths of 6 mm are possible to print, and small radii up to 20 mm do not form a problem with regard to tow steering defects. Complex shapes are therefore possible that were not possible to manufacture with automated tape layering machines.

Some deviations in printed dimensions are noticed. Especially a small increase in layer height during printing, which indicates that the layers are not pressed sufficiently together without air voids. A main factor in this is the fact that glass fibres are protruding out of the matrix after printing, and before solidification of the matrix material. At the sides of the printed products, a small amount of printed material is squeezed to the outside of the printed area, leading to slightly larger outer dimensions.

The increased volume after printing is measured to be around 18%. It is expected that for larger products this volume increase will be lower, since the height deviation is not expected to change after multiple layers. The amount of air voids found during a microscopic study is approximately the same, based on the higher estimation.

The process of printing continuous fibre reinforced filament is stable. No large deviations in mechanical properties of the printed products are found. However, there is found to be a large difference in mechanical properties given by the manufacturer and several tested samples. The main reason for this is identified to be the volume fraction of air voids inside the products. The main topic for improvement in the design the consolidation pressure exerted by the printer nozzle. In order to consolidate with a higher pressure, two things need to be improved. Most important being the location of the exerted pressure. This needs to be done during the solidification stage, so a smooth and stable surface of the print is achieved. Secondly the stiffness of the printer frame needs to be improved. By doing so, mainly the first layers will gain improved bonding. A possible improvement in fibre distribution in the printed product can be achieved by lowering the process temperature.

# 7 Conclusion and recommendations

This chapter summarizes the main achievements and findings of the research. In the second sub chapter an overview is given of the most important design improvements and recommendations for further research.

## 7.1 Conclusion

During the research a working prototype has been developed for a machine that can print fibre reinforced material. The goal to achieve the freedom of creation that is found in the Fused Deposition Modelling is achieved. The built and tested setup is therefore a promising design to automate the production of small and complex composites.

Before printing of fibre reinforced material was possible, a suitable feed material needed to be selected. This is done based on availability, fibre volume percentage and diameter. Since the material was not readily available, a machine is designed to create it from comingled TwinTex yarns, consisting of 34 volume percent of E-glass, surrounded by strands of polypropylene matrix material. The chosen pre processing method is pultrusion, which yielded visually smooth filaments that were suitable for further processing with a 3D printer.

After the processing of the feed material, an open source Fused Deposition Modelling 3D printer is configured to process the continuous fibre reinforced filament. The main developed feature is the new printing head with a specialized nozzle and cutting mechanism. The specialized nozzle differs from a common FDM nozzle because its cross sectional area had to remain the same during the process, in order to avoid jamming by the glass fibres. The developed cutting mechanism is developed to cut the glass fibres to free the print head for a movement to a new location.

Before the adapted 3D printer could work, a number of software adaptations are made. The printer firmware is adapted so it could automatically control the cutting device. Further an algorithm is written to convert standard printer code into updated code for the glass fibre reinforcement printer. It is optimized to automatically detect the places where to insert a cutting command.

With these adaptations a highly automated process is created, without necessary user input during the process of printing. Results for the printed test parts show a reliable and stable process, which does not change over time. Inside the printed products, average air void concentrations of around 19% are found.  This is almost twice as high as for general FDM printed ABS products (10%).

The main cause for the air voids is found to be the behaviour of the glass fibres just after extrusion by the printing head. They tend to move to a less compressed state after being printed, while the matrix material is still not solidified. This causes a rough and irregular surface on which it is difficult to print a new layer without air inclusions.

The flexural properties of several test beams are studied with results of a three point bending test. The average flexural modulus is found to be around 44% of the modulus that was expected based on perfectly consolidated material properties. In general FDM products made from ABS this is found to be approximately 60%. The main reason for this is found to be the larger air void content.

## 7.2 Recommendations

For further research a few recommendations are made. They are shortly explained in the next sub chapters in order of importance.

### 7.2.1 Decrease of leakage

During the pultrusion and printing process some leakage of melted polypropylene is observed. This is measured to be around $10\%_v$ of the total processed volume. This decrease in matrix material makes it more difficult to create good bonding between the printed layers, since this is a process of the matrix material only. It can be stopped by redesigning the connection of the guidance with the nozzle.

### 7.2.2 Increase of consolidation pressure

In order to achieve a decrease in the air void fraction, the printer head needs to exert more consolidation pressure. In the current design this is limited by two factors. For the first layers, the stiffness of the printer frame is found to be too low (522.5N/m). This causes the first layers to increase in height until the frame is pre tensioned enough to exert the required pressure to flatten the next layers to the right extend.

The second factor that limits the consolidation pressure is found to be the location where it is exerted. It is physically impossible to exert a high pressure on the lower side of the melted matrix material by pushing at the top side. When the pressure is increased, the matrix material is just squeezed to the sides. This is not expected to increase the consolidation under the melted matrix in a high degree. It does on the other hand affect the behaviour of the glass fibres. The more they are compressed, the more they tend to move backwards after the nozzle. This is possible for a short time, since the matrix material takes time to solidify. This observed behaviour creates a rough surface with protruding fibres. It is expected that this causes additional air voids between this layer and the next. The printer nozzle could be improved to exert pressure at a larger surface, so the matrix is solidified under pressure. A larger surface of exerting pressure increases the requirement of a stiffer frame.

### 7.2.3 Microscopic study

The results of the microscopic study are difficult to interpret, due to changing light conditions and insufficiently polished surfaces. It should be carried out again to establish more reliable data about the air void content. Further it can be extended by a study to the fibre alignment in the print. This can be done by imaging cross sections of specimen that are parallel to the fibre direction. This would yield more insight in the possible effect of fibre alignment on the mechanical properties.

# 8 Table of pictures

# 9 Works Cited


[1] A. Jacob, "The popularity of carbon fibre," *Reinforced Plastics,* pp. 22-24, March 2006.

[2] "ProtoPasta," ProtoPasta, Vancouver, Washington, [Online]. Available: www.proto-pasta.com. [Accessed 25 05 2014].

[3] T. De Bruin, "DEVELOPING A PROCESS FOR CONTINUOUS FIBRES IN FUSED DEPOSITION MODELLING," University of Twente, Enschede, 2013.

[4] J. Sloan, "ATL and AFP: defining the megatrends in composite aerostructures," 30 06 2008. [Online]. Available: http://www.compositesworld.com/articles/atl-and-afp-defining-the-megatrends-in-composite-aerostructures. [Accessed 2 11 2014].

[5] D. H.-J. Lukaszewicz, C. Ward and K. D. Potter, "The engineering aspects of automated prepreg layup: History, present and future," *Elsevier,* vol. 43, p. 13, 2011.

[6] M. Lamontia, M. Gruber and B. Waibel, "Conformable compaction system used in automated fiber placement of large composite aerospace structures.," in *23rd Sampe conference*, Paris, France, 2002.

[7] Åström, "Manufacturing of polymer composites," Chapman & Hall, London, UK, 1997.

[8] "RepRap.org," 09 02 2010. [Online]. Available: http://forums.reprap.org/read.php?1,35533. [Accessed 2 10 2014].

[9] "www.3ders.org," 06 10 2013. [Online]. Available: http://www.3ders.org/articles/20131006-6-axis-3d-printer.html. [Accessed 16 03 2015].

[10] S. Anderson, "Students Develop 6-Axis Robotic 3D Printer Inspired by Spiderwebs," 02 02 2015. [Online]. Available: http://3dprint.com/41183/robotic-6-axis-3d-printer/. [Accessed 16 03 2015].

[11] Fab@Home, "http://www.fabathome.org," [Online]. [Accessed 10 January 2014].

[12] IPS, "Installing pipes; Butt fusion welding of polypropene," [Online]. [Accessed 9 January 2014].

[13] Equistar, "Injection Molding Technical Tip," [Online]. [Accessed 09 January 2014].

[14] [Online]. Available: http://fiberglassindustries.com/twintex.htm. [Accessed 5 4 2014].

[15] "http://compositetape.com/," Comp Tape. [Online]. [Accessed 10 Janurary 2014].

[16] NEN, "Fibre-reinforced plastic composites — Determination of flexural properties," no. Reference number: ISO 14125:1998(E), 1998-03-01.

[17] "Arduino.cc," Arduino, [Online]. Available: www.arduino.cc. [Accessed 10 10 2014].

[18] WOT, “Werkgroep OntwikkelingsTechnieken,” [Online]. Available: www.wot.utwente.nl. [Accessed 2014].

[19] E. Zalm, “Marlin firmware,” [Online]. Available: https://github.com/ErikZalm/Marlin/tree/Marlin_v1/Marlin. [Accessed 10 11 2014].

[20] A. Ranellucci, “Slic3r,” [Online]. Available: http://slic3r.org/. [Accessed 10 11 2014].

[21] “RepRap Wiki,” RepRap, [Online]. Available: http://reprap.org/wiki/Leveling_the_Print_Bed. [Accessed 10 11 2014].

[22] “MATERIAL SELECTION GUIDE,” Curbell Plastics, [Online]. Available: http://www.curbellplastics.com/. [Accessed 30 05 2015].

[23] A.-C. I. F. E. e. a. Schindelin J., “Fiji: an open-source platform for biological-image analysis,” *Nature methods,* vol. 9, no. 7, pp. 676-682, 2012.

[24] C. Ziemian, M. Sharma and S. Ziemian, “Anisotropic Mechanical Properties of ABS Parts Fabricated by Fused Deposition Modelling,” in *Mechanical Engineering, Dr. Murat Gokcek (Ed.)*, InTech.

[25] J. F. RodríguezJames, P. ThomasJohn and E. Renaud, “Mechanical behavior of acrylonitrile butadiene styrene (ABS) fused deposition materials. Experimental investigation,” *Rapid Prototyping Journal, ,* vol. 7, no. 3, pp. 148 - 158, 2001.

[26] F. B. J.-A. M. P.-O. Hagstrand, “The influence of void content on the structural flexural performance of unidirectional glass fibre reinforced polypropylene composites,” *Composites,* vol. Part A, no. 36, p. 705–714, 2005.

[27] S.-Y. Fu and B. Lauke, “The elastic modulus of misaligned short fiber reinforced polymers,” *Composites Sciences and Technology,* vol. 58, no. PII, pp. 389-400, 1998.

[28] MarkForged, “https://markforged.com/,” MarkForged, 28 February 2014. [Online]. [Accessed February 2014].

[29] M. Creemers, P. Leijendeckers, M. v. Maarschakerwaart, J. Rijnsdorp and S. Tysma, Poly-technisch zakboekje (43e druk), Arnhem: Koninklijke PBNA BV, 1989.

[30] C. Lee, S. Kim, H. Kimb and S. Ahn, “Measurement of anisotropic compressive strength of rapid prototyping parts,” *Journal of Materials Processing Technology 187–188,* Vols. 187-188, p. 627–630, 2007.

[31] D. Hull and T. W. Clyne, An Introduction to Composite Materials, Cambridge: University of Cambridge, 1996.

# ATTACHMENTS

# 1 Advantages of pushing vs. pulling of filament

Pushing of the fibres through heater block has several advantages above pulling it after heating. The advantages are elaborated below.

- **Exact control of amount of material to feed**
  The material will be solid before heating. Designing a system that drives solid filament is much easier than a system that drives melted filament. Slipping of the filament will barely occur. When pulling the hot melted tape, slipping will occur, unless only the fibres are pulled. This will cause a huge deformation of the matrix material and will result in very flat end material.

- **Sticking to drive system**
  When the filament is driven after the heating stage, the PP matrix material is very sticky. It will stick to the drive system, unless the drive system has a very smooth contact area or cooled actively. The first will cause less grip on the tape, the latter will cool the tape below the desired temperature. Sticking to the driving system is avoided when pushing the non melted filament through the heater.

- **No dead volume in driving system**
  When finished with one printed trace, the fibres must be cut so the printer can start on a new place with printing the filament. During this movement the printer is not extruding filament. In the case of a pulling system, the material in the drive system is cooling down during this moving stage. Bonding this dead volume to the printed work to start a new trace is not possible when cooled down. Pushing the material back to heat it again might be possible, but when all dead volume has entered the heating element, there is nothing left to pull it out again.

- **Consolidation force**
  If successful tests are performed, and pushing the feed material through a heater block is proven to be possible, it is also possible that a certain pressure can be maintained at the outlet of the heater channel. If this pressure can be increased enough without blocking the heater channel, it can be used to press the heated material onto the print. This would eliminate the need for a separate consolidation system.

# 2 Tests with pushing filament though a heater block

This chapter describes a series of tests performed on a setup where the filament is pushed through a heater block. This block transfers the heat through conduction to the tape. Two tests are performed, each of the following sub chapters describe the goal, setup and outcomes of the tests. Then a conclusion is found in the last sub chapter.

## 2.1 Test 1 (manual feed, manual temperature control)

**What to test**

The first test is to discover if it is possible at all to push heated tape with 30%v E-glass reinforcement through a heater block for conductional heating. The heating of the block is done with a gas torch. The temperature can be checked by pushing a rest piece of the material against the heater block. When it is possible to leave a sticky mark on the surface with the PP matrix material, the temperature becomes close to the desired print temperature. When the material on the surface starts to produce smoke or becomes brownish, the material is degrading and the temperature is too high. The used feed material for the test is obtained from CompTape BV and has nominal dimensions of 5 x 0.5 mm [15].

The feed rate is done by hand. This is the most simple test to do, since it does not require a complicated design. With the manual feeding, it is easy to get a rough understanding of the behaviour of the pushed tape with different speeds.

If it is possible to push a significant amount (0.5m) of material through the heater channel without visual buckling of the fibres, it will give reason to perform further tests. If it appears to be impossible to push fibres, due to buckling or clogging of the channel, it gives reason to invest more time in designing a pull setup.

**Design of setup**

The heater block is designed of two aluminium blocks of 20 x 20 x 10 mm. One of the blocks is equipped with a milled heater channel of 0.5 x 5 mm (+-0.01mm). The two halves are bolted together with M3 x 35 bolts and nuts. The edges of the inlet are chamfered with 1mm x 45 degrees. Pictures of the heater block and primitive usage are given in Figure 103 and Figure 104.

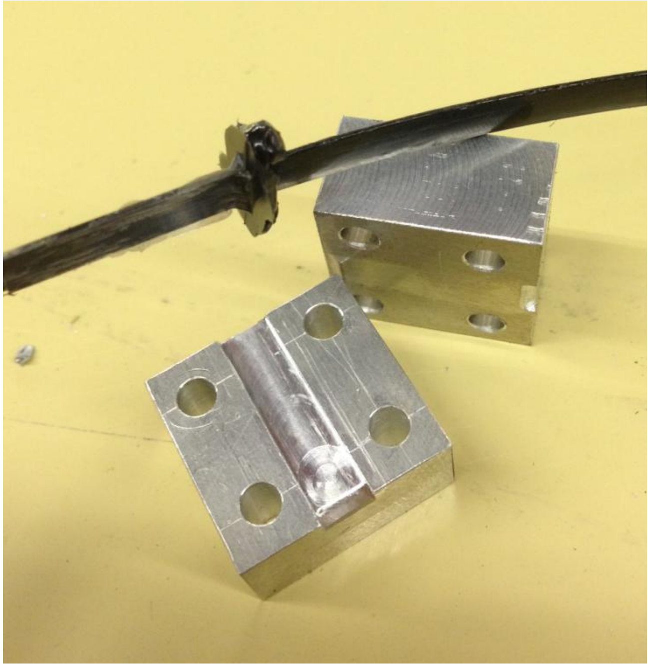

Figure 103: Design of the aluminium heater block

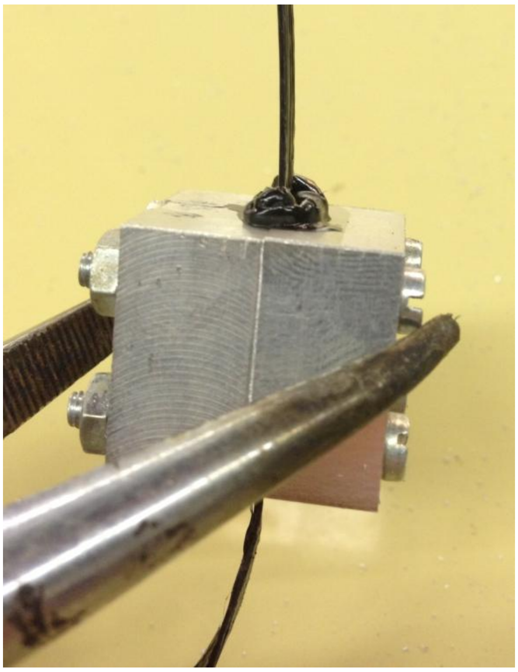

Figure 104: Temperature control with gas torch and pliers

**Test + outcome**

After heating it turned out to be possible to push the tape through the heater channel. The feed rate is approximately 2 mm/s. A faster rate yields a much higher resistance. Since the torch was kept away from the block during extrusion, the temperature dropped below melting point of the PP after extruding approximately 20 s. To ensure that all the material inside the channel is molten, several tests are done by extruding material that remained for longer time (10s) inside the heater block.

The fibres in the filament remained visually straight after extrusion. When inserting the tape under an angle, some of the outside fibres are breaking because they are pressed against entrance of the channel. These broken fibres are however not blocking the throughput. They are dragged out of the channel by the flow, and recognized by sinusoidal waves on the extruded filament. A picture of an extruded filament that is taken out of the heater is given in Figure 105. The waves seem to decrease after extrusion of more material. It is important to test if this is true for different extrusion temperatures and feed rates. The tape has two main sides: one smooth surface, and one rough surface where the fibres protrude through the surface. The glass fibres are probably roller pressed from this side into the PP matrix during manufacturing. The fibres only show the waving behaviour at the rough side of the tape. A filament with better enclosure of the fibres might reduce the wavy phenomenon.

Figure 105: Manually extruded tape with sinusoidal wave of fibres on the rough surface and a lump of PP formed at the entrance of the heater channel

At the top of the heater block a lump of melted PP is formed. This is partly due to the fact that the filament does not have accurate dimensions. The width and height of a cross section vary with +-0.1 and +-0.4mm respectively. Since the inlet of the block is heated above melting temperature, the excess material is scraped away to the top surface. A guidance channel (not heated) would resolve this issue. The problem is however that the cold filament does not fit in a guidance channel of the nominal dimensions. This can be solved by selecting a different kind of filament with lower tolerances on its dimensions.

The fact that the filament gives a lot of resistance above a certain feed rate, is probably due to the variation in dimensions of the filament. At the entrance, the excess material outside the nominal dimensions of the tape is melted away, so the tape fits in the channel. When the feed rate is too high, this excess material is not melted away fast enough, giving a significant resistance. To solve this, a different kind of filament should be selected, with more consistency in dimensions.

**Conclusion test 1**
The outcome of the test shows that it is possible under certain conditions of temperature and feed rate to push material through a heater block. More tests are required to identify the boundaries of temperature and feed rate.

It is important to take good note during further test to see if broken fibres are not blocking the extruder during longer extrusions. If broken fibres are accumulating inside the heating channel, the system is potentially not suitable for printing products. This can be visually checked by the sinusoidal waves on the surface of the extruded filament. If the quantity of the fibres in the wave increase during extrusion, blocking of the extruder is expected over time.

Further it shows that the variations from the nominal dimensions of the tape causes problems during the extrusion process. A round extruded filament of PP filled with fibres is therefore preferred, since this can be bought with lower engineering tolerance on its diameter.

## 2.2 Test 2 (manual feed, temperature control system)

Since the outcome of Test 1 is positive, a new test is designed to control a new parameter of the test. A temperature control system is designed to power the heating. Heating with a gas flame is not very controlled, and care must be taken to avoid burning of the out coming filament. A controlled system makes it possible to test over a longer time under the same conditions, which makes the outcome more reliable.

**What to test**

The maximum and minimum temperature to extrude will be tested with a control system. The minimal temperature is where the PP matrix barely melts. The maximum is where the PP or some of its filler material starts to degrade. This is notable by grey smoke and smell. The allowable process temperature for PP is found to be between 180°C and 230°C [14].

Further a longer extrusion time is tested (60s), to see if blocking of the channel will occur. This will be done for several temperature setpoints.

**Design of test**

*Heater block*

In the heater block a 7mm hole is drilled for a 5W power resistor of 6.8 Ohm. This is done in the part with the channel. A drawing is given in Figure 106. Connected to a 12V power supply it will draw 1.8A, which yields a power consumption of approximately 21Watts. However the resistor is only rated at 5W, this is no problem since the rated power is valid for uncontrolled use. The electronics will control the maximum temperature and the resistor will not get overheated. The power resistor is wrapped in aluminium foil for improved heat transfer to the aluminium block and inserted in its hole.

On the back side a small hole of 2ø x 8 mm is drilled to house the thermocouple. This sensor is also wrapped in aluminium foil and kept in place with a small plate. The position of the sensor is chosen to be only 2mm away from the heating channel, near its exit. The temperature at the exit is the most important place to know and control. The sensor is attached to a thermocouple amplifier, which converts the signal of a few mV to serial data in logic voltage (5V).

The whole unit is bolted on a thermosetting plastic frame, supported by a metal leg. The setup is given in Figure 107.

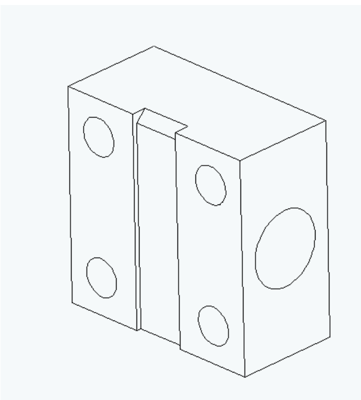

Figure 106: Drawing of heater block

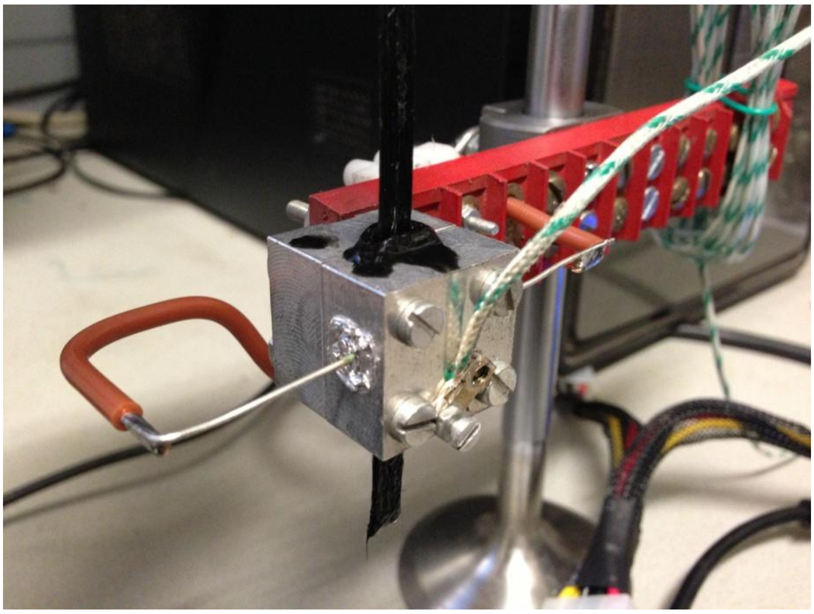

Figure 107: Frame and setup

*Electronics*

To control the software, an Arduino Uno R3 is used. It can read the serial data from the thermocouple and control a power mosfet (IRLZ34N) which switches the resistor. The mosfet is switched by the Arduino with Pulse Width Modulation (PWM) at a frequency of 120Hz. Since the width of each pulse is configurable from 0 (off) to 255 (100% duty cycle), the power to the resistor (and thus the temperature) can be regulated accurately.

To make alterations of setpoint easy, a display shield with 5 functional buttons is added. The display shows the current temperature (C), the internal temperature of amplifier chip (Ta), and the setpoint temperature (Ts) (Figure 108). With the buttons the setpoint temperature can be changed from 0 to 240 $^{0}$C. The temperature can be logged in real-time on the computer to test the settings of the control system (Figure 109).

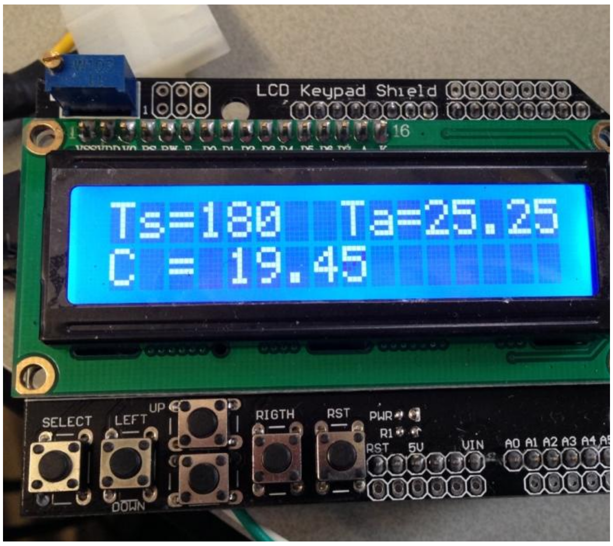


Figure 108: Display layout of Arduino controller

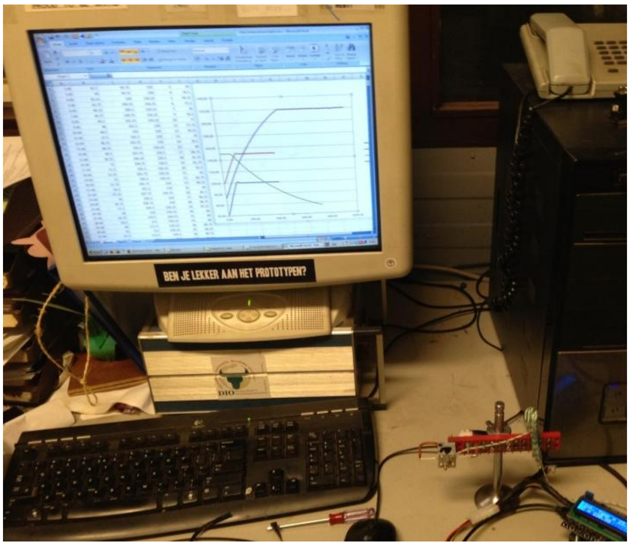


Figure 109: Data plotting of temperature with different parameters and setpoints

*Program*

Two programs are tested on the Arduino. One with a simple on/off regulation. When the measured temperature is higher than the setpoint, the program switches the temperature off. If the temperature is lower than the setpoint, the program switches the power resistor fully on. The frequency of this control is approximately 5Hz. In systems with a lot of thermal mass, and a long thermal distance (conductivity x distance), this will result in a high overshoot. In the current system, where the sensor is placed close to the resistor and the aluminium block is relatively small, the overshoot is relatively small (~1 $^{0}$C)

An improved program is written with a PID controller to minimise the overshoot. The parameters of the PID are designed to be overdamped, so overshoot will not occur. A big disadvantage is that such a system is much slower in response. Heating this system from ambient temperature to printing temperature takes almost two times longer than the program that uses simply an on/off regulation. To prevent this, an improved program is written that uses the relay switching control when the error |Tc-Ts| > 5 $^{0}$C, and very conservative overdamped parameters if the error becomes smaller than 5

°C. The adaptive PID controller gives an overshoot of 0.75 °C. The extruder temperature with the different control systems is given Figure 110.

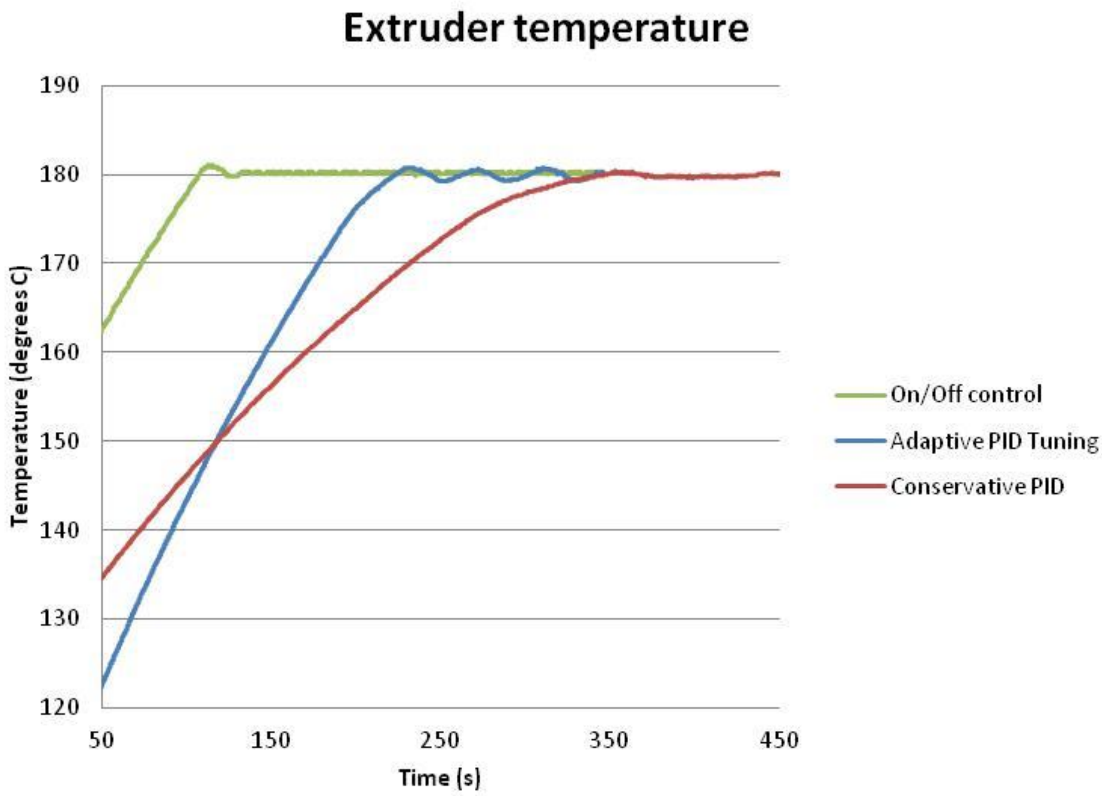


Figure 110: Data plot of extruder temperature with different control systems without line smoothing

The parameters of the PID controller are experimentally determined. They can be improved with closer analysis, since there is a constant oscillation with an amplitude of 0.75°C around the setpoint. From Figure 110 can be seen that both the simple On/Off and the PID control systems give a relatively small maximal error of less than 1°C. It is expected that the Adaptive PID controller is more flexible to use in other systems, since it can be tuned to a higher degree than the On/Off system. With other extruder blocks, a simple On/Off system can give totally different results, without the possibility to tune (See Figure 7). For this reason the future tests will be performed with the Adaptive PID controller.

**Test + outcome**

During the test 5 samples of tape of 100 mm are cut. They are fed into the heater block until they come out at the bottom (20mm). The rough side of the tape is facing the milled part of the heater channel. Then timing is started, and the pieces are pushed manually through the heater channel at a rate where scraping sounds are not heard and scratching vibrations not felt. This is repeated for five different temperatures and logged in Figure 112.

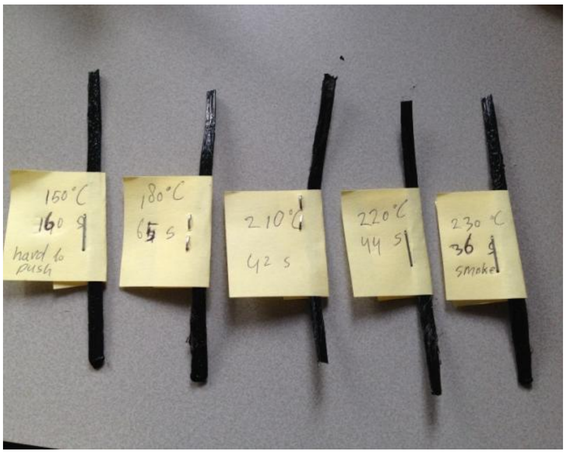


Figure 111: Test samples after extrusion

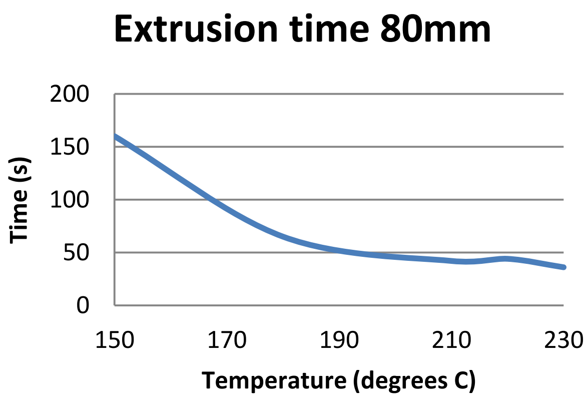


Figure 112: Plot of extrusion time vs. temperature

At 150 $^{0}$C the lowest temperature is reached where PP starts to melt. The highest allowable temperature is determined to be < 230 $^{0}$C. From 230$^{0}$C smoke is starting to form.

It is tried to keep the required force equal throughout the tests. Only light manual pushing is done with a rough estimation of 2.5N. When pushing with more force, weak but distinct scraping sounds and vibrations are noticed.

All samples show that the phenomena of dislocated fibres after extrusion are damped out over extrusion length. Wavy patterns occur at the start of each sample, but at the end they have disappeared. This might be caused by pulling the last bit out of the extruder, which is to be determined in further tests.

**Conclusion test 2**
Test 2 gives satisfying result with manually pushing the tape through a heated channel. Temperature control is accurate enough to approximate the highest allowable temperature without degrading the matrix material, which is around 220$^{0}$C. From 200-230$^{0}$C there is no noticeable difference in extrusion speed with the used criteria of allowable pushing force. The tested feed rate of the material within this temperature region is 2 mm/s.
A new test can be designed to discover the relations between temperature and feed rate. With a fixed temperature and feed rate, it is also interesting to test if the layer consolidation pressure can be achieved by the extruder motor. This seems a viable assumption, since no form of buckling and channel blocking has occurred during tests.

## 2.3 Setup of test system 3 (automatic feed, temperature control system)

Since the outcome of test 2 was positive, a drive system for the tape can be designed to test the behaviour of pushing fibre reinforced material through a heated channel at different speeds.

**What to test**
Different feeding rates can be tested to determine limits of extrusion the tape through the channel.

**Design of test 3**

A simple drive system is created with a stepper motor and a wheel. The stepper motor is controlled by an Arduino Uno R3 via a stepper driver card. A drawing is given in Figure 113 and the built setup in Figure 114.

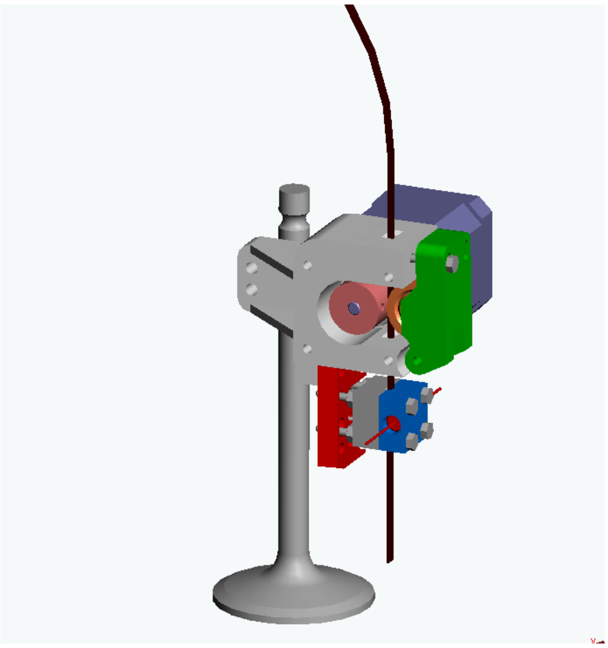

Figure 113: Simple drive system and heater block

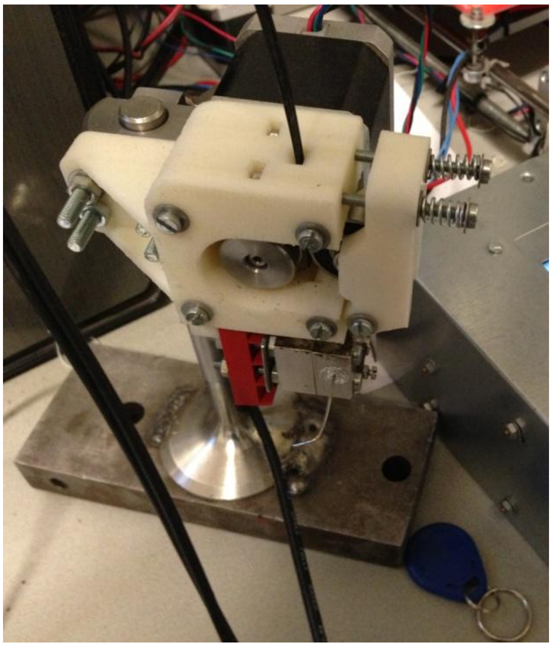

Figure 114: Built driver/heater assembly

**Test + outcome**

At a fixed temperature of 220°C several drive speeds up to 5 mm/s were achieved without clogging of the channel or buckling/breaking of the fibres. Above 5 mm/s the drive wheel slipped on the filament. From 3 mm/s it is noticed that only the outer layer of the tape is melted. At lower speeds it turned out that it is possible to press the heated tape on an existing tape with only the motor force. The results are achieved with a limited amount of tape (300mm), of which some parts were already extruded in previous tests. CompTape BV stopped the production of the tape, and it was not available anymore.

**Conclusion test 3**

Since the tests is only carried out with a small amount of tape, no solid conclusions can be drawn. It can be stated carefully that it appears to be possible to use the heater to exert consolidation force.

# 3 Modifications to printer firmware Marlin

This attachment describes the modifications to the Marlin firmware to control a digital I/O pin with M352 in a Gcode file.

In the C++ code of the firmware at the tab pins.h a new variable is created:

```
#define CUTTER_PIN          27 // Pin 27 corresponds with A4 on
                               extension pin header
```

Then a setup function is created to initialize pin 27 as output in Marlin_main.cpp:

```
void setup_cutterpin()        //   Code for initializing extension
                                   pin D27 (AI4) for cutting
                                   actuation.
{
  #ifdef CUTTER_PIN
    #if (CUTTER_PIN > -1)
    SET_OUTPUT(CUTTER_PIN);
    WRITE(CUTTER_PIN, LOW);
    #endif
  #endif
}
```

This function is called in the same file with:

```
setup_cutterpin();            //   Call function to initialize pin
                                   for cutting actuation.
```

Then the new Mcode 'M352' is created. When called, this function will finish all the commands in the local buffer of the printer, then makes a HIGH signal on pin D27 for 1000ms.

```
    case 352:
     {
      st_synchronize();       //   same as G4 P0 or M400.
                                   Waits up to all moves are finished
                                   from printer buffer before new
                                   commands can be send from host
      #ifdef CUTTER_PIN
        #if (CUTTER_PIN > -1)
          WRITE(CUTTER_PIN, HIGH);
          _delay_ms(1000);
          WRITE(CUTTER_PIN, LOW);
        #endif
      #endif
     }
    break;
```

With these adaptations the printer firmware recognizes M352 as a valid Mcode to change the pin state to HIGH for 1000ms to actuate the cutter mechanism.

# 4 Circuit of pultrusion electronics

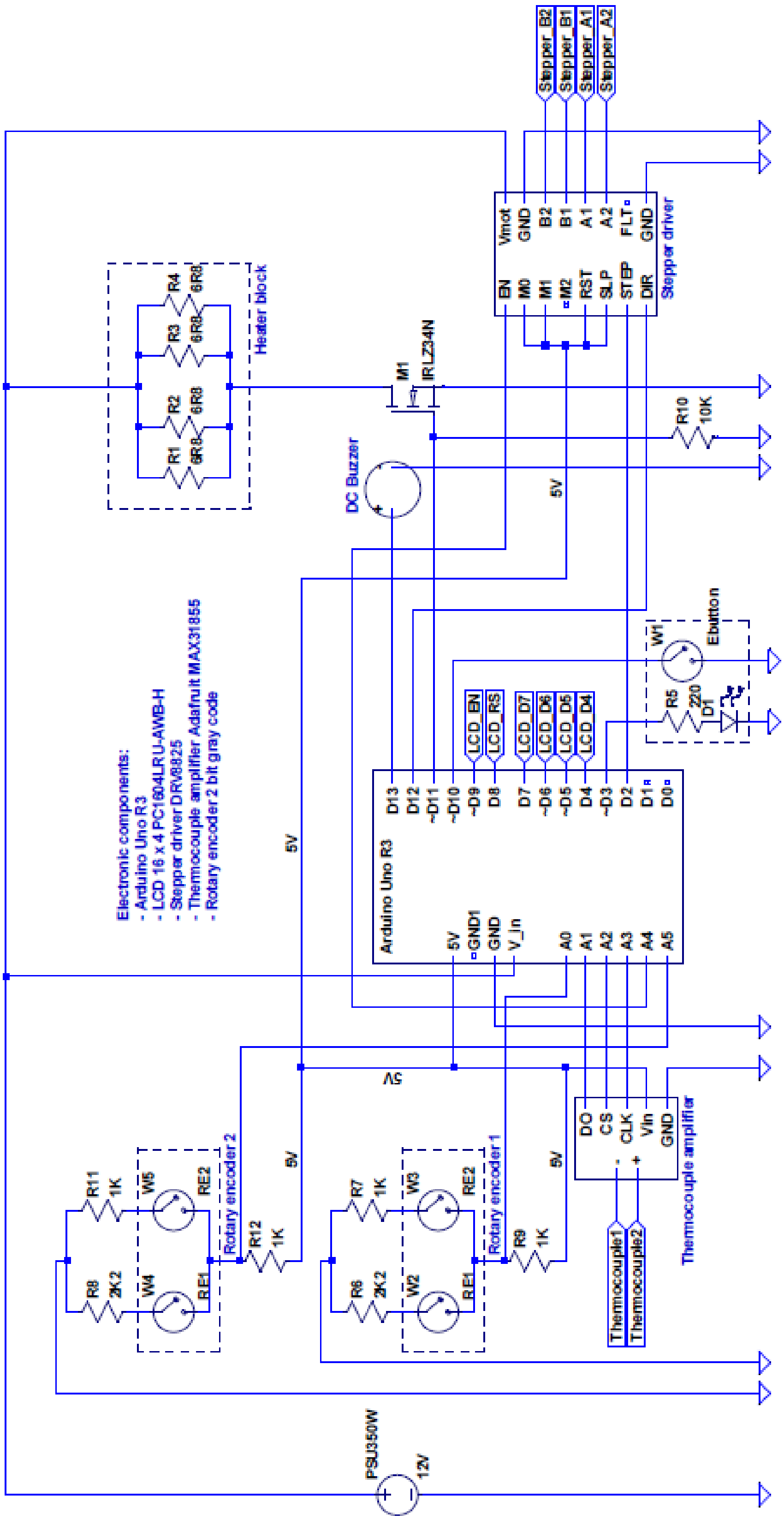


Figure 115: Circuit of pultrusion electronics

# 5 MarkForge 3D printer

During this research, MarkForged© introduced a new FDM printer that combines continuous fibres and FDM printing in one machine, the MarkOne [28]. This is a similar machine as the one that is described in this research. Feed material exists of Carbon Fibre, Fibreglass and Kevlar® embedded in a Nylon filament. The resolution in Z-direction is reported to be 0.1 mm. Achieved stress-strain behaviour of printed specimen (scaled by mass) are compared with injection moulded ABS and aluminium in Figure 116.

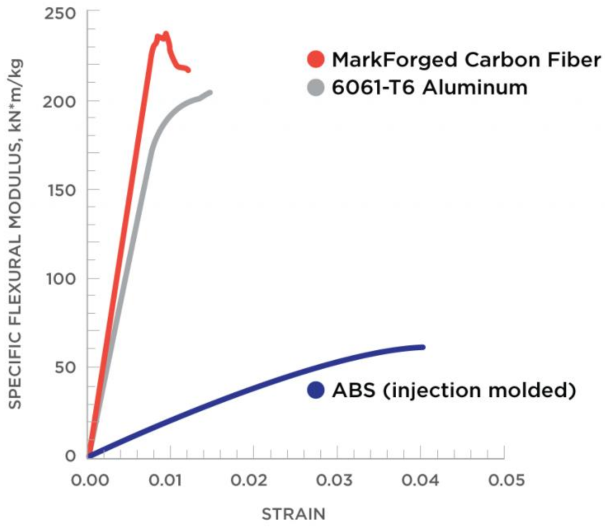


Figure 116: Comparison Stress-Strain curves [28]

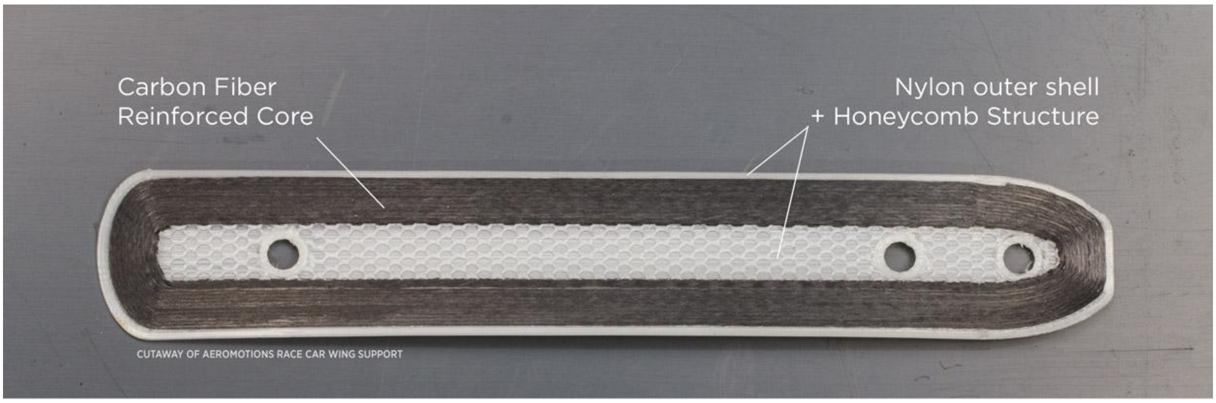


Figure 117: Cutaway of aeromotions race car wing support printed by the Mark One 3D printer[28]

A US patent is requested under number US2014328964 at 06-11-2014 (with priority date 22-03-2013), but is currently (April 2015) in the A1 category which means that is not granted yet.

# 6 Results three point bending tests

Dimensions of tested samples are found in Table 6. Span for setup L=40mm, v=1mm/min, $R_2$ = 1/16" (ø 3.175mm), $R_1$ = 1/8" (ø6.35mm) (See Figure 89)

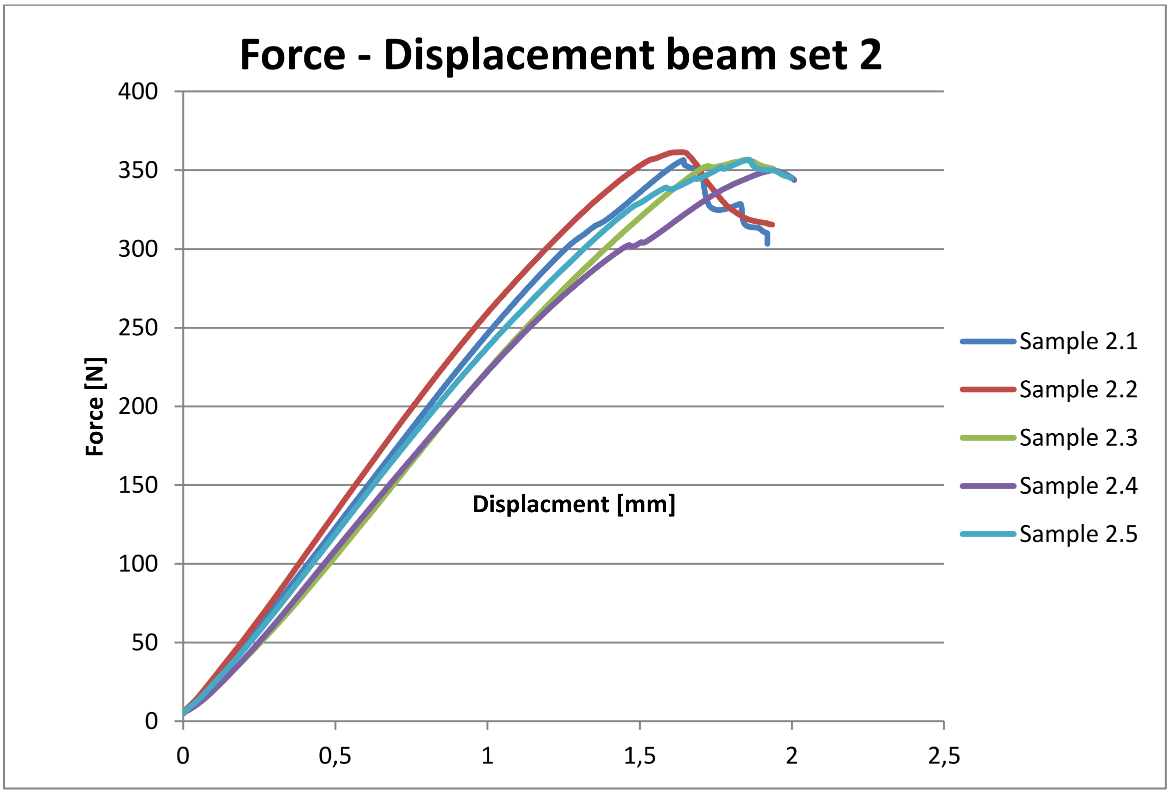


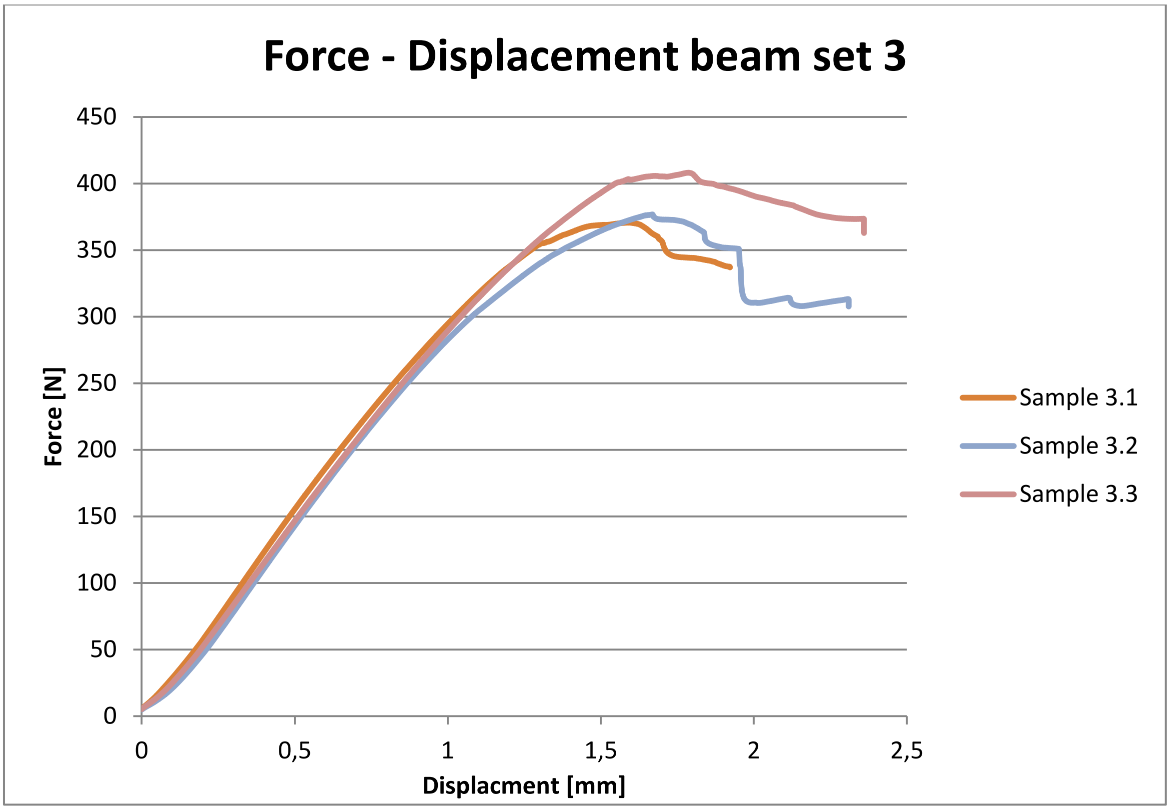

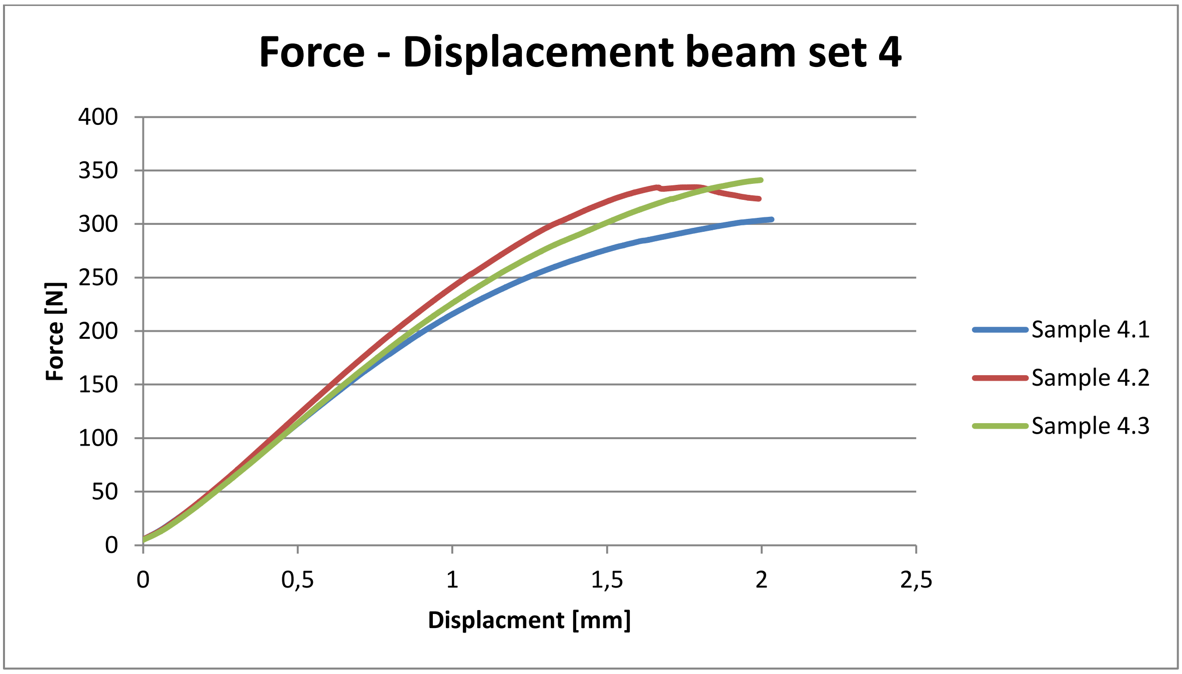
Force - Displacement beam set 4
Force [N]
400
350
300
250
200
150
100
50
0
0
0,5
1
1,5
2
2,5
Displacment [mm]
Sample 4.1
Sample 4.2
Sample 4.3

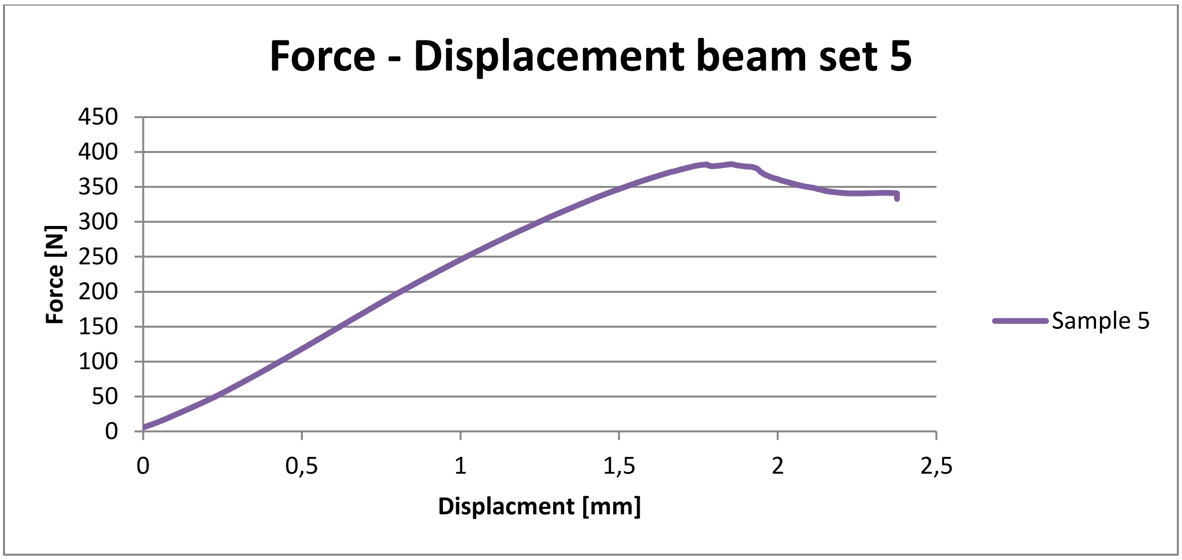
Force - Displacement beam set 5
Force [N]
450
400
350
300
250
200
150
100
50
0
0
0,5
1
1,5
2
2,5
Displacment [mm]
Sample 5

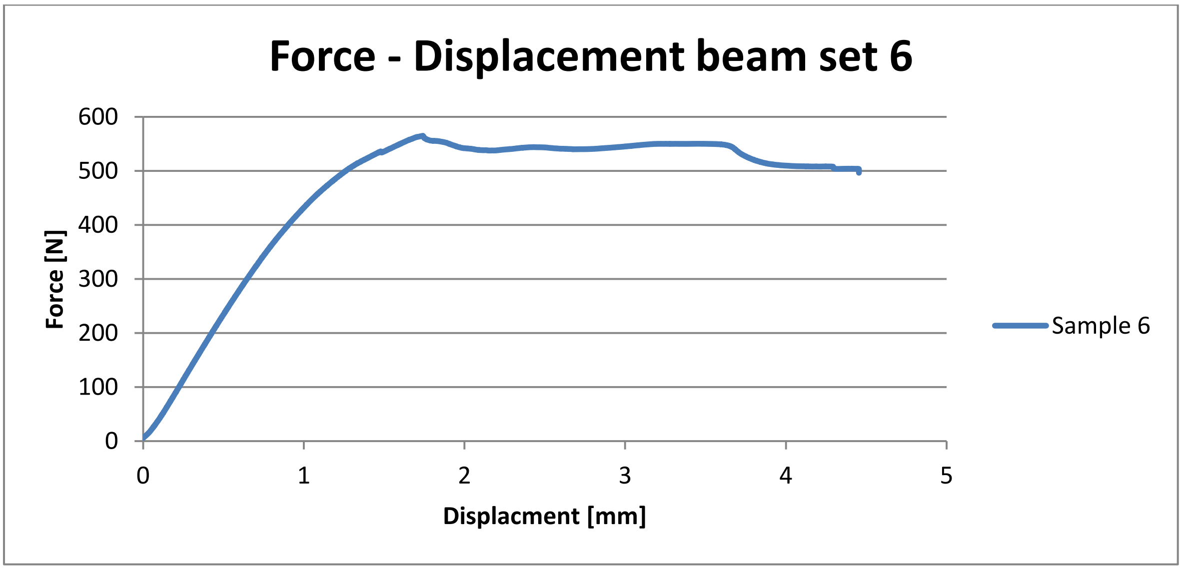
Force - Displacement beam set 6
Force [N]
600
500
400
300
200
100
0
0
1
2
3
4
5
Displacment [mm]
Sample 6